OTH Amberg-Weiden

Master's Thesis

Techno-economic Analysis and Experimental Investigation of a Floating Turbine Coil Pump (FTCP)

Techno-ökonomische Analyse und experimentelle Untersuchung einer schwimmenden Turbinen-Spulenpumpe (FTCP)

Axel Popp

M.Eng. International Energy Engineering
Department Mechanical Engineering / Environmental Technology

1. Examiner:	Prof. Dr.-Ing. Andreas P. Weiß
2. Examiner:	Prof. Dr.-Ing. Marco Taschek
Date of assignment:	02 February 2025
Date of submission:	01 August 2025

Confirmation in Accordance with § 27 ASPO

I, Axel Popp, hereby confirm that I have written this Master's thesis independently, have not submitted it elsewhere for examination purposes, have not used any sources or aids other than those indicated, and have identified all quotations and paraphrases as such.

Amberg, 31 July 2025   ....

Statement on the Usage of Artificial Intelligence Tools

In the preparation of this master's thesis, artificial intelligence (AI) tools were utilized to support specific tasks related to literature research, translation, and image processing. The suggested literature was reviewed, only its actual content was used, and the sources were cited accordingly. The following applications were employed:

- DeepL (Translation)
- Copilot (Translation / Literature research)
- ChatGPT, including Scholar GPT (Literature research / Image processing)

These tools were used as supportive instruments under the author's full academic responsibility. Only individual words or short phrasing elements were incorporated into the thesis, never entire sentences or full paragraphs. Images that have been processed with the help of AI are identified accordingly by their captions. As such, with this statement, no explicit marking or referencing within the main text was deemed necessary. All interpretations, analyses, and conclusions presented in this thesis are the result of independent scholarly work.

Abstract

This thesis investigates the technical feasibility and economic viability of a Floating Turbine Coil Pump (FTCP) as a decentralized irrigation solution for regions with limited access to electricity. Based on the principles of the Wirtz pump, the FTCP utilizes the kinetic energy of flowing water to operate without external power sources. A theoretical analysis presented the performance parameters submerged ratio, number of hose coils, drum and turbine diameter, rotational speed, and hose diameter as well as the key parameter flow velocity.

These influence of these parameters were examined through 186 measurements on a custom-built test apparatus. Flow rate and maximum achievable pump head were measured for different configurations. Energy efficiency and volumetric efficiency were calculated from these and other measurements, and the influence of the routing of the stationary delivery hose was investigated.

Subsequently, a functional FTCP prototype was constructed using potentially locally available materials and tested under real-world conditions in the river Vils. The pump achieved a flow rate of 1.2 l/min at a pump head of 1.7 m, confirming proof of concept.

An economic comparison with conventional submersible pumps revealed that FTCPs are not competitive in industrialized contexts such as Germany. However, in developing regions, their simplicity, repairability, and independence from grid infrastructure offer distinct advantages. The findings suggest that FTCPs could serve as a low-cost, locally maintainable irrigation solution in remote areas, provided that suitable watercourses are available.

Diese Arbeit untersucht die technische Machbarkeit und wirtschaftliche Rentabilität einer schwimmenden Turbinen-Spulenpumpe (FTCP) als dezentrale Bewässerungs- lösung für Regionen mit begrenztem Zugang zu Elektrizität. Basierend auf den Prinzipien der Wirtz-Pumpe nutzt die FTCP die kinetische Energie fließenden Wassers, um ohne externe Energiequellen zu arbeiten. Eine theoretische Analyse ergab die Leistungsparameter Eintauchverhältnis, Anzahl der Schlauchwindungen, Trommel- und

Turbinendurchmesser, Drehzahl und Schlauchdurchmesser sowie den Schlüssel-parameter Strömungsgeschwindigkeit.

Der Einfluss dieser Parameter wurde anhand von 186 Messungen an einer speziell angefertigten Testvorrichtung untersucht. Für verschiedene Konfigurationen wurden die Durchflussrate und die maximal erreichbare Förderhöhe gemessen. Aus diesen und weiteren Messungen wurden die Energieeffizienz und der volumetrische Wirkungsgrad berechnet und der Einfluss der Führung der stationären Förderleitung untersucht.

Anschließend wurde ein funktionsfähiger FTCP-Prototyp aus potenziell lokal verfügbaren Materialien gebaut und unter realen Bedingungen im Fluss Vils getestet. Die Pumpe erreichte eine Förderleistung von 1,2 l/min bei einer Förderhöhe von 1,7 m, was den Nachweis der Funktionsfähigkeit erbrachte.

Ein wirtschaftlicher Vergleich mit herkömmlichen Tauchpumpen ergab, dass FTCPs in industrialisierten Gebieten wie Deutschland nicht wettbewerbsfähig sind. In Entwicklungsregionen bieten sie jedoch aufgrund ihrer Einfachheit, Reparatur-freundlichkeit und Unabhängigkeit von der Netzinfrastruktur deutliche Vorteile. Die Ergebnisse deuten darauf hin, dass FTCPs als kostengünstige, lokal handhabbare Bewässerungslösung in abgelegenen Gebieten dienen könnten, sofern geeignete Fließgewässer vorhanden sind.

Keywords: Wirtz Pump, coil Pump, floating turbine coil pump, irrigation, development
Stichworte: Wirtz-Pumpe, Spulenpumpe, schwimmende Turbinen-Spulenpumpe, Bewässerung, Entwicklung

Acknowledgement

Table of Contents

Table of Figures

Table of Equations

Table of Tables

List of Formula Symbols

Parameter	Symbol	Unit
area	A	m^2
circumference	C	m
operational expenditures	c	EUR/a
power coefficient according to Betz	$c_{p,Betz}$	--
real power coefficient	$c_{p,real}$	--
diameter	D	m
degrees of freedom	df	--
energy	E	J
gravitational acceleration	g	m/s^2
pump head	H	m
height difference	Δh	m
length	l	m
mass	m	kg
mass flow rate	$\dot{m}$	kg/s
number of correlated value pairs	n	--
number of revolutions	n	--
number of turns / coils	n	--
power	P	W
electricity price	p	ct/kWh
pressure difference	Δp	Pa
flow rate	Q	m^3/s
correlation coefficient	r	--
radius	r	m
t-statistic	t	--
time	t	min
time difference	Δt	s

Parameter	Symbol	Unit
volume	V	m^3
volume flow	$\dot{V}$	l/min
velocity	v	m/s
efficiency	η	--
density	ρ	kg/m^3
rotational speed	ω	1/min

List of Abbreviations

CAPEX	capital expenditures
EUR	Euro
FTCP	floating turbine coil pump
H_2O	water
kin	kinetic
MZN MT	Mozambican Metical
OPEX	operational expenditures
pot	potential
SR	submerged ratio
tur	turbine

1   Introduction

Climate change is one of the key global challenges of the 21st century, exerting profound impacts on global agricultural systems. Rising temperatures, erratic rainfall patterns, and prolonged droughts threaten the stability of food production across the globe. As these environmental shifts intensify, many regions must expand and adapt their irrigation practices to sustain current levels of agricultural productivity (Makar et al. 2022). This situation is particularly critical in developing and emerging countries, where small-scale agriculture often forms the backbone of livelihoods and food security (Thornton et al. 2019).

In many rural areas of Sub-Saharan Africa, such as Mozambique, the need for reliable irrigation is growing rapidly. However, small-scale farmers frequently face a significant barrier: A lack of stable electricity infrastructure. Grid electricity is either unavailable, unreliable, or overly expensive in remote farming communities, restricting the use of conventional electrically powered irrigation pumps. The theoretical possibilities of electrifying rural areas using solar-based off-grid systems often fall short due to poor market access, uncertain safety conditions and, last but not least, the often expensive credit-financed investment costs (Baruah and Coleman 2019). Diesel-powered pumps, while common, pose environmental concerns and create a dependency on volatile fuel markets, placing additional strain on farmers with limited resources (Mindú et al. 2021).

Floating turbine coil pumps (FTCPs), as seen in online videos, might represent a simple yet promising solution for small-scale irrigation in remote areas (Tiller 2018; Meneses 2015). By using the kinetic energy of existing rivers, they do not require any external power source. As a floating structure the design potentially adapts independently to different water levels and flow conditions. Their seemingly simple structure appears to be replicable even without special knowledge in engineering or manufacturing.

1.1   Research Questions

Recognising the need for alternative pump systems and based on the videos mentioned above, the following research questions arise:

- Is it technically possible to create a functioning FTCP from locally available materials and by hand using basic equipment?
- At what price can such a pump be built and operated, and how does this compare with other available pump systems?

1.2   Methodological approach

In order to answer the research questions, the first step is to gain a deeper understanding of the principles of coil pumps. To this end, theoretical and experimental studies and work will be presented. The future operating environment of the FTCP in watercourses will also be outlined.

Subsequently, the assumptions and findings from the literature will be practically verified and tested in a test setup. Taking into account the results of these tests, a functioning model of an FTCP will then be designed, manufactured and tested for functionality.

In the event of a successful proof of concept, the costs for implementation will then be quantified. In order to ensure that the economic analysis is applicable in developing countries, the investment costs for a potential country of use will be estimated as accurately as possible. A review of the operating costs of the system in comparison to alternatives concludes this thesis.

2   Theoretical and Previous Work

This chapter is focused on presenting the theoretical principles that are relevant to this work. To this end, the principle of the original Wirtz pump is first examined, followed by a discussion of its modification as a coil pump. Finally, a brief consideration of possible turbines in flowing water is provided.

2.1   The Wirtz Pump

A Wirtz pump, displayed in historic drawings in Figure 1, was invented by H. A. Wirtz in 1746. It is a spiral of pipe partly submerged into water in a vertical plane and powered by an external source such as the kinetic energy of a river. When rotating this spiral the open end of the pipe on the outer edge dips into a liquid once per revolution and therefore collects it. After surfacing, a plug of air is automatically taken in for the remaining rotation. Through constant rotation, the spiral gradually fills with water plugs, each separated from the others by air plugs. At the inner end of the spiral, the pipe is connected to a rotary coupling. From there, the water and air plugs are transferred to a stationary pipe, the delivery pipe. As the water plugs in the delivery pipe are elevated, pressure builds up in the system. This pressure creates a cascade of manometric effects in the spiral (Deane and Bevan 2018).
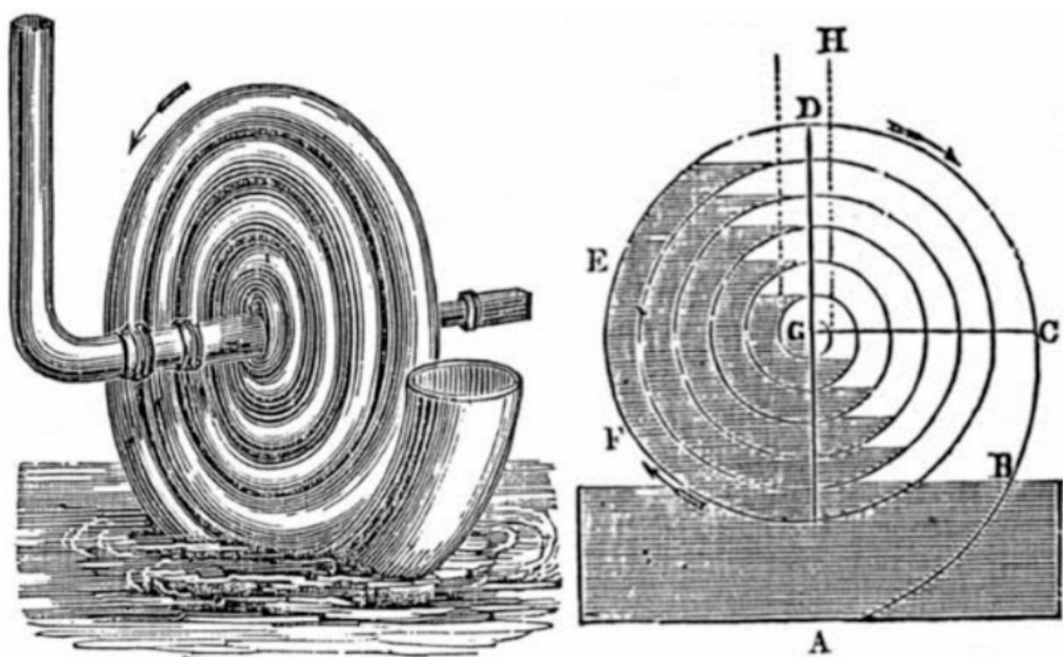
Figure 1: Wirtz pump drawing from 1842 (Meseret et al. 2024)

Figure 2 shows a single manometer (a), three manometers in series (b) and the arrangement of the manometers in a spiral. In the single manometer (a), the pressure difference $p_1 - p_0$ is proportional to the difference in height Δh of the water levels on both sides of the manometer. According to Pascal's Law, this assumption is valid for incompressible, stationary liquids. With a slowly rotating spiral, the system can be considered to be in a stationary state and water can be considered to be incompressible. Transferred to the triple manometer (b), it can be concluded that the new pressure difference $p_3 - p_0$ is now proportional to the sum of the height differences given as $\Delta h_1 + \Delta h_2 + \Delta h_3$. The same applies to the spiral (c) (Deane and Bevan 2018). Since such a spiral can consist of an indefinite number of turns n, a general relationship must be established here. Accordingly, every pressure difference between points n and 0, given as $p_n - p_0$ is proportional to the sum of the corresponding height differences, given as $\sum_{i=1}^{n} \Delta h_i$. The pressure pushes the individual water columns from the centre of the spiral slightly towards the inlet.
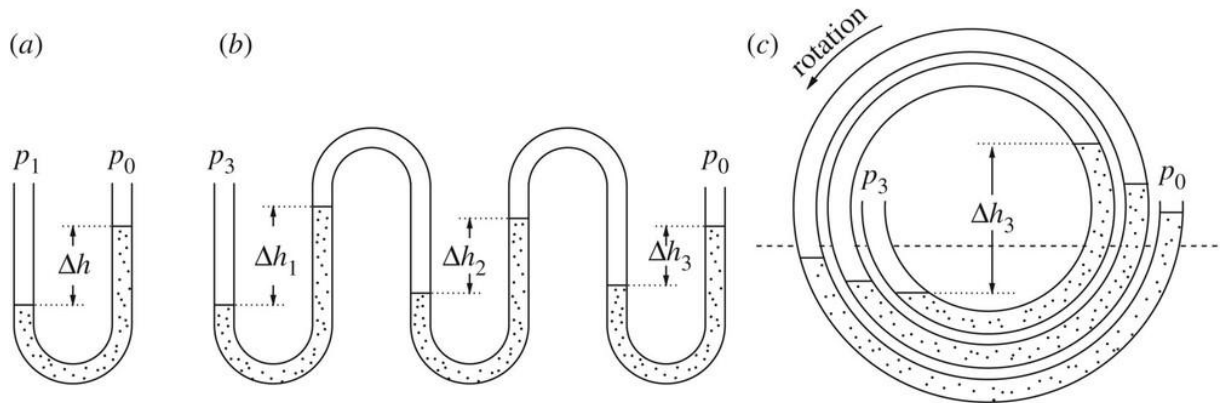
Figure 2: Illustration of a single manometer (a), three manometers in series (b) and the arrangement of manometers in a spiral (c) (Deane und Bevan 2018)

It is therefore essential that the water and air columns remain intact during operation. If air were to pass through the water columns, this would compensate for the differences in height described above and the system would be unable to generate pressure. In summary, it can be stated that the pump works on the principle that columns of water and air alternate in the system. The high-density fluid water is displaced and exerts pressure on the low-density fluid air. This pressure then elevates the fluids in the delivery pipe (Deane and Bevan 2018). Since this thesis refers to a variation of the Wirtz pump, the coil pump, a more in-depth examination of the original design will not be pursued.

2.2 The Coil Pump

The coil pump is based on the same principle as the Wirtz pump. However, the coils are not spiral- but coil-shaped in or around a cylinder (Mortimer 1988). Figure 3 presents the structure of a coil pump based on a helical drum. During functional operation, water and air are alternately drawn in at the inlet. The plugs then move from left to right through the coils, in accordance with Figure 3, and are discharged from the drum into a rotating horizontal piece of pipe after passing through the last coil. After that, they are fed through the rotary coupling into the stationary delivery pipe. There, water and air are elevated to the upper tank. Depending on the pump head, which in Figure 3 would be the height of the upper tank, the air plugs in the pump are compressed. The higher the pump head, the greater the compression and the greater the height differences in the individual coils (Mortimer 1988).
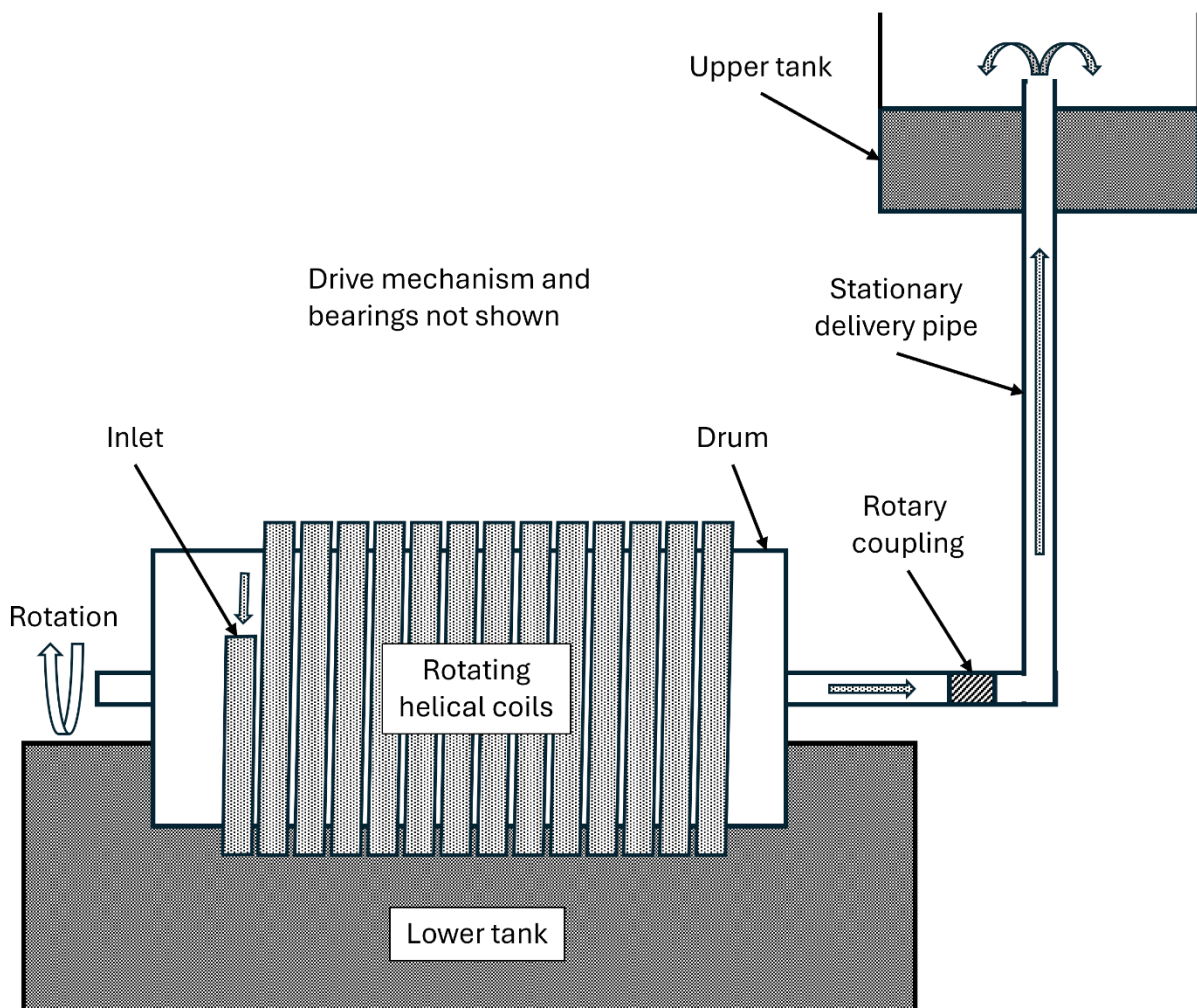
Figure 3: Structure of a coil pump (Own illustration according to Mortimer 1988)

2.2.1 Limitation in the Operation of a Coil Pump: Spilling

Spilling occurs when the water column in a coil exceeds the highest point on the inside of the pipe. The previously stable water column splits, as the compressed air remains in the upper part of the pipe and the water below can flow through into the next coil. The water always flows back into the next coil in the direction of the inlet. This triggers a chain reaction from the affected coil to the inlet, where water
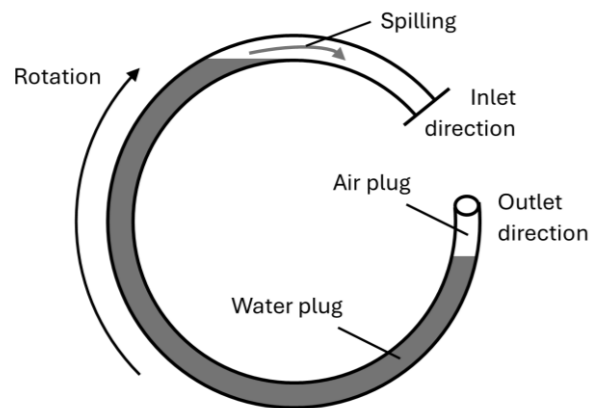
Figure 4: Illustration of the spilling mechanism (Own illustration according to Mortimer 1988)

finally shoots out of the pump. Figure 4 illustrates the occurrence in the first coil affected by spilling. Possible reasons for spilling include either excessive rotational speed or excessive pressure in the system (Mortimer 1988). Although there are no clear statements on this in the literature, spillage must result in a loss of head in the stationary delivery pipe due to the loss of water at the inlet. As this is a rapid and dynamic change, it is to be expected that the momentum of this drop will amplify the spilling effect.

2.2.2 Parameters of an Operational Coil Pump

Whether a coil pump is functional and what pump head and flow rate it can achieve depends on its configuration and operation. The following subsections provide a theoretical overview of the respective variables and their influence on pump performance. If the influence of one parameter is investigated, the rest of the setup is not changed. For instance, for all results investigating the influence of the submerged ratio the same configuration of number of coils, drum diameter and pipe internal diameter is used. The descriptions mostly refer to two experimental studies by the same authors, as the data available for this application is not yet very extensive. Since the studies do not explain all the correlations in detail, some own explanatory approaches are presented after the presentation of the results. It should be noted that these are purely theoretical considerations that are not evidence-based.

2.2.2.1 Effect of the Submerged Ratio

The submerged ratio describes the ratio of the cross-sectional area of the rotating cylinder that is submerged. Theoretically, values above 0 % and below 100 % are possible. At 0 %, no water would be absorbed, and at 100 %, no air would be absorbed. In both cases, the pump would not function.

Figure 5 displays the results of an experimental study. The experiments have shown that the submerged ratio has little effect on the maximum achievable pump head as long as it varies between 15 % and 85 %. However, at a submerged ratio of over 85 %, the maximum achievable pump head decreases at constant rotational speed and, as expected, drops to 0 m when 100 % is reached. At a submerged ratio of less than 15 %, the maximum achievable pump height also decreases and returns to 0 m at 0 % (Kassab et al.
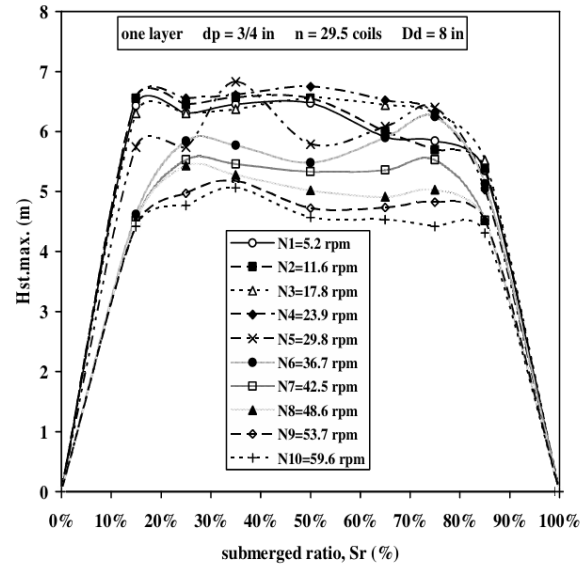
Figure 5: Variation of maximum achievable pump head with submerged ratio for different rotational speeds (Kassab et al. 2005)

2005). In theory, it should be noted that the system tends towards spilling more easily with a high submerged ratio, as the difference in height between the water edge and the highest point on the inside of the pipe becomes smaller as the submerged ratio increases (Mortimer 1988). This might be the reason why the maximum achievable pump head decreases at values above 85%.

7

Figure 6 shows the results with regard to the flow rate. Here, an increase in the submerged ratio from 15 % to 85 % is accompanied by an increase in the flow rate. The increase is approximately linear. Up to a submerged ratio of just under 100 %, the flow rate continues to increase slightly, but above 95 % it no longer reaches the measurement height for all rotational speeds. At 100 %, just like at 0 %, no flow could be measured. (Kassab et al. 2005). This insight is easy to understand logically: the higher the

Figure 6: Variation of flow rate with submerged ratio for different rotational speeds (Kassab et al. 2005)

submerged ratio, the more water is taken in per revolution. Presuming that a fixed pump head can be achieved, more water is pumped per revolution. At a constant rotational speed, this leads to a higher flow rate.

2.2.2.2 Effect of the Number of Coils

Experiments show a clear correlation between the number of coils and the maximum achievable pump head (Figure 7). Between 5 and 30 coils, the maximum achievable pump head increases continuously with increasing number of coils (Kassab et al. 2005). In simple terms, this can be explained as follows: Each additional coil introduces an additional air plug into the system. When this additional volume is compressed, an additional manometer is created in which additional pressure can build up. This pressure then enables the additional pump head.
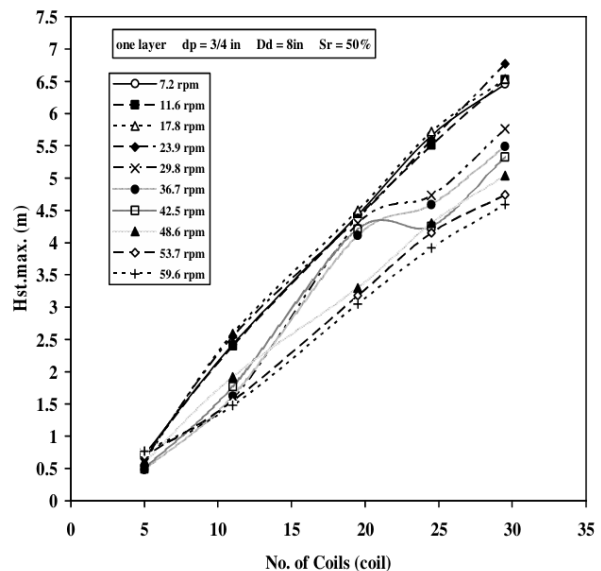
Figure 7: Variation of maximum achievable pump head with different numbers of coils for different rotational speeds (Kassab et al. 2005)

The relationship between the number of coils and the flow rate is shown in Figure 8. It could not be generally proven that the number of coils also has an effect on the flow rate. For rotational speeds of up to 30 rpm, the flow rate remained approximately constant regardless of the number of coils. Only when the number of coils was increased from 24 to 30 did the flow rate decrease slightly. It should be noted that no experiments with more than 30 coils were carried out in this study. The behaviour with very large numbers of coils cannot therefore be assessed here (Kassab et al. 2005).
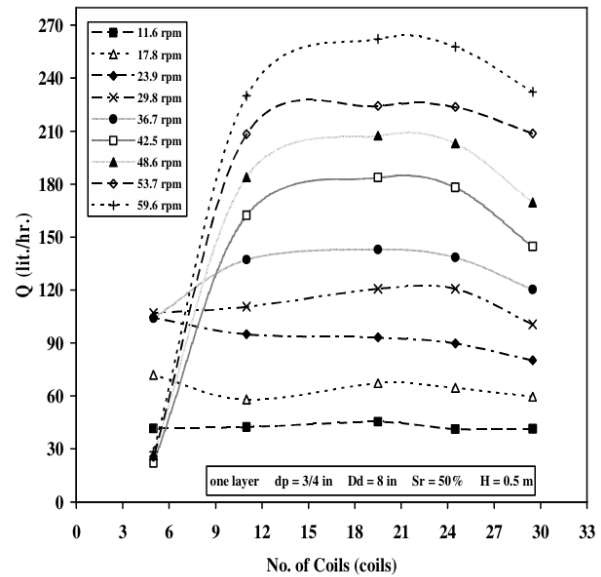
Figure 8: Variation of flow rate with different numbers of coils for different rotational speeds (Kassab et al. 2005)

2.2.2.3 Effect of the Rotational Speed

Referring to the results of the same experimental study, a correlation between the maximum achievable pump head and the rotational speed can be concluded. Specific measurements, illustrated in Figure 9 for submerged ratios above 85 %, show that,
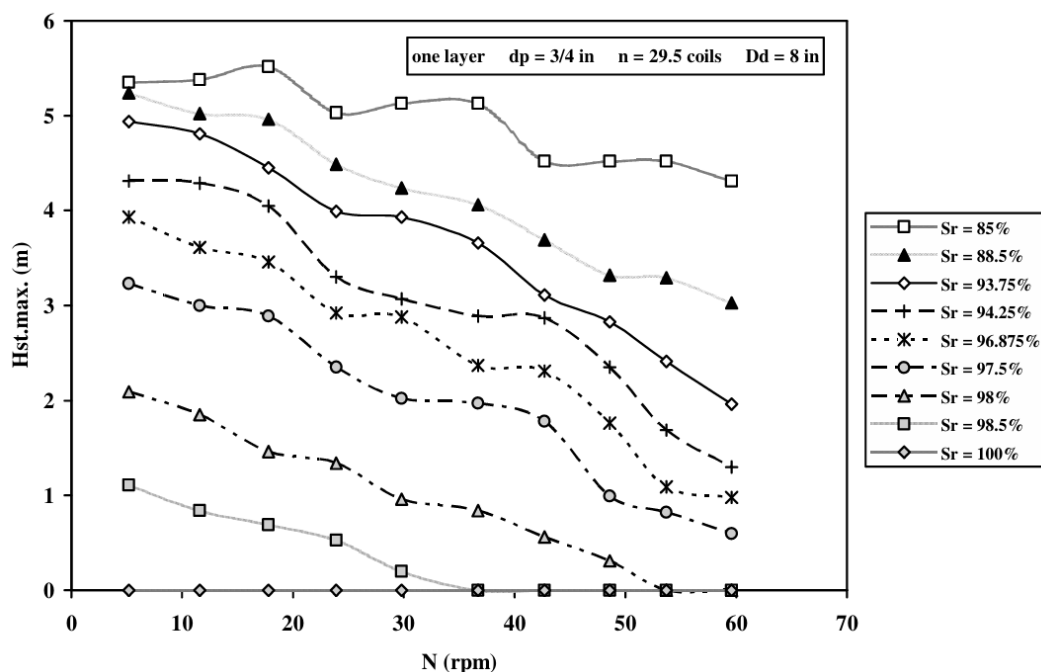
Figure 9: Variation of maximum achievable pump head with different rotational speeds for different submerged ratios from 85 % to 100 % (Kassab et al. 2005)

9

with the pump configuration otherwise unchanged, higher pump heads could be achieved at lower rotational speeds. The correlation also applies to lower submerged ratio values, but no equivalent graphical representation could be found in the study. In addition, when measuring the flow rates, the curves shown in the graphs for higher rotational speeds trend towards 0 l/hr at lower pump heads. However, it should be noted here that a wide range of rotational speeds is being compared, from about 5 rpm to 60 rpm. The authors of the study therefore consider minor changes in rotational speed to be of little significance. The study does not provide an explanation for the changes (Kassab et al. 2005). One possible theoretical explanation might be the increase in friction. Higher rotational speeds result in a higher flow velocity relative to the pipe and therefore a higher flowrate. As the pressure losses are proportional to the cubed square velocity, the increase in rotational speed increases the share of the static pressure that is dissipated as a pressure loss. Additionally, the increased friction on the inner wall of the pipe might cause the water plugs to follow the pipe's movement and therefore move further up towards the inlet. This would lead to spilling occurring at lower pump heads.

Provided that the pump was functioning properly, meaning that the flow rates were significantly above 0 l/h, it was clearly demonstrated that increasing the rotational speed had a positive effect on the flow rates as can be seen in Figure 10. This behaviour is explained by the increased water absorption due to higher rotational speeds and is easily
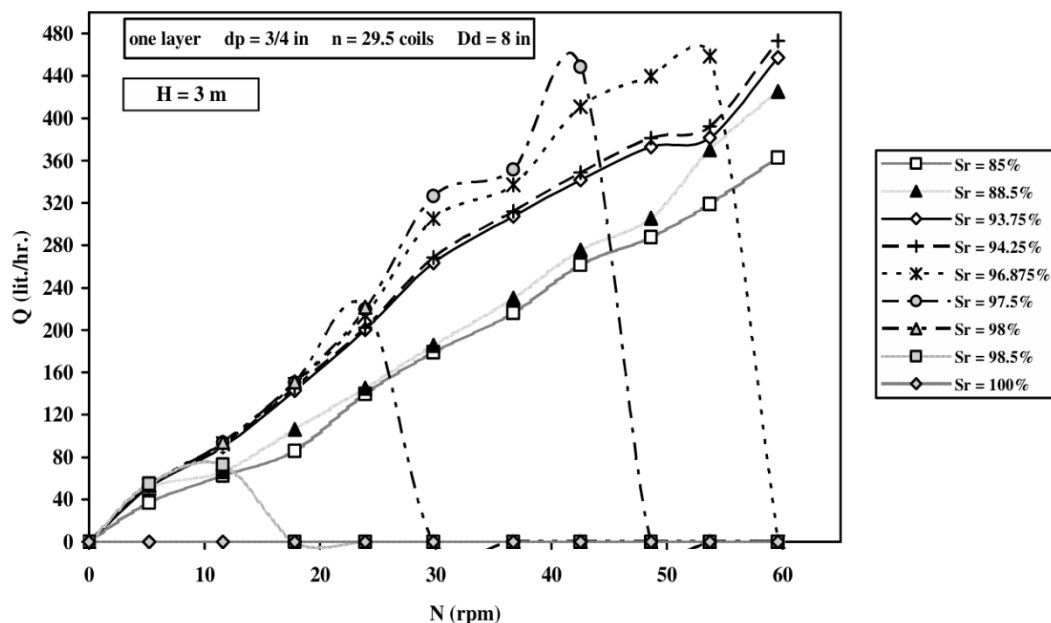
*Figure 10: Variation of flow rate with different rotational speeds for different submerged ratios from 85 %
to 100 % (Kassab et al. 2005)*

comprehensible. However, as already mentioned in the previous paragraph, excessive rotational speed can prevent the desired pump head from being reached and cause the pump to fail completely. Figure 10 represents these results for submerged ratios above 85 % (Kassab et al. 2005). This aspect should be taken into account when implementing the system in practice.

2.2.2.4 Effect of the Drum Diameter

In the experiments of a further study, the change in the drum diameter was investigated. It was found that the maximum achievable pump head increases with a larger drum diameter. The authors explain this behaviour by stating that the larger diameter allows more air to be absorbed. A graph showing the drum diameter on the x-axis and the maximum achievable pump head on the y-axis is not included in the study (Kassab et al. 2006). A slightly more detailed explanation for the correlation than the one given in the study would be that the larger diameter in each coil increases the length of the air plugs. This increases the absolute distance between the water edge and the inner upper edge of the pipe. Given an otherwise unchanged configuration, the pump can therefore generate more pressure with a larger drum before the pressure causes a height difference in the coils, which causes spilling.

According to the results of the study, the flow rate also increases with increasing drum diameter. Figure 11 depicts the measurement results of the study in graphical form. The reason for this is said to be the increased water absorption under otherwise constant conditions (Kassab et al. 2006). The following explanation can be given: The larger diameter increases the length of the water plugs and thus the volume of water per coil. Provided that a specified pump head
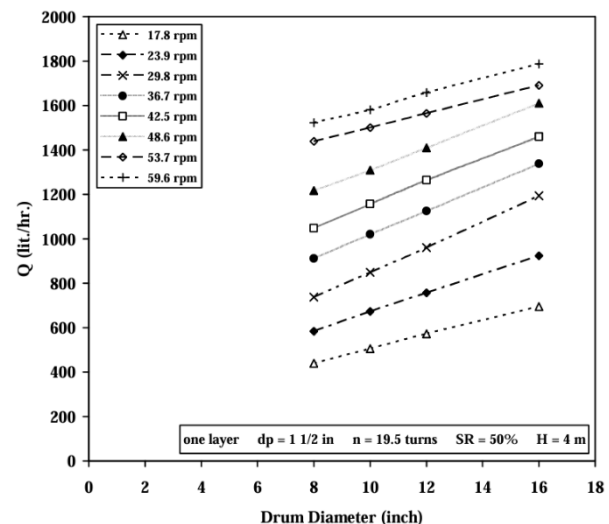
Figure 11: Variation of flow rate with different coil/drum diameters for different rotational speeds (Kassab et al. 2006)

is achieved at a constant rotational speed, more water is transported through the pump and thus into the upper tank per coil. An increased flow rate can then be measured.

2.2.2.5 Effect of the Pipes Internal Diameter

No clear information is provided on the effect of the internal diameter of the pipe or hose used (both terms are used in the studies for the same components) on the maximum achievable pump head. Nor can any trend be identified from the graphs provided (Kassab et al. 2006).

However, what is clearly highlighted is the effect of the inner diameter of the hose used on the flow rate of the pump. Figure 12 shows the measurement results for different hose diameters depending on the rotational speed. From 1/2" to 3/4" to 1", the flow rate already increases noticeably. However, the increase in flow rate from 1" to 1 1/2" is significantly greater. The authors of the study cite two reasons for this. As the inner diameter of
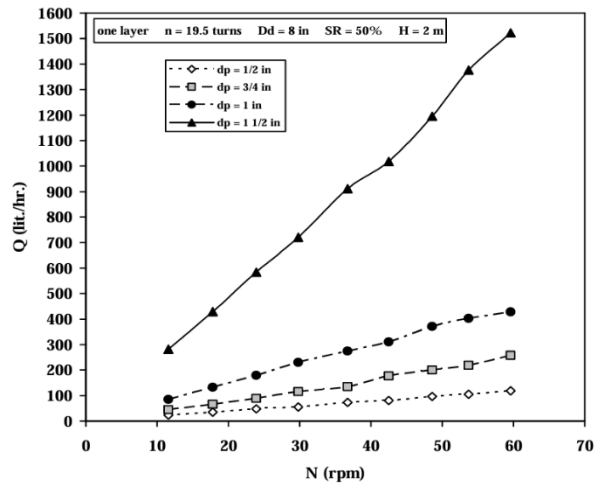
Figure 12: Variation of flow rate with different rotational speeds for different internal diameters of the hose (Kassab et al. 2006)

the hose increases, so does the cross-sectional area of the inlet, which in turn leads to a higher flow rate at the inlet. This continues through the pump and is measured as an increased flow rate at the outlet. In addition, the larger inner diameter reduces friction losses per unit volume inside the pump (Kassab et al. 2006). It should be noted that the inlet area increases quadratically with the pipes' radius. This explains the increasing differences of the graphs in Figure 12 with the increasing internal diameters of the pipes.

2.2.3 Conclusions for an Optimal Coil Pump Design

With regard to the optimal design for achieving maximum pump head and maximum flow rate, the following configuration and operation would therefore be advisable based on the findings of this study:

Configuration/operation	Maximum pump head	Maximum flow rate
Submerged ratio (SR)	< 85 %	High, but < 100 %
Number of coils (n)	High	< 30 coils
Rotational speed (ω)	Low	High
Drum diameter ($\varnothing D_{drum}$)	High	High
Internal diameter of hoses ($\varnothing D_{hose}$)	No indication	High

Table 1: Optimized configurations and operations for maximum pump head and maximum flow rate of a coil pump (Own table)

Depending on practical requirements, the configuration and operating mode can be taken into account in the pump design. However, it should be noted that a sufficiently powerful drive is required to achieve high performance, meaning high flow rates at high pump heads. When implementing a pump as an FTCP, the drive is always determined by the properties of the given water flow. It should be noted that the table provides only indications on the pump design. A general statement on one optimal design cannot be derived from the information provided in previous works.

2.3   The Floating Turbine Coil Pump

The central objective of this work is to develop an FTCP for existing water bodies. A schematic representation of such an FTCP is shown in Figure 13. It should be noted that neither the floating bodies nor the pump anchorage are shown here. Essentially, the design barely differs from that of the coil pump as illustrated in Figure 3 in Chapter 2.2. Unlike the original coil pump, however, the drive mechanism of the FTCP is precisely defined. The FTCP is driven exclusively by a turbine that exploits the flow of the given water body. Here, the water body serves as the lower tank. The torque generated at the turbine is transmitted via a fixed connection to the cylindrical drum to which the rotating hose is attached. This causes the pump to alternately draw in air and water at the inlet and transport both to the rotary coupling. From there, both are transported via the delivery hose to the upper tank. It is important to note that this is only a schematic representation. The design and orientation of individual parts may be modified in practical implementation, provided that their basic functions remain unchanged.
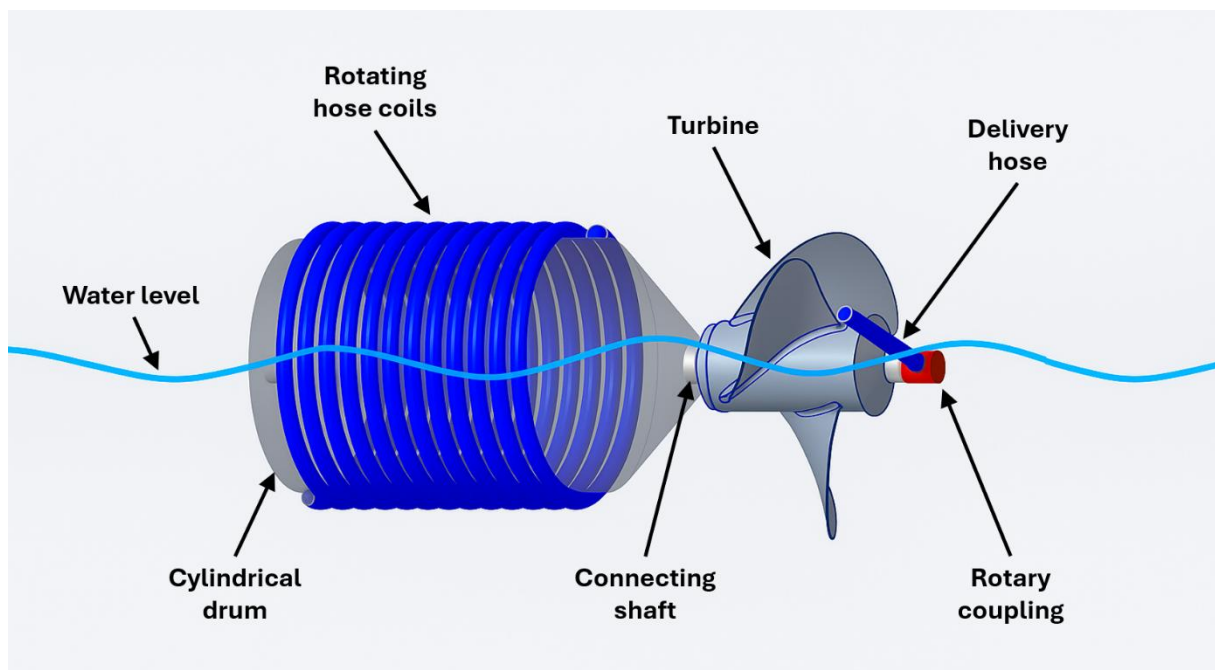
Figure 13: Schematic representation of an FTCP (Illustration by C. Heuermann with own AI-assisted adjustments)

The following sections describe the theoretical power that can be supplied to the system by a flowing water body for the pumping work.

2.3.1 Power Calculation of a Water Flow

The power in this case is defined as the quotient of the kinetic (kin) energy of the water (H_2O) over time as described in Equation 1.

Equation 1: Power of a water flow (Ruff 2022)

$$P_{H_2O} = \frac{E_{kin,H_2O}}{\Delta t} = \frac{\frac{1}{2} * m_{H_2O} * v_{H_2O}^2}{\Delta t} = \frac{1}{2} * \dot{m}_{H_2O} * v_{H_2O}^2$$

With:

P	power	$[W]$
E	energy	$[J]$
Δt	time difference	$[s]$
m	mass	$[kg]$
v	velocity	$\left[\frac{m}{s}\right]$
$\dot{m}$	mass flow rate	$\left[\frac{kg}{s}\right]$

Since the mass flow rate is difficult to measure in practice, the equation needs to be broken down further. As it also depends on the size of the turbine (tur), this is introduced as a variable. The calculation is presented in Equation 2.

Equation 2: Mass flow rate of a water flow (Ruff 2022)

$$\dot{m}_{H_2O} = \rho_{H_2O} * Q_{H_2O} = \rho_{H_2O} * A_{tur} * v_{H_2O} = \rho_{H_2O} * r_{tur}^2 * \pi * v_{H_2O}$$

With:

ρ	density	$\left[\frac{kg}{m^3}\right]$
Q	flow rate	$\left[\frac{m^3}{s}\right]$
A	area	$[m^2]$
r	radius	$[m]$

For the calculation, the last term from Equation 2 is now inserted into Equation 1. This means that the power of a water flow theoretically available for the cross-section of a turbine, as shown in Equation 3, mainly depends on the turbine radius and the flow velocity. Since the flow velocity affects the power to the third power, it is the key variable to consider (Ruff 2022).

Equation 3: Power of a water flow (Ruff 2022)

$$P_{H_2O} = \frac{1}{2} * r_{tur}^2 * \pi * \rho_{H_2O} * v_{H_2O}^3$$

2.3.2   Power Calculation of a Floating Turbine Coil Pump

With an FTCP, it cannot be assumed that the entire power of a water flow can be converted directly into pump power. This subchapter therefore considers the limitations applicable in the case of FTCPs.

The first limitation generally applies to all free flow turbines that extract energy from a flow. According to the calculations of Alfred Betz, the power coefficient is introduced here, describing the share of energy that can be extracted from a flow. He states that this power coefficient cannot exceed a maximum value of 16/27 or about 59 % (Betz 1926). Higher values would lead to the flow slowing down further passing the turbine, decreasing the mass flow rate through the turbine by causing stagnation of the flow behind the turbine.

This would cause, in case of a free flow turbine without alterations in the river course, nozzles or diffusers, larger parts of the flow to bypass the turbine. Figure 14 depicts the progression of pressure and speed in qualitative terms. The increase in pressure in front of the turbine, point -2, reduces the usable mass flow rate and therefore the power provided by the flow. The power coefficient according to Betz describes the theoretical optimum and leads to exploiting the flow through the turbine and decreasing the flow rate through the turbine (Ruff 2022). In this case, the flow velocity after the turbine v_3
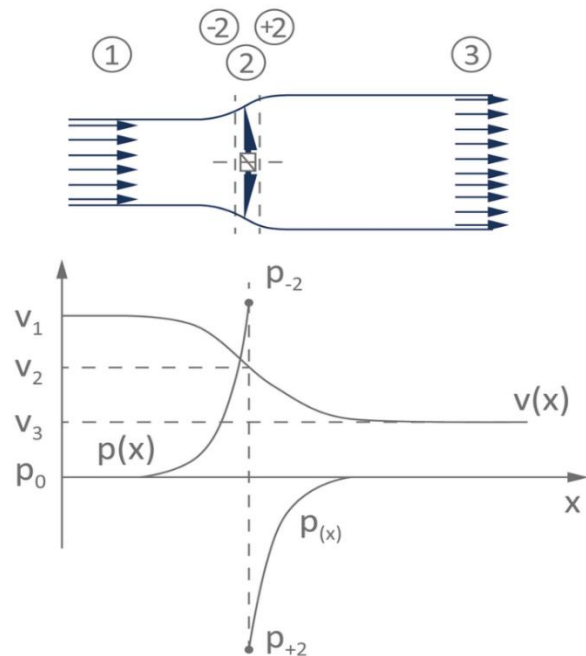
Figure 14: Fluid pressures and velocities at different positions of a turbine (Bundesverband WindEnergie e.V. 2022)

corresponds to exactly one third of v_1. The flow velocity at the turbine v_2 then equals two thirds of the initial velocity v_1 (Bundesverband WindEnergie e.V. 2022).

Secondly, the shape of the turbine must also be taken into account. Losses can occur here if the turbine is not optimally designed for the flow velocity, flow direction, and rotational speed of the pump. The product of Betz's optimal power coefficient and the efficiency of the turbine can be combined to give the real power coefficient of the turbine.

The third limitation concerns the submerged ratio of the turbine. Assuming that the pump is horizontal in the water, the turbine is point-symmetrical about the centre, and has the same radius as the rotating coils, the submerged ratio of the pump corresponds to the submerged ratio of the turbine. The part of the turbine that is above water does not contribute to the drive of the pump. If one of the above aspects does not apply, the submerged ratio of the turbine must be measured to calculate the available power. This allows the performance of an FTCP to be represented as shown in Equation 4. All other losses, such as for example for friction, are included in the term η_{other}.

Equation 4: Power of a Floating Turbine Coil Pump (Own calculations according to Ruff 2022)

$$P_{FTCP} = \frac{1}{2} * r_{tur}^2 * \pi * \rho_{H_2O} * v_{H_2O}^3 * c_{p,Betz} * \eta_{tur} * SR_{tur} * \eta_{other} =$$

$$= \frac{1}{2} * A_{tur} * SR_{tur} * c_{p,real} * \eta_{other} * \rho_{H_2O} * v_{H_2O}^3$$

With:

$c_{p,Betz}$	*power coefficient according to Betz*	$[-]$
η	*efficiency*	$[-]$
SR	*submerged ratio*	$[-]$
$c_{p,real}$	*real power coefficient*	$[-]$

3   Development of a Test Apparatus

After gaining a basic theoretical understanding of how Wirtz and coil pumps work, the next step was to design, build and test a test setup. The aim of this setup was to be able to verify the theory through experimental proof. The setup was also intended to serve as the basis for the development of a functional FTCP.

3.1   Construction and Assembly of the Test Apparatus

An Intermediate Bulk Container (IBC) with a capacity of 1,000 litres, which is ideally suited for test purposes, serves as the basis. Since the container is mounted on a plastic pallet, it can be easily transported. The outlet at the bottom also allows for quick filling and emptying. The upper crosspieces were removed from the container first, followed by the lid, using an angle grinder. The tank was then cleaned, and the resulting opening was measured.

On the basis of the size of the container, a steel frame was then designed as a mounting. Several designs were created using AutoCAD software, which were optimized in consultation with the university's central workshop. The final version, depicted as a model in Figure 15, was then produced using square steel tubes sized 40 × 40 × 2 mm. The upper part was designed to rest on two opposite sides of the IBC container frame. On the other sides, additional square steel tubes were attached vertically downwards in a U-shape in the centre. The bearing blocks for the hose holder will later be attached to these parts. To prevent the frame from excessive slipping, short steel tubes pointing downwards were attached in such a way that the mounting is held securely on the frame of the container. To prevent rust, the entire mounting was hot dip galvanised at an external facility. This meant that several holes had to be drilled in the individual parts in advance. This was the only way to ensure that the parts would not deform or burst due to the high temperatures. Another hole was drilled for the attachment of the drive. This will be explained in more detail in a separate paragraph below.

Figure 15 shows the final CAD model in 3D, which was used as the basis for subsequent production. The bearings for the rotating hose holder are already included in the drawing. Since drawing the bearings would have been very time-consuming, a 3D CAD model was downloaded from an online source, and inserted into the drawing of the mounting (SKF GmbH 2025). The holes for attaching
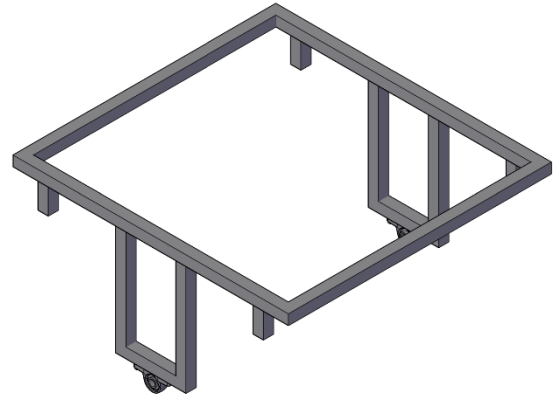
Figure 15: 3D CAD model of the mounting (Own CAD model)

the drive and for galvanisation are not depicted. The finished component is 1,100 mm wide, 1,050 mm long and 480 mm high, excluding the bearings. The short steel tubes for securing the component, which are 100 mm long, were attached at a distance of 100 mm from the outer edge of the mounting. The U-shaped attachments for the hose holder are 280 mm wide and 440 mm high.

The hose holder was also designed in several steps, first digitally using AutoCAD. The basic aim was to provide as much space as possible for attaching the hose while still offering all the necessary functionality for testing. Figure 16 shows the final CAD model of the hose holder, which served as the framework for practical implementation.

A 25 mm diameter steel shaft measuring 1,070 mm in length serves as the basis for the hose holder. At the upper end of the shaft, as shown in the model, a 90 mm deep hole was drilled into the centre of the shaft's top end. This hole is intended to allow water to flow out of the shaft through a coupling into the stationary hose and has a diameter of 12 mm. Another hole on the mantle surface just above the upper ring will later be used for the transition from the rotating hose to the shaft. This hole has a diameter of 11 mm and a depth of about 8 mm. This connects the two holes and creates a continuous transition from the rotating hose to the stationary hose. Following that, a 3/4" external thread was cut onto the drilled end of the shaft, onto which the coupling was later screwed. The thread is not shown in the model.

Figure 16: 3D CAD model of the hose holder (Own CAD model)

Twelve flat steel bars with dimensions 300 × 25 × 5 mm were cut to size and then drilled through three times each. The flat steel bars were then welded onto the shaft in two rings, with an angle of 30° between every two flat steel bars. At the lower end of the shaft shown in Figure 16, a distance of 80 mm was selected, and at the upper end, a distance of 120 mm was selected. These distances were designed to leave just enough space for the bearings and all further attachments, thus providing the maximum width for hose coils in between the two rings. The holes in the flat steel will later accommodate M10 threaded rods onto which the rotating hose will then be wound. To ensure sufficient space for a coating to prevent rust, a hole diameter of 11 mm was selected. The holes were designed so that their centres are spaced 180 mm, 230 mm and 280 mm measured from the shaft's centre. The distances between the outer edges of opposite threaded rods are therefore approximately 370 mm, 470 mm and 570 mm.

To drive the test setup, a bicycle sprocket was attached below the lower ring shown in Figure 16. Since it was not possible to weld the sprocket directly to the shaft, six steel nuts were used. First, one nut was welded to each flat steel bar. The sprocket was then welded to the nuts. The resulting distance between the flat steel bars and the sprocket was therefore determined by the thickness of the steel nuts and measures 10 mm. To ensure an airtight transition from the rotating hose to the shaft, a reducing sleeve with two internal threads was welded onto the hole on the shaft's outer surface. The 1/2" to 3/8" sleeve was attached to the shaft with the 3/8" side so that the 1/2" internal thread was available for attaching the rotating hose with a Geka[1] coupling.

A transition piece was needed to connect the rotating shaft to the stationary hose. Figure 17 shows the individual parts of the transition (left) and the transition in its final form (right). This was achieved using an ABA Beul[2] 3/4" water plug-in coupling. This can be screwed onto the thread turned onto the shaft. The included sealing ring on the internal thread of the coupling automatically seals the screw connection. A hose plug can be attached to the other side of the coupling, which also seals without any further modification. The plug can rotate freely in the coupling. Theoretically, it would have been possible to attach the stationary 3/4" hose directly to the plug with a hose clamp. However, this would not have been an option for the 1/2" hose, which was also to be tested later, as the plug is not designed for this size. In addition, space for the stationary hose in the IBC container was very limited and without modification of the setup it might have become kinked. Therefore, the plug was first shortened using an angle grinder and then welded to a 90° pipe elbow. This pipe elbow has a 1/2" external thread onto which Geka couplings of various sizes can be screwed. In the planned application, the Geka coupling will rotate together with the shaft around the custom-made plug to which the stationary hose is attached.

---

[1] Name of coupling type
[2] Brand name of the manufacturer

Figure 17: Transition from the shaft to the stationary hose as individual parts (left) and assembled (right) (Own photograph)

After completing the work described, the hose holder had to be protected against rust. Due to the parts used, especially the sprocket, the holder could not be hot dip galvanised. There would have been the risk of individual parts deforming due to the heat during the process. The hose holder was therefore powder-coated by an external company, with the thread on the shaft, the reduction sleeve and the sprocket being masked off beforehand. The colour grey was chosen because it was much quicker to process than other colours. In order to keep track of the rotational speed of the hose holder and therefore the pump in later tests, one flat steel on each of the rings was marked with a red colour. Figure 18 shows the hose holder in this form. The Geka couplings and transitions for the hose connections are already attached to the holder in the picture.

Figure 18: Hose holder after coating and colouring (Own photograph)

The shaft of the hose holder had to be reworked before assembling the holder and the mounting. Due to the coating and the resulting slight increase in diameter, the shaft no longer fit into the bearings. The coating was therefore removed from the ends of the shaft using an electric file. Afterwards, the shaft could be secured using the safety screws contained in the bearings. Figure 19 shows the mounting and hose holder assembled and turned upside down. The threaded rods have already been inserted here and secured with nuts on the outside of the rings. During a test that was supposed to confirm whether the shaft was properly installed in the bearings, a grinding noise was heard. A quick check revealed that the Geka coupling at the transition from the rotating hose to the shaft was grinding on the mounting. The space for the coupling had been designed slightly too small. As a quick fix, the couplings were filed down at their widest points on the outside using an electric file. This removed a few millimetres of material and allowed the hose holder to rotate freely in the mounting.
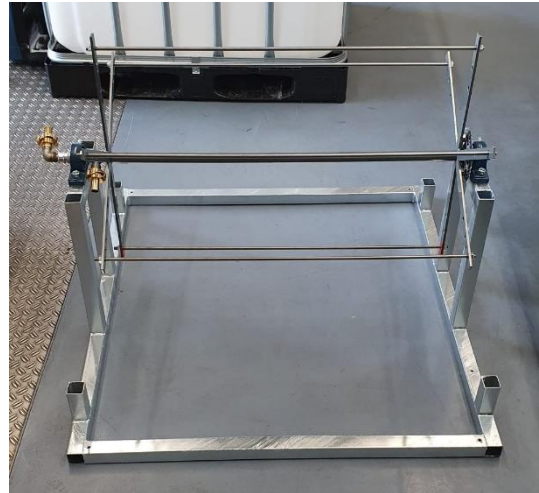
Figure 19: Assembled test apparatus without the drive gear upside down (Own photograph)

In the next step, the drive gear shown in Figure 20 had to be completed. The sprocket was already attached to the shaft as described above. An old bicycle was dismantled to provide the counterpart for the mounting. The crank was separated from the frame using a cut-off grinder so that it could still be attached to the mounting with a screw. Since the two larger sprockets were already heavily worn, it was decided to use the smallest sprocket for the drive. This also has the advantage of reducing the transmission ratio from the drive to the shaft, allowing low rotational speeds to be controlled more accurately. The pedal on the side of the

Figure 20: Prepared bicycle crank for the drive (Own photograph)

sprockets was removed, as it would otherwise have collided with the hose holder during rotation. The frame of the bicycle was painted black for aesthetic reasons as well as to prevent rust.

Two new bicycle chains were then purchased and connected to each other to transfer power from the drive sprocket to the shaft. Once the chain was fitted to both sprockets, the crank was placed on the bracket such that it was as taut as possible. In this position, the points where the crank was to be attached were marked. This was done by drilling a suitable hole in the mounting and securing the crank with a screw, nut, and washers. The assembled apparatus, still without hoses and with an open drive chain, is depicted in Figure 21.
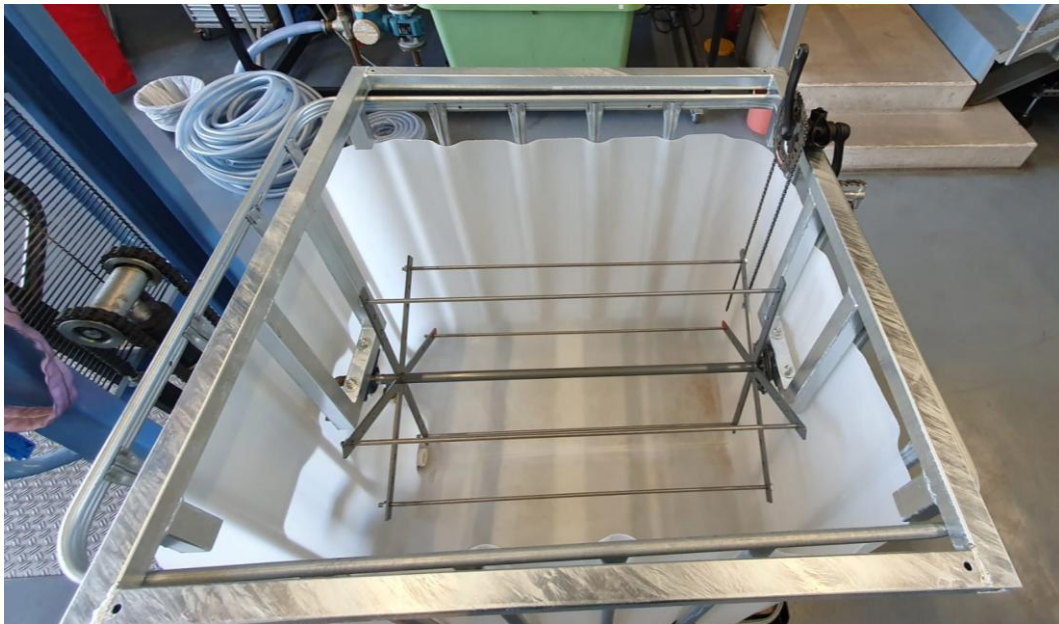
Figure 21: Assembled test apparatus in the lab (Own photograph)

3.2 Experiments on the Test Apparatus

The following sections describe the measurements performed on the test apparatus. First, the test location, the necessary preparations, and the methodology are described. This is followed by a presentation of the results sorted by measured variable, along with a discussion of qualitative observations. Finally, this chapter concludes with an analysis of the results presented.

3.2.1 Location and Preparations for the Testing

The eastern external staircase, seen in Figure 22, of the MB/UT building at OTH Amberg-Weiden, Amberg site, served as the location for the tests. This location is characterised by good access, easily measurable pump heads of 1.45 m, 4.55 m and 7.35 m, and reasonably good protection from wind. The IBC container was standing on a flat, paved surface and the shaft was supported at a height of 0.75 m above the ground. A thin rope with a knot was attached to one side of the structure. This was led diagonally upwards to a deflection roller and then vertically downwards. The other end of the rope was attached to a bucket on the ground. This allowed the bucket to be lifted vertically to a height of 7.60 m above the ground. The setup is shown in Figure 22.

A water supply was set up on site to fill the container. To achieve this, a garden hose was connected to one of the taps in a nearby Formula Student seminar room and fed outside through a window. In addition, the necessary hose lengths for various test configurations were calculated and a test sequence was created. In order to limit the tests in terms of time, it was decided at this stage to restrict the drum diameters to 0.57 m and 0.37 m. These closely approximate the inner diameters of oil drums in sizes 200 l and 60 l. If the drum diameter of 0.47 m had been included, significantly more measurements would have been required in purely numerical terms. In addition, the calculated hose lengths would have considerably increased the number of modifications between the individual configurations.

After filling the tanks for the first time, a 3/4" hose with 25 coils was wound onto the apparatus and attached to the shaft using the prepared couplings. Cable ties were used to attach the hose to the coil. The stationary 3/4" hose was attached to the outlet of the

shaft, which was then pulled to the maximum height of the stairs. In this configuration, the setup was tested for functionality without the aim of taking specific measurements. It is important to note that the filling level of the container was several centimetres above the shaft, meaning that all couplings and hose connections were completely submerged.

The first noticeable problem was the transition from the shaft to the stationary hose. Even at low pump heads and therefore low pressure in the system, air bubbles were visible at the screw connection of the ABA Beul coupling. When checking the coupling, it was noticed that damage to the rubber seal that had occurred during production was causing air to escape. Fortunately, a replacement part could be obtained quickly, and the fault rectified. Another weak point was the screw connection between the rotating hose coupling and the shaft. Air was escaping at several points where the Geka coupling connected to the reduction sleeve. This problem was solved by applying sealing tape to the thread of the coupling.

To rule out further leaks, the setup was tested several times after these modifications. No further problems were identified, and the test series could begin. For this purpose, the container was filled so that the water level at rest before the tests stood approximately 8 cm above the centre of the shaft. The reason for this procedure was to ensure that all couplings and hose connections remained constantly submerged. This made it possible to quickly identify any leaks. As a result, the submerged ratio for all tests was greater than 50 %.

Figure 22 shows the initial setup of the test apparatus next to the MB/UT building in Amberg. It should be noted that the image was taken with a fisheye lens due to lack of space and therefore appears distorted. The stationary hose is fed out of the tank to the left rear as seen from the camera, onto the floor and only then upwards. The upper edges of the railing on the three landings served as the measuring heads. The thin white rope that runs diagonally upwards on the left wheel of the tank is attached to a bucket via a deflection roller. This was later used to determine the energy efficiency.

Figure 22: Setup of the test apparatus before the measurements (Own photograph)

3.2.2 Methodology

In order to achieve comparable results in the tests, a standardised procedure was used for all initial tests. Between each measurement, regardless of whether it was of the flow rate, the maximum achievable pump head or the energy efficiency, the stationary hose was always drained as far as possible. This was done by turning the coil pump backwards until the last stable water column had retracted to the outlet of the shaft. In addition, the pumped water volume was poured back into the tank to ensure a constant submerged ratio. The procedure was as follows:

1. Attachment of the hose to the hose holder with the desired diameter and the desired number of coils.
2. Fastening of the stationary hose at 7.35 m above the shaft.
3. Checking for leaks at a rotational speed of approximately 6 rpm.
4. Draining of the stationary hose by turning the shaft backwards.
5. Only for configurations with 1/2" hose:
   a. Measurement of the maximum achievable pump head at 20 rpm.
   b. Measurement of the maximum achievable pump head at 12 rpm.
   c. Measurement of the maximum achievable pump head at 6 rpm.
6. Fastening of the stationary hose at the desired measurement pump head above the shaft.
7. Measurement of the flow rate at 20 rpm, 12 rpm and 6 rpm as soon as water first started filling the measuring cup for one minute, or until a total of approximately 5 l of water has been pumped. The rotational speed was kept as constant as possible manually. For this purpose, the pump operator was provided with a stopwatch and given a time specification per revolution. With a speed of 12 rpm, for instance, the target was 5 s per revolution. The pump heads of 7.35 m, 4.55 m and 1.45 m describe the vertical distance from the shaft to the highest point of the stationary hose.

8. Determination of the energy efficiency:

    a. Manually pumping the water at 12 rpm until just below the desired measurement pump head.

    b. Locking the coil in this position either by hand or with the help of a metal rod.

    c. Pulling up the bucket filled with water.

    d. Winding the rope around the coil and then securing it with a knot.

    e. Releasing the coil for pumping powered by the lowering bucket.

    f. Measurement of the pumped water volume and estimation of the impact velocity of the bucket.

9. Shortening the rotating hose to the next required length.

Once all measurements with the 3/4" hose had been completed, both the rotating hose on the coil and the stationary hose were replaced with 1/2" hoses. The reason for this was to ensure that subsequent practical implementation would be as simple and inexpensive as possible. If the rotating and stationary hoses are of the same diameter, only one hose needs to be procured. After the first series of tests with the 3/4" hose and a low number of coils frequently failing to achieve the desired pump heads, it was decided to reduce the number of coils three times in increments of 5 instead of 10 for the 1/2" hose.

Towards the end of the tests, the procedure had to be modified slightly. The reason for this was that, in the course of advanced observations, possible optimisations of the setup were to be tested. This concerned the run of the stationary hose: in the original configuration shown in Figure 23, it was fed out of the tank and laid down on the floor. The hose was then pulled vertically upwards only to the extent necessary to reach the required pump head. This resulted in several coils remaining on the floor next to the IBC container.

Figure 23: Original configuration of the stationary hose (Photograph: M. Salih)

Unfortunately, the remaining coils on the ground are not visible in any of the available pictures.

The first adjustment was therefore to pull the stationary hose out of the tank and raise it almost vertically so that the water was pumped upwards continuously. This setup is depicted in Figure 24. As the hose might be difficult to see due to its colour, the orange arrow was added alongside it. This image, too, was taken with a fisheye lens and therefore appears slightly distorted. With these adjustments, the maximum achievable pump heads were measured, along with flow rates and energy efficiencies for the following configurations:
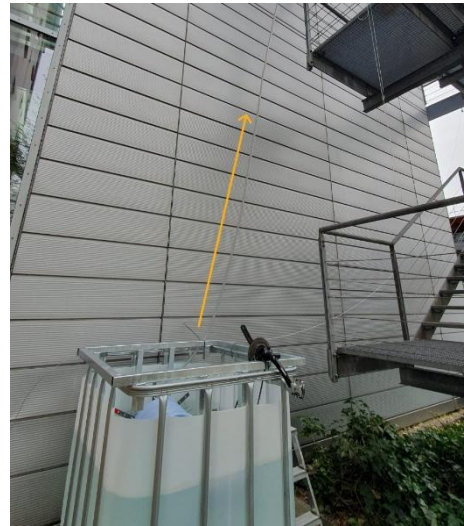
Figure 24: Vertical configuration on the stationary hose (Own photograph)

- 1/2" hose with a coil of ⌀ 37 cm and 20 coils

- 1/2" hose with a coil of ⌀ 37 cm and 15 coils

However, during practical use of the pump in a river, it is to be expected that the stationary hose will be fed out of the coil in an almost horizontal position, as the hose will float on the surface of the water. Unfortunately, due to space constraints, it was not possible to feed the hose out horizontally in the test setup. The hose was therefore fed upwards out of the top of the container and then laid horizontally over a wooden board and a flat surface for a distance of approximately 2.5 m. It was then brought upstairs in variant 1 via the staircase with an incline of approximately 35°. In variant 2, the hose was pulled vertically upwards after the horizontal section. Both variants are displayed in Figure 25. Since the 1/2" hose had already been shortened to a drum diameter of 37 cm with 15 coils at the time these variants were tested, the tests were only carried out in this configuration. For both variants, only the maximum achievable pump head was measured for rotational speeds of 20 rpm, 12 rpm and 6 rpm.

It should be noted that all measurements with adjustments to the setup were performed in addition to the measurements with the original setup. This ensures comparability both with the previous measurements and between the original and adjusted measurements.

Figure 25: Horizontal configuration of the stationary hose as variant 1 via the stairs (left) and as variant 2 straight up (right) (Own photographs)

3.2.3   Test Results

A total of 186 measurements were taken. Of these, 54 were flow rate measurements and 18 were measurements for the determination of the energy efficiency using the 3/4" hose. The 1/2" hose was used to measure the flow rate 60 times, for the determination of the energy efficiency 24 times, and the maximum achievable pump head 30 times. To keep the text concise, from this point onwards the configurations are abbreviated as follows: inner diameter of the hose used | drum diameter | number of coils. Changes to the setup of the stationary hose are, where applicable, marked with an additional section |. The results are presented and compared in the following sections, sorted by measurement variable. Tabular overviews of all results are attached to this paper as appendices.

3.2.3.1 Flow Rates

The first section displays the flow rates in the order in which the tests were performed. Each diagram represents a fixed configuration of hose diameter, drum diameter, and number of coils. The measurement results are thus displayed as a function of the pump head. The flow rates were measured at pump heads of 1.45 m, 4.55 m, and 7.35 m for each rotational speed. The graphical representation is therefore not indicative of results for pump heads between these values.

Figure 26 shows the results for the configuration 3/4" | ⌀ 57 cm | 25. The flow rate remains approximately constant at 6 rpm with 1.5 l/min at 1.45 m and 1.8 l/min at 4.55 m and 7.35 m. At 12 rpm, an increase from 3.8 l/min at a measuring head of 1.45 m to 4.2 l/min at 4.55 m was observed. At 7.35 m, however, only 2.5 l/min were pumped. It was noted that a flow rate could not be measured throughout the entire minute of measurement, as the flow stopped completely after about 30 s. At a speed of 20 rpm, flow rates of 6.4 l/min were measured at 1.45 m and 4.55 m respectively. The pump head of 7.35 m could not be reached, and the flow rate is therefore documented as 0.0 l/min.
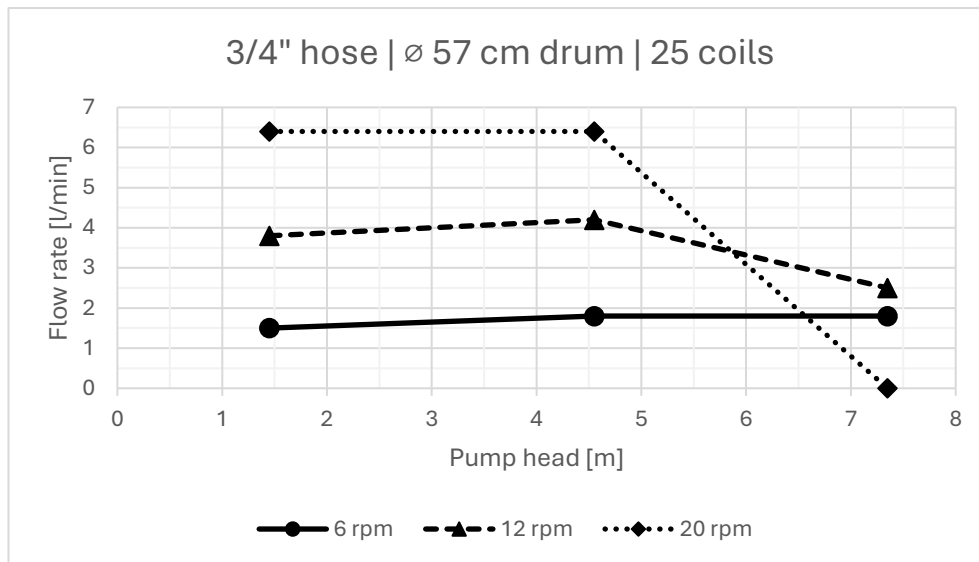
Figure 26: Flow rates for the 3/4" hose with a ⌀ 57 cm drum and 25 coils (Own diagram)

The results of the setting 3/4" | ⌀ 37 cm | 25 are illustrated in Figure 27. Driven at 6 rpm, an almost linear decrease in the flow rate from 1.2 l/min at a head of 1.45 m to 0.5 l/min at 4.55 m and 0.0 l/min at 7.35 m was observed. The last head could not be reached at all, while a very irregular flow was observed at the middle head. With the increased speeds of 12 rpm and 20 rpm, flow rates could only be measured at 1.45 m. These amounted to 1.9 l/min at 12 rpm and 3.5 l/min at 20 rpm. For heads of 4.55 m and 7.35 m, 0.0 l/min was logged in each case.
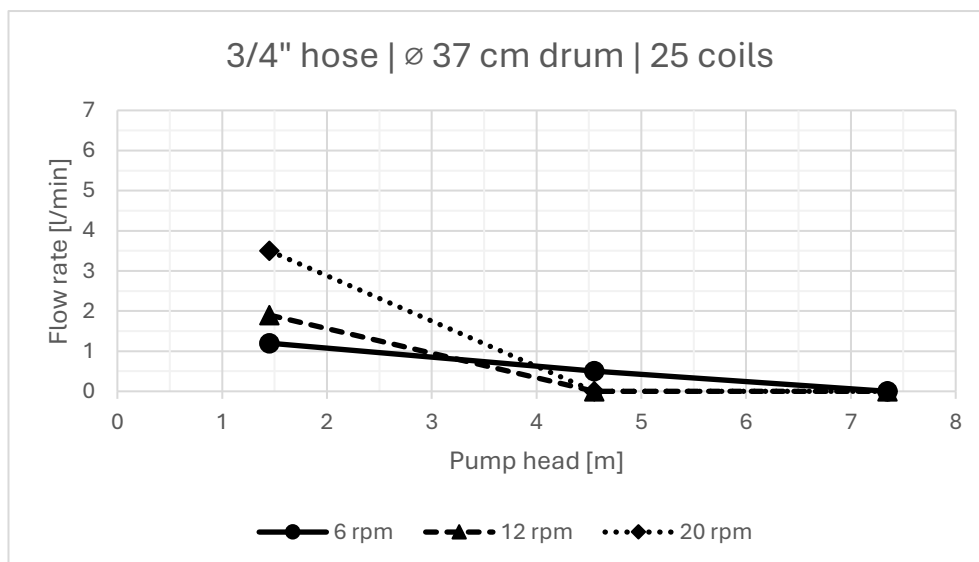
Figure 27: Flow rates for the 3/4" hose with a ⌀ 37 cm drum and 25 coils (Own diagram)

The results for the setup 3/4" | ⌀ 57 cm | 15 are shown in Figure 28. Whilst the values for 6 rpm at the lower two pump heads are similar with 1.7 l/min at 1.45 m and 1.5 l/min at

4.55 m the highest measurable head of 7.35 m could not be reached. For both 12 rpm and 20 rpm water was only pumped at 1.45 m. With the rotational speed of 12 rpm 4.0 l/min were pumped, for 20 rpm 4.5 l/min. At 4.55 m and 7.35 m 0.0 l/min were documented.
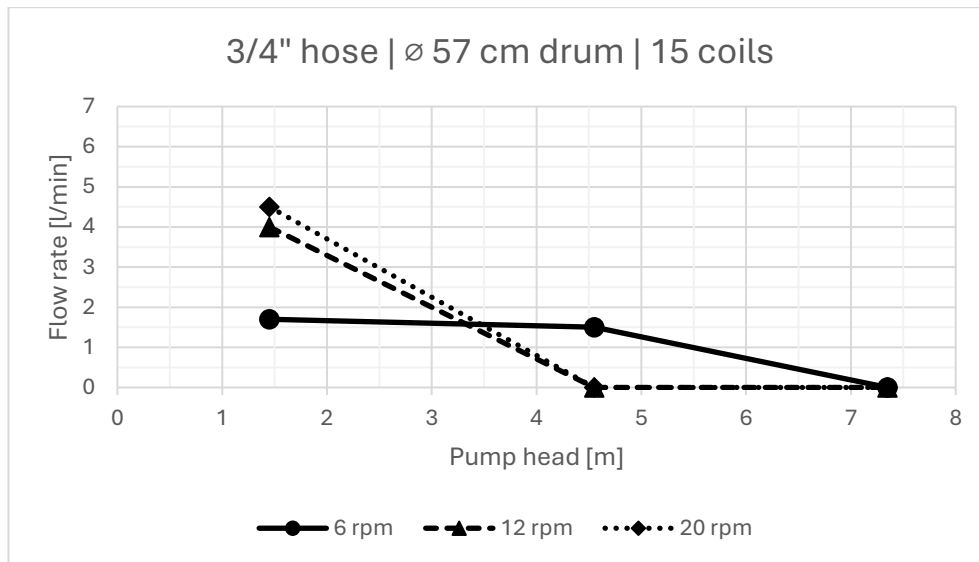
Figure 28: Flow rates for the 3/4" hose with a ∅ 57 cm drum and 15 coils (Own diagram)

The results of the setting 3/4" | ∅ 37 cm | 15 are illustrated in Figure 29. The pump heads 4.55 m and 7.35 m were not reached for any of the given rotational speeds. Therefore, only the values for 1.45 m are given as above 0.0 l/min here. The measured flow rates amount to 1.1 l/min at 6 rpm, to 1.8 l/min at 12 rpm and to 3.8 l/min at a rotational speed of 20 rpm.
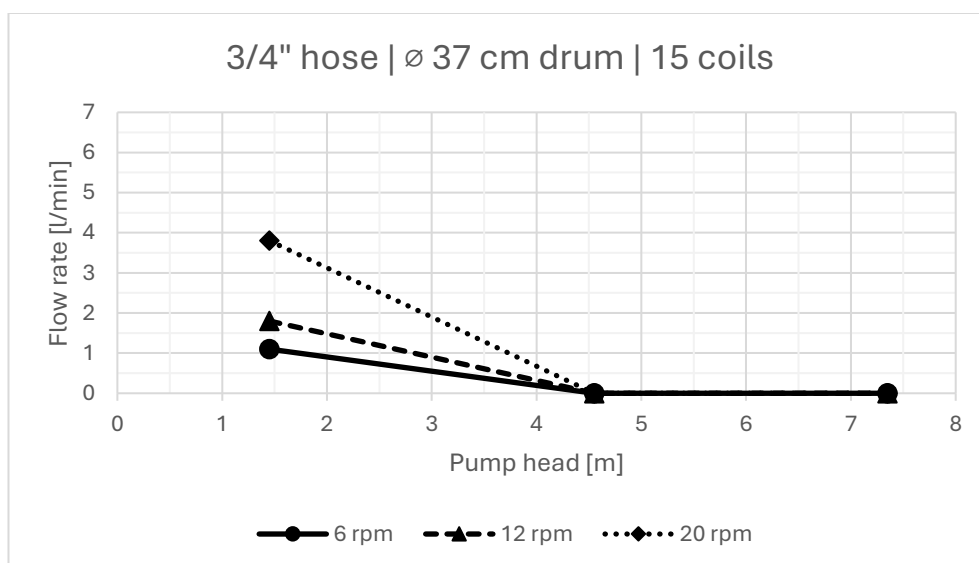
Figure 29: Flow rates for the 3/4" hose with a ∅ 37 cm drum and 15 coils (Own diagram)

Figure 30 shows the results for the configuration 3/4" | ⌀ 57 cm | 10. Regardless of the rotational speed the pump heads 4.55 m and 7.35 m again could not be reached. At the head of 1.45 m flow rates of 1.5 l/min were measured at 6 rpm, 3.6 l/min at 12 rpm, and 5.5 l/min at 20 rpm.
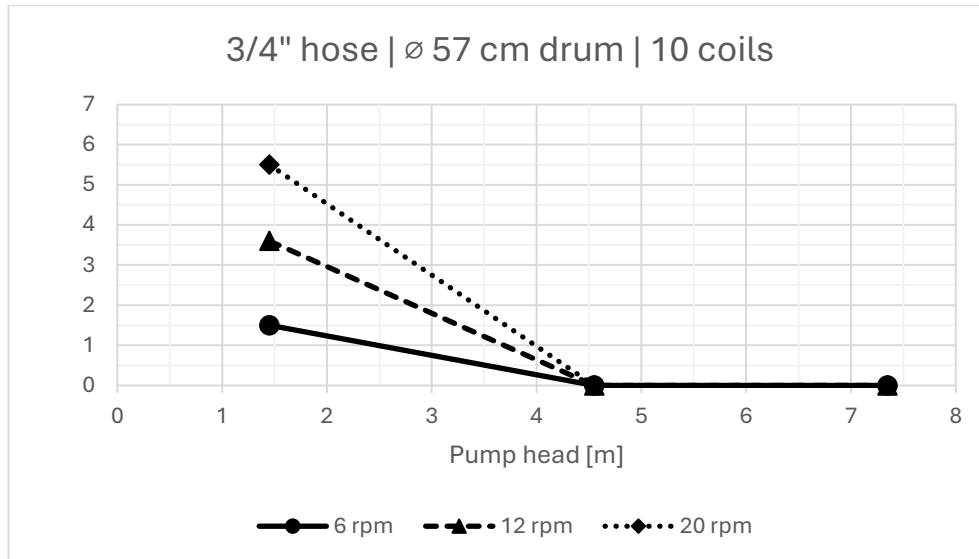
Figure 30: Flow rates for the 3/4" hose with a ⌀ 57 cm drum and 10 coils (Own diagram)

During the test with the setting 3/4" | ⌀ 37 cm | 10 none of the given pump heads were reached at all. Therefore, all values are given as 0.0 l/min for all rotational speeds in Figure 31.
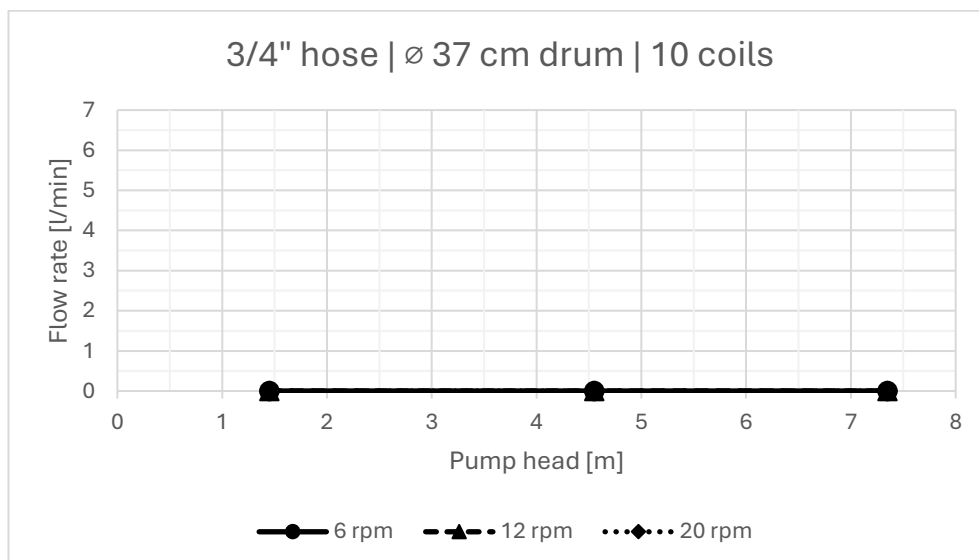
Figure 31: Flow rates for the 3/4" hose with a ⌀ 37 cm drum and 10 coils (Own diagram)

The setup was then modified and equipped with 1/2" hoses. The first configuration tested was 1/2" | ⌀ 57 cm | 25. As can be seen in Figure 32, the flow rates at 6 rpm are almost identical with 1.0 l/min at a head of 1.45 m and 1.1 l/min at 4.55 m. The values at these heads are higher at 12 rpm, reaching 1.9 l/min at 1.45 m and 1.7 l/min at 4.55 m. At 20 rpm, 3.1 l/min were pumped at a head of 1.45 m. No flow could be measured at a head of 4.55 m. At 7.35 m no water was pumped for any of the applied rotational speeds.
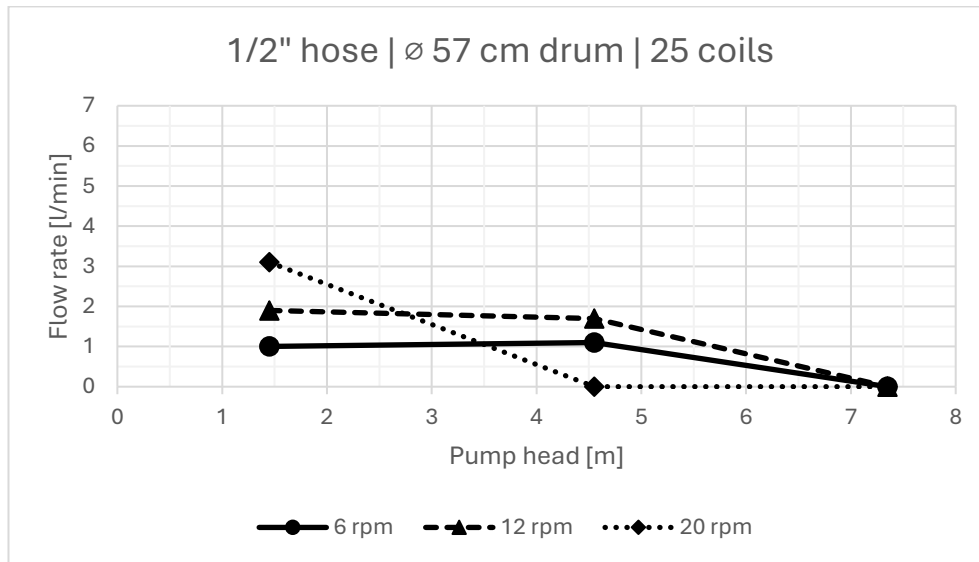
Figure 32: Flow rates for the 1/2" hose with a ⌀ 57 cm drum and 25 coils (Own diagram)

Figure 33 displays the results for the configuration 1/2" | ⌀ 57 cm | 20. At 6 rpm, 1.1 l/min could be pumped to 1.45 m and 1.0 l/min to 4.55 m. As the rotational speed was increased to 12 rpm, the flow rate at these heads also increased to 1.9 l/min at 1.45 m and 1.7 l/min at 4.55 m. No flow was measured at 7.35 m for either rotational speed. At a rotational speed of 20 rpm, a flow rate of 3.1 l/min could be measured at 1.45 m. The pump heads of 4.55 m and 7.35 m could not be achieved in this configuration and the flow rate is therefore documented as 0.0 l/min.
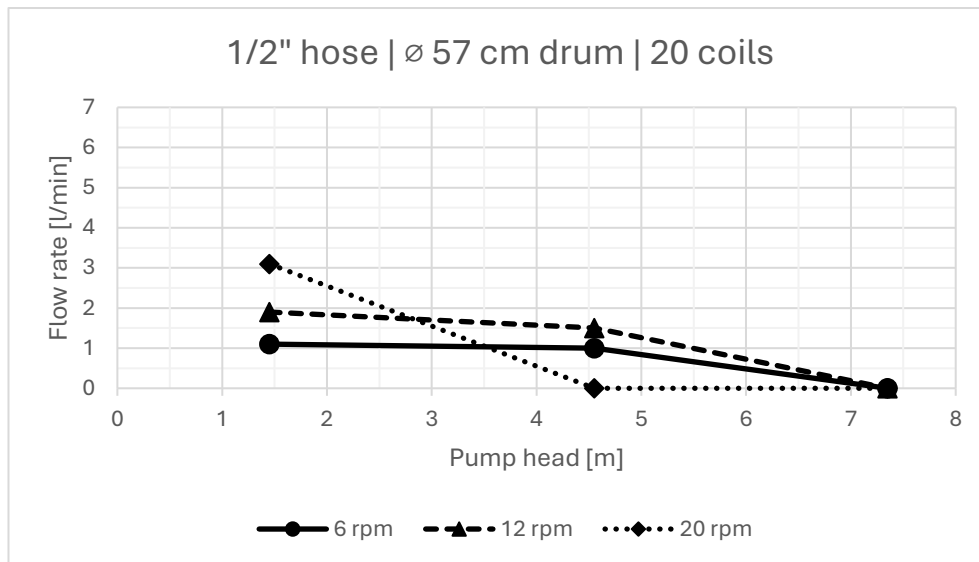
Figure 33: Flow rates for the 1/2" hose with a ⌀ 57 cm drum and 20 coils (Own diagram)

The results of the setting 1/2" | ⌀ 37 cm | 25 are illustrated in Figure 34. At 6 rpm flow rates of 0.7 l/min were measured at 1.45 m and 0.5 l/min at 4.55 m. Rotating at 12 rpm in this configuration 0.9 l/min were pumped to a head of 1.45 m and 0.0 l/min to 4.55 m. At 20 rpm the flow rate amounted to 1.5 l/min at 1.45 m and again to 0.0 l/min at 4.55 m. The head 7.35 m was not reached regardless of the rotational speed.
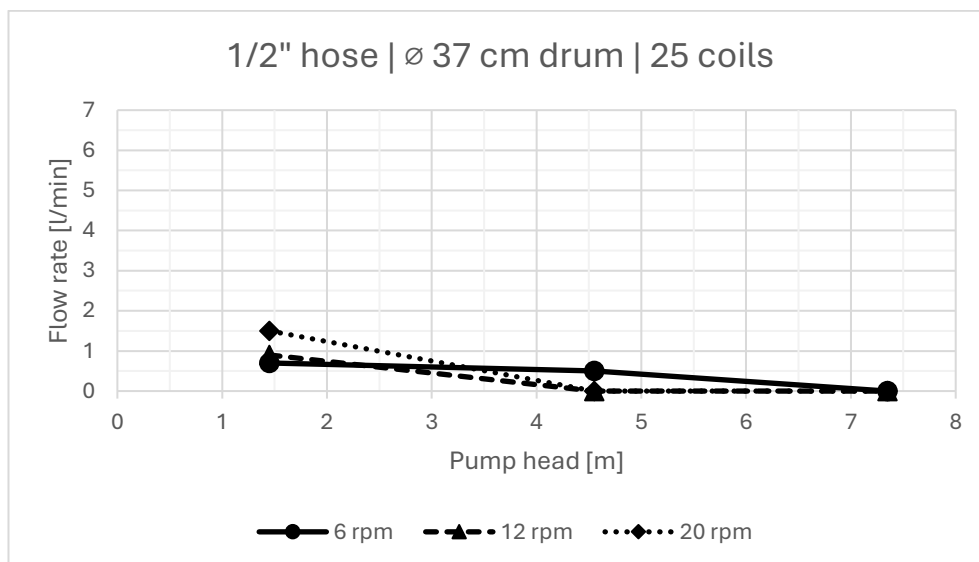
Figure 34: Flow rates for the 1/2" hose with a ⌀ 37 cm drum and 25 coils (Own diagram)

Figure 35 depicts the results for the configuration 1/2" | ⌀ 57 cm | 15. The flow rates were measured as 1.1 l/min for 6 rpm, 1.8 l/min for 12 rpm and 2.3 l/min for 20 rpm all at a pump head of 1.45 m. As the heads 4.55 m and 7.35 m were not reached, the results are documented as 0.0 l/min for all tests.
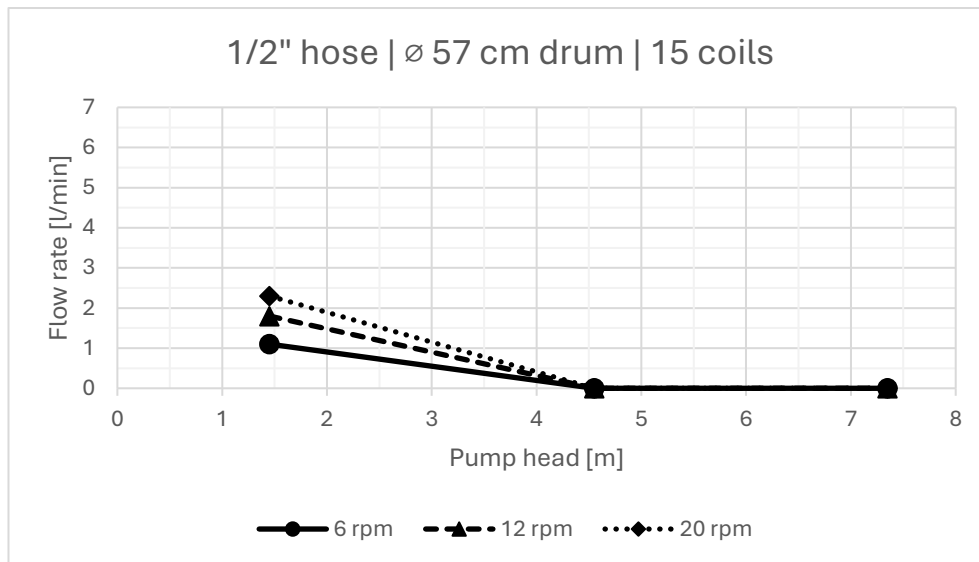
Figure 35: Flow rates for the 1/2" hose with a ⌀ 57 cm drum and 15 coils (Own diagram)

Testing the setup 1/2" | ⌀ 37 cm | 20 again only at a head of 1.45 m water was pumped. As displayed in Figure 36 the flow rates amount to 0.8 l/min at 6 rpm, 1.2 l/min at 12 rpm and 1.3 l/min at 20 rpm. All other values are documented as 0.0 l/min.
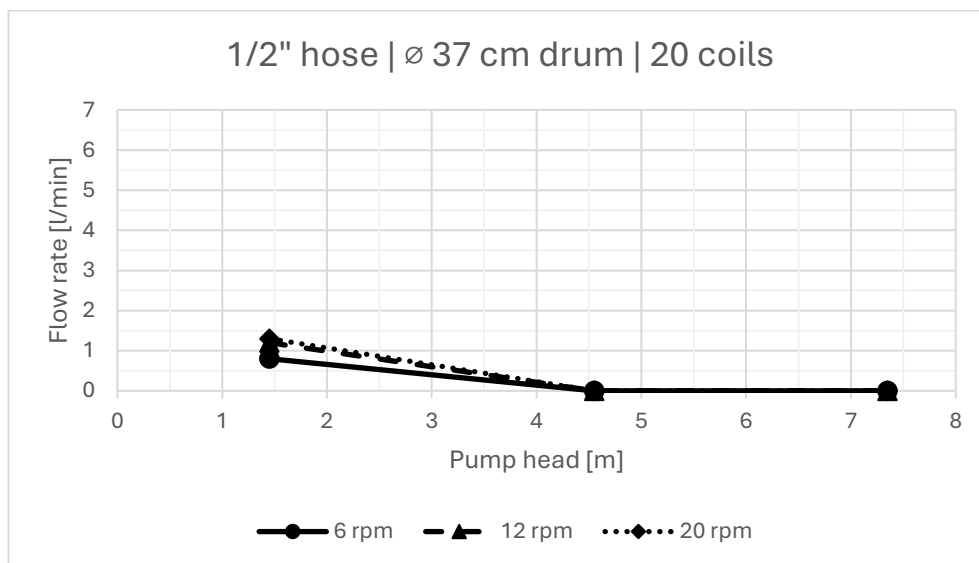
Figure 36: Flow rates for the 1/2" hose with a ⌀ 37 cm drum and 20 coils (Own diagram)

After modifying this configuration with an almost vertical stationary hose to the setup 1/2" | ⌀ 37 cm | 20 | 'vertical', displayed in Figure 37, the measurements at a head of 1.45 m were repeated. The flow rates here came out as 0.8 l/min for 6 rpm, 1.1 l/min for 12 rpm and 1.4 l/min for 20 rpm. Since the individual values would hardly be discernible in the previous format of display, the chart type has been changed here.
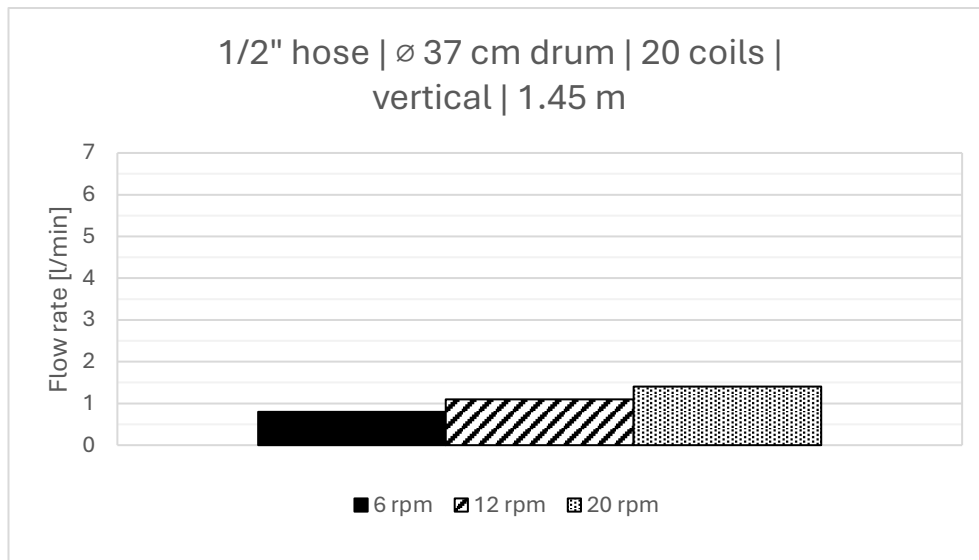
Figure 37: Flow rates for the 1/2" hose with a ⌀ 37 cm drum and 20 coils with a vertical stationary hose at 1.45 m (Own diagram)

The last tested configuration was given as 1/2" | ⌀ 37 cm | 15. The achieved flow rates at 1.45 m are shown in Figure 38. With a rotational speed of 6 rpm 0.5 l/min were pumped, with 12 rpm 1.1 l/min and with 20 rpm 1.8 l/min. The pump heads 4.55 m and 7.35 m again were not reached, and the flow rates therefore noted as 0.0 l/min.
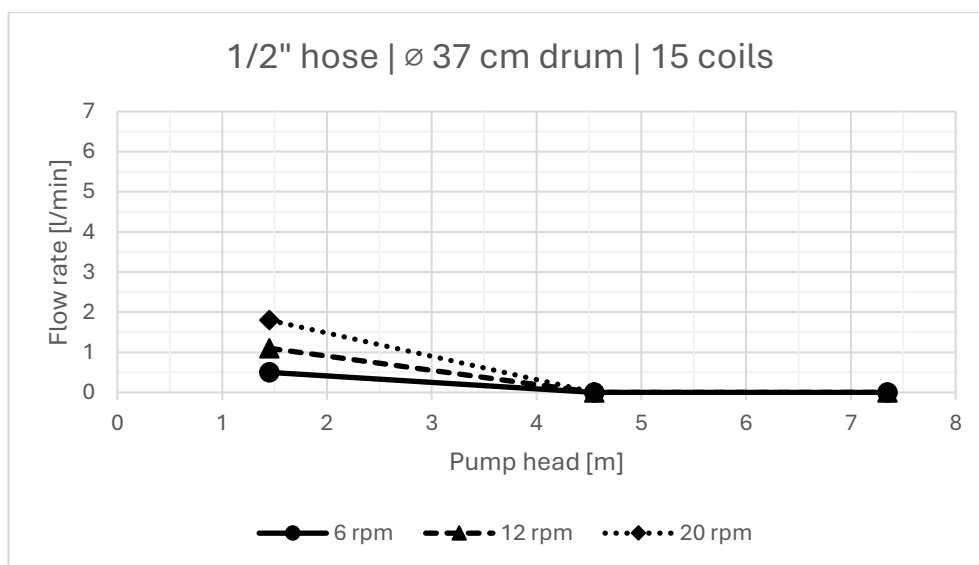
Figure 38: Flow rates for the 1/2" hose with a ⌀ 37 cm drum and 15 coils (Own diagram)

Once again, the measurements were repeated with the adjustment on the stationary hose to 1/2" | ⌀ 37 cm | 15 | 'vertical' for a head of 1.45 m. The flow rates, displayed in Figure 39, were now measured as 0.6 l/min for 6 rpm, 1.0 l/min for 12 rpm and 1.7 l/min for 20 rpm. Again, the chart type has been altered for better visualization.
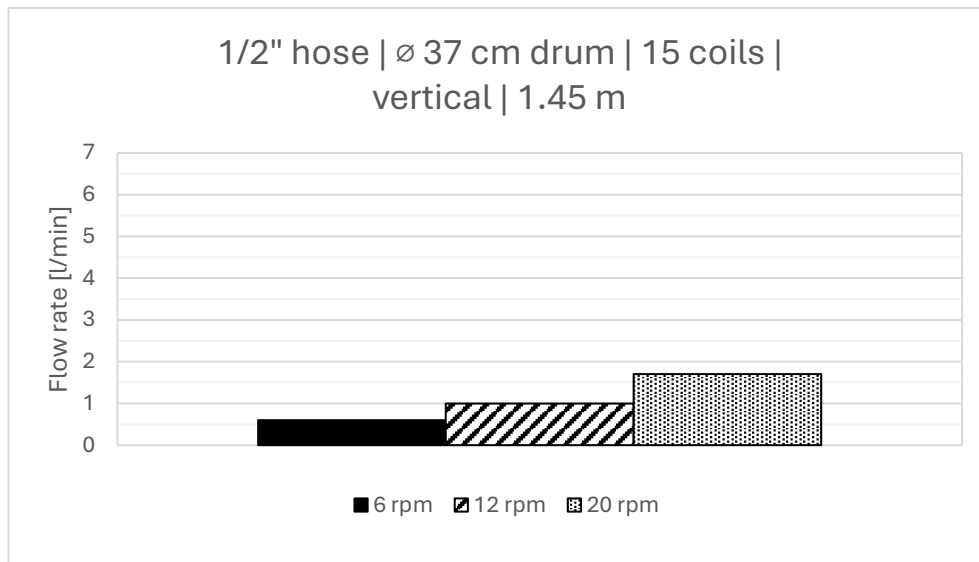
Figure 39: Flow rates for the 1/2" hose with a ⌀ 37 cm drum and 15 coils with a vertical stationary hose at 1.45 m (Own diagram)

3.2.3.2 Maximum Pump Heads

This section presents the results of measurements of the maximum pump heads that were achieved. These measurements were only carried out for the 1/2" hose. It should be noted that the measurements were taken on the delivery hose just before the occurrence of spilling, and no water was actually delivered to these heads. The first three diagrams of this part depict the heads for a fixed drum diameter as a function of the number of coils and the rotational speed. The fourth diagram deviates from this representation, as the results would no longer be readable. It displays the maximum achievable pump heads for a fixed combination of drum diameter and number of coils. The values here depend on the rotational speed and the configuration of the stationary hose.

It should be noted that the values shown below actually represent the maximum achievable pump heads. These heads were generally not stable over longer periods of time, as the water-air columns collapsed immediately after these heads were reached. In some cases, the maximum heads could not be reached again after the first collapse when pumping continued. Only after a pause, during which the stationary hose was emptied, the heads could be replicated.

Figure 40 displays the maximum achievable pump heads for the configuration 1/2" | ⌀ 57 cm. Using a rotational speed of 6 rpm maximum heads of 4.50 m were reached with 15 coils, 6.05 m with 20 coils and 7.30 m with 25 coils. At 12 rpm the maximum head

with 15 coils came out at 4.00 m, with 20 coils at 5.85 m and with 25 coils at 6.05 m. With the highest tested rotational speed of 20 rpm maximum heads of 3.15 m were measured whilst using 15 coils, 3.65 m whilst using 20 coils and 4.60 m whilst using 25 coils.
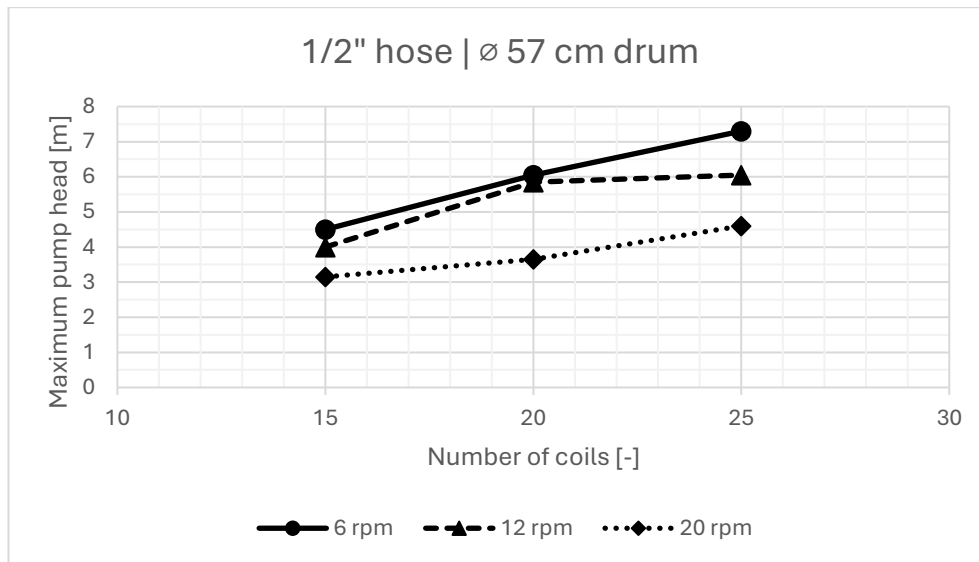
Figure 40: Maximum pump heads for the 1/2" hose with a ∅ 57 cm drum (Own diagram)

The results for the setup 1/2" | ∅ 37 cm are shown in Figure 41. Spinning at 6 rpm the coil pump produced maximum heads of 2.40 m with 15 coils, 3.55 m with 20 coils and 4.70 m with 25 coils. At 12 rpm the measured heads are 2.15 m with 15 coils, 3.45 m with 20 coils and 4.55 m with 25 coils. At 20 rpm, 1.95 m was reached as a maximum whilst rotating the drum with 15 coils, 3.15 m with 20 coils and 3.20 m with 25 coils.
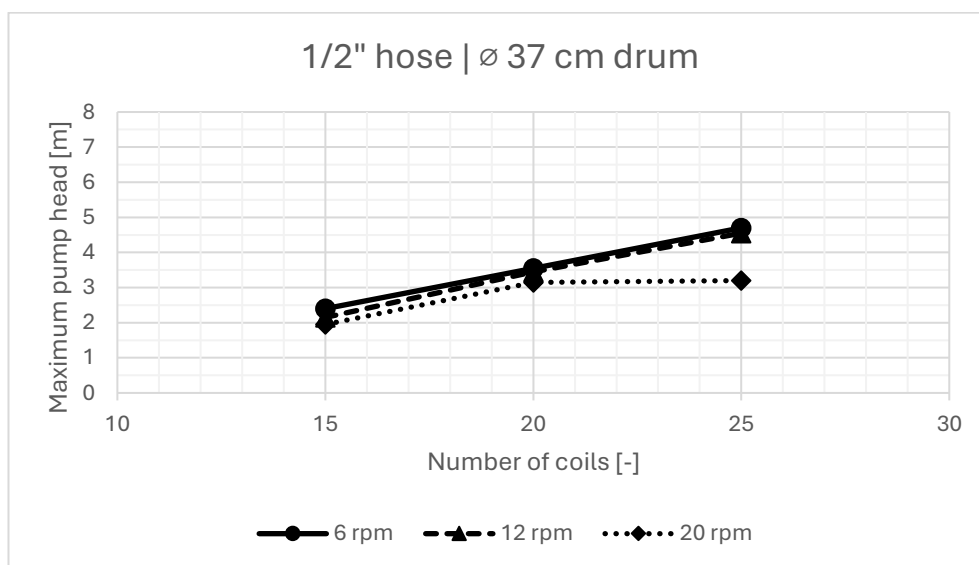
Figure 41: Maximum pump heads for the 1/2" hose with a ∅ 37 cm drum (Own diagram)

As the setup of the stationary hose was believed to be an influencing factor in the performance of the test apparatus it was also modified for some of the measurements of the maximum achievable pump head. Figure 42 displays the setup with an almost completely vertical stationary hose and therefore the configuration 1/2" | ∅ 37 cm | 'vertical'. The new measurements for 6 rpm came out at 5.20 m with 15 coils and 6.60 m with 20 coils. For 12 rpm 4.85 m were measured using 15 coils and 5.15 m using 20 coils. At a rotational speed of 20 rpm the maximum heads were 4.00 m with 15 coils and 3.95 m with 20 coils.
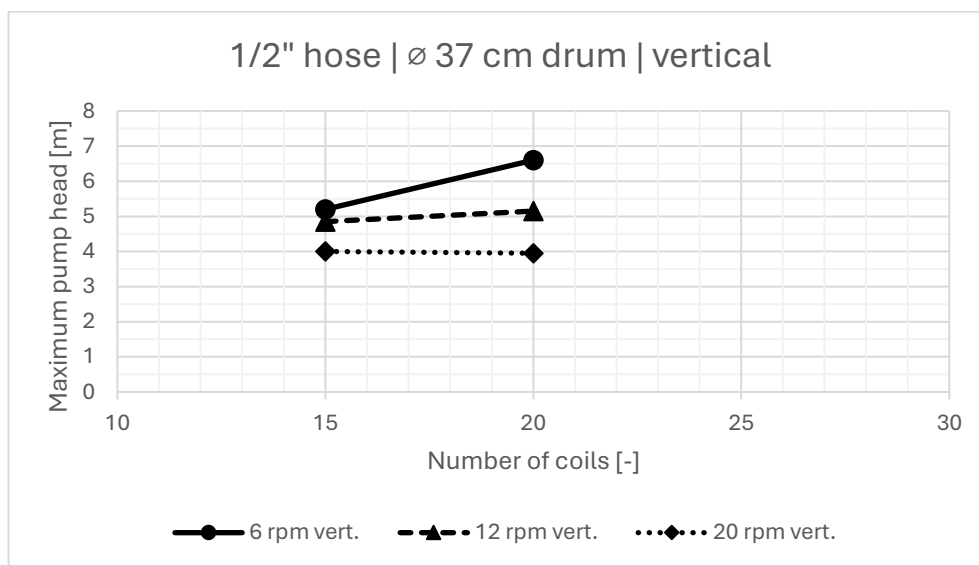
Figure 42: Maximum pump heads for the 1/2" hose with a ∅ 37 cm drum with a vertical stationary hose (Own diagram)

An overview over all measurements with a modified stationary hose in the configuration 1/2" | ∅ 37 cm | 15 is given in Figure 43. As the illustration in the format of the previous diagrams did not seem suitable for these results, again a bar chart was chosen for the presentation of the maximum pump heads. The values for the vertical modification, indicated with 'vert.', are the same as in the previous diagram for 15 coils. When the hose was led horizontally out of the tank as described above and then pulled up via the stairs, indicated as 'hor. 1', 3.85 m were reached at 6 rpm, 3.75 m at 12 rpm and 3.10 m at 20 rpm. When the hose was pulled up vertically after the same horizontal distance, indicated as 'hor. 2', the maximum achievable pump heads were measured at 3.90 m at 6 rpm, 3.65 m at 12 rpm and 3.45 m at 20 rpm.
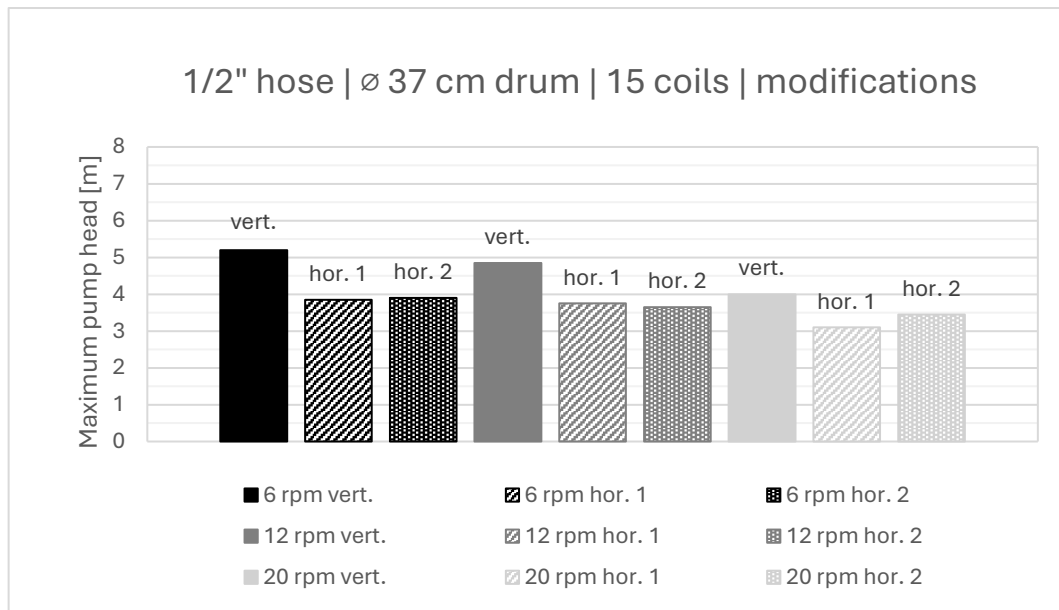
Figure 43: Maximum pump heads for the 1/2" hose with a ⌀ 37 cm coil and 15 coils with modified stationary hoses (Own diagram)

3.2.3.3 Energy Efficiencies

For determining the energy efficiency of the system, a bucket was filled with water, sealed with a lid and its total weight then measured. The lid was required to prevent water from spilling out and thus to ensure that the total weight of the bucket remained constant. The bucket was then connected to the pump by means of a rope and a deflection roller. Since the impact velocity of the bucket on the ground was not yet clear at the start of the tests, the area directly beneath the bucket was covered with cardboard. This was intended to cushion the impact and prevent damage to the bucket. Figure 44 shows the setup as seen from the pump. The orange circle over the bucket was added and highlights the position of the
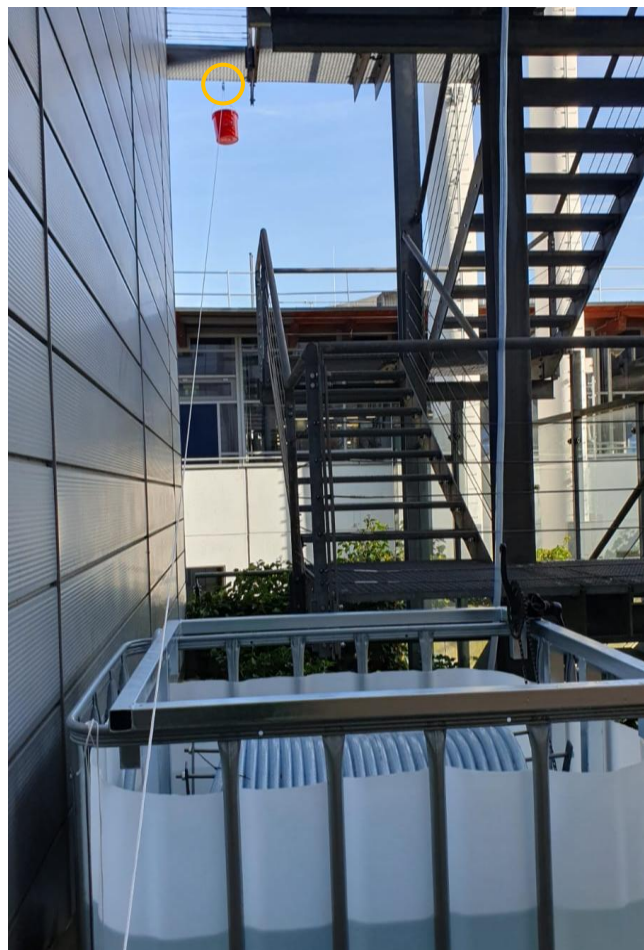
Figure 44: Setup for the energy efficiency measurements (Own photograph)

43

deflection roller. By winding the rope around the coil and then releasing it, the bucket can drive the pump. As the bucket drops below the hedges seen in the background of the picture, the impact area is not visible from this perspective.

For the calculation of the energy efficiency, it is necessary to determine the energy input and the energy output, as well as the losses that occurred. In this setup, the bucket drives the system with its potential (pot) energy. The energy input is therefore the potential energy of the bucket which can be calculated with Equation 5. In all further calculations the value for the gravitational acceleration is taken to be 9.81 m/s².

Equation 5: Potential energy of the bucket (Own calculation)

$$E_{pot,bucket} = m_{bucket} * g * \Delta h_{bucket}$$

With:

g	*gravitational acceleration*	$\left[\frac{m}{s^2}\right]$

As the goal of the pump is to deliver water to a desired head, the potential energy of the pumped water volume is the energy output. The calculation given here goes accordingly to the one of the potential energy of the bucket and is given in Equation 6. As the pumped water is measured as a volume, it is required to transfer this value into a mass by multiplying it with the density of water. For all calculations a density of 1,000 kg/m³ was assumed.

Equation 6: Potential energy of the pumped water volume (Own calculation)

$$E_{pot,H_2O} = V_{H_2O} * \rho_{H_2O} * g * H_{H_2O} = m_{H_2O} * g * H_{H_2O}$$

With:

V	*volume*	$[m^3]$
H	*pump head*	$[m]$

The losses were determined as the kinetic energy of the bucket upon impact with the ground based on its impact velocity. The calculation is shown in Equation 7. Friction losses between the air and the bucket and at the deflection roller were not considered.

Equation 7: Kinetic energy of the bucket at impact (Own calculation)

$$E_{kin,bucket} = \frac{1}{2} * m_{bucket} * v_{bucket}^2$$

Having obtained these values, the total energy efficiency of the pump can be calculated as displayed in Equation 8 as the quotient of energy output and the difference of energy input and losses. To receive a value in percent, the result must then be multiplied by 100 %.

$$\eta_{energy} = \frac{E_{output}}{E_{input} - E_{losses}} * 100\ \% = \frac{E_{pot,H_2O}}{E_{pot,bucket} - E_{kin,bucket}} * 100\ \%$$

The results of these calculations, based on the respective measured values, are shown in the following diagrams. The actual measured values for the variables used in the formulas are provided in the appendix. Each of the diagrams represents one fixed combination of hose diameter and drum diameter and the results are therefore displayed as functions of the pump head and the number of coils on the coil. The last diagram displays the results for the modified stationary hose.

Figure 45 illustrates the efficiencies for the setup 3/4" | ⌀ 57 cm. At a head of 1.45 m the efficiency with 10 coils was calculated as 10.9 % and with 15 coils as 8.3 %. No water was pumped for this number of coils at the heads 4.55 m and 7.35 m. The efficiencies are therefore documented as 0.0 %. With 25 coils an efficiency of 7.2 % was reached at 1.45 m, 31.3 % at 4.55 m and 64.5 % at 7.35 m. Referring to the flow rate measurements, this efficient configuration 3/4" | ⌀ 57 cm | 25 yielded 1.8 l/min at 6 rpm and 2.5 l/min at 12 rpm to a head of 7.35 m. At 20 rpm the pump did not deliver any water to this head.
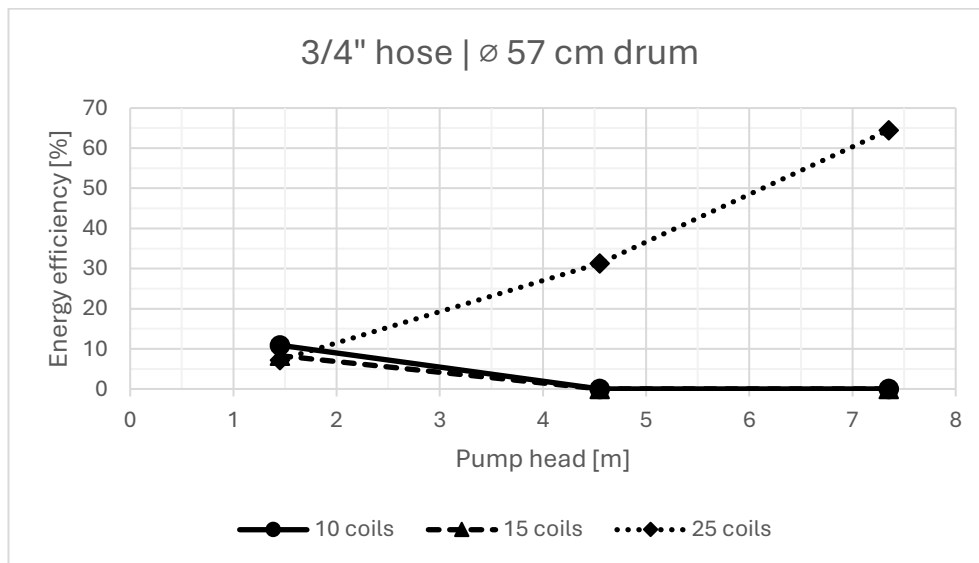
Figure 45: Energy efficiencies for the 3/4" hose with a ⌀ 57 cm drum (Own diagram)

The results for the configuration 3/4" | ∅ 37 cm are displayed in Figure 46. At 1.45 m no water was pumped with 10 coils. With 15 coils the efficiency was determined as 3.9 % and as 8.3 % with 25 coils. The heads 4.55 m and 7.35 m were not reached with this configuration.
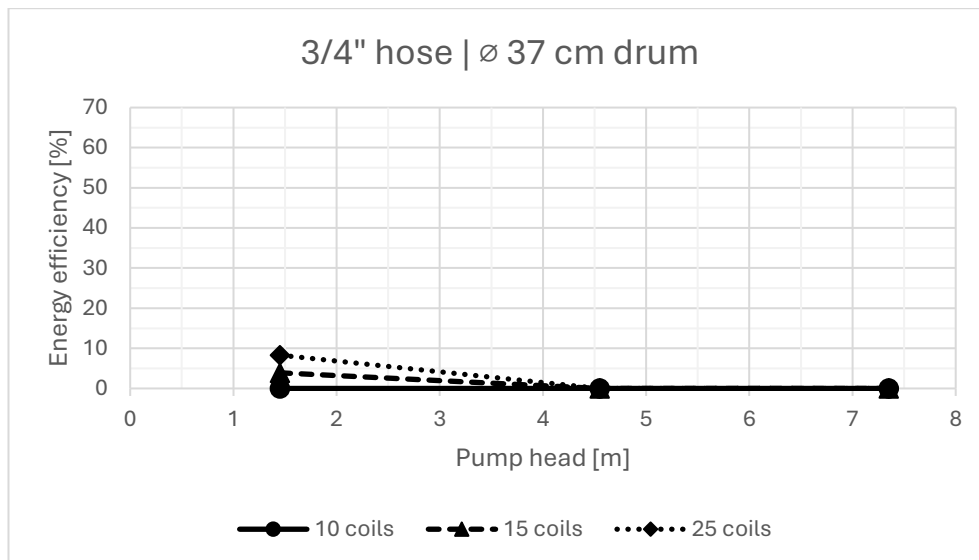
Figure 46: Energy efficiencies for the 3/4" hose with a ∅ 37 cm drum (Own diagram)

Figure 47 depicts the efficiencies for the combination 1/2" | ∅ 57 cm. With 15 coils the only efficiency above 0.0 % was measured at the head 1.45 m and calculated as 5.5 %. With 20 coils efficiencies of 6.2 % was determined at 1.45 m, 24.4 % at 4.55 m and 0.0 % at 7.35 m. In the configuration with 25 coils the results were 6.2 % at 1.45 m, 24.3 % at 4.55 m and again 0.0 % at 7.35 m.
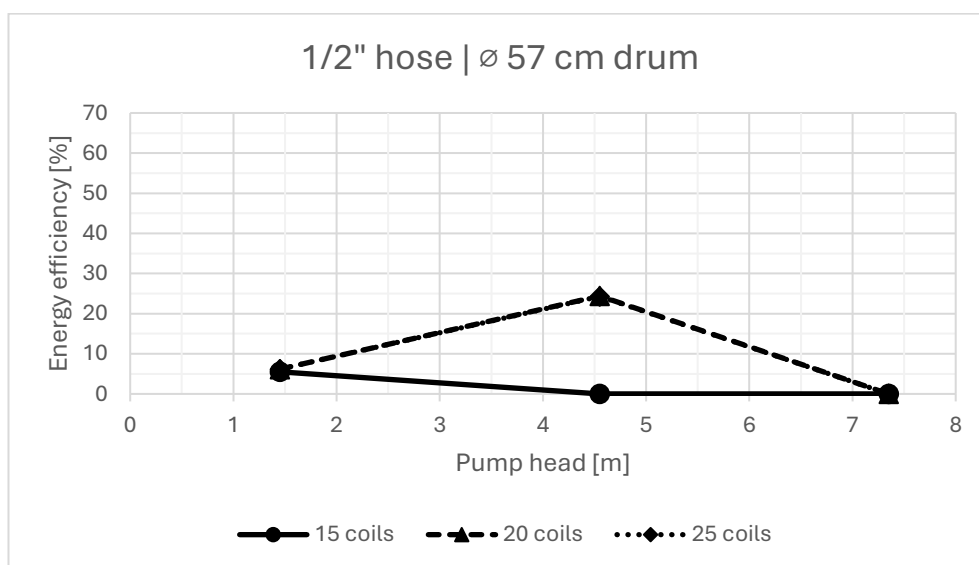
Figure 47: Energy efficiencies for the 1/2" hose with a ∅ 57 cm drum (Own diagram)

The calculated results for the setup 1/2" | ⌀ 37 cm are shown in Figure 48. Only at a head of 1.45 m water was delivered into the measuring cup. This resulted in efficiencies of 0.8 % with 15 coils, 4.7 % with 20 coils and 6.2 % with 25 coils. All other values were noted as 0.0 %.
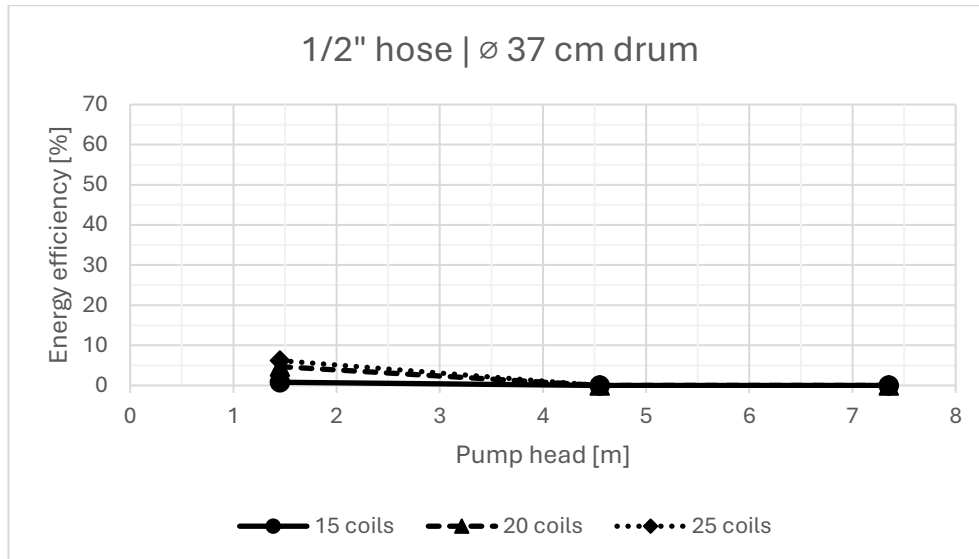
Figure 48: Energy efficiencies for the 1/2" hose with a ⌀ 37 cm drum (Own diagram)

As the hose had been shortened before implementing the adjustments for the first time, the configuration 1/2" | ⌀ 37 cm | 'vertical', displayed in Figure 49, only includes results for 15 and 20 coils. Both measurements were successful only at 1.45 m, with efficiencies of 0.8 % with 15 coils and 5.5 % with 20 coils.
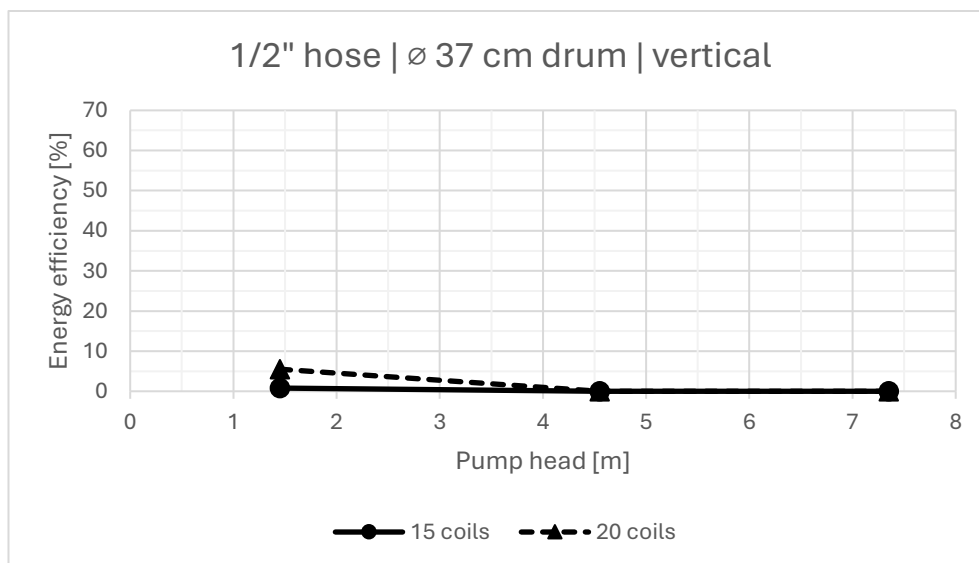
Figure 49: Energy efficiencies for the 1/2" hose with a ⌀ 37 cm drum and a vertical stationary hose (Own diagram)

It should be noted that while the bucket had a total weight of 3.5 kg for the configurations 3/4" | ⌀ 57 cm | 25, 3/4" | ⌀ 37 cm | 25, and 3/4" | ⌀ 57 cm | 15, the weight was decreased to 2.5 kg for all other configurations. During the tests it became clear that the bucket was too heavy for smaller configurations and therefore spun the coil too fast. This resulted in bad performances of the pump.

3.2.3.4 Volumetric Efficiencies

Following the experiments, the volumetric efficiencies were to be calculated based on the measured flow rates whilst pumping by hand. This means that for the results presented later in this chapter, the values from chapter 3.2.3.1 were used and not those from the energy efficiency measurements. For determining the volumetric efficiency, there are two different approaches: Both use the amount of water pumped during the observation period, later called the pumped flow rate, as a reference value. The volume in the pump available to achieve these pumped flow rates, however, can be assessed in different ways. One possible approach is to consider the total volume of the pump, in this case the combined volume of the stationary and rotating hose. To determine this volume, it would be essential to know the exact lengths of the hoses used, which unfortunately cannot be verified at the time of assessing volumetric efficiency, especially for the stationary hose. The second approach does not consider the volume of the pump, but rather the volume of air and water that the pump was able to absorb at the inlet during the observation period. The value for the second approach can be calculated using known variables as in Equation 9.

$$\dot{V}_{inlet} = A_{hose} * l_{hose} * 1000 \ \frac{l}{m^3} =$$

$$= \left(\left(\frac{D_{hose}}{2}\right)^2 * \pi\right) * \left(C_{drum} * \frac{n}{t}\right) * 1000 \ \frac{l}{m^3} =$$

$$= \left(\left(\frac{D_{hose}}{2}\right)^2 * \pi\right) * \left((D_{drum} * \pi) * \omega\right) * 1000 \ \frac{l}{m^3}$$

With:

$\dot{V}$	volume flow	$[l/min]$
l	length	$[m]$
D	diameter	$[m]$
C	circumference	$[m]$
n	number of revolutions	$[-]$
ω	rotational speed	$[rpm]$
t	time	$[min]$

To determine the volumetric efficiency of the pump, the ratio of the pumped flow rate to the volume flow at the pump inlet must now be calculated. This can be seen in Equation 10.

Equation 10: Volumetric efficiency of the pump (Own calculation)

$$\eta_{volume} = \frac{\dot{V}_{pumped}}{\dot{V}_{inlet}} * 100 \ \%$$

The following Figure 50 displays the values for volumetric efficiency separated by hose diameter. It should be noted that only tests with the original routing of the stationary hose, meaning from the container across the floor and then vertically upwards, are included. The highest calculated efficiency of 90.8 % is achieved in configuration 1/2" | ⌀ 37 cm | 20 | 6 rpm. The lowest efficiency above 0.0 % was calculated for setup 3/4" | ⌀ 37 cm | 25 | 6 rpm at 25.2 %. For the hose diameter 3/4", the value 0.0 % was obtained 32 times, and for the 1/2" hose 31 times. It should be noted that configurations with 25 coils, 15 coils and 10 coils were tested for the 3/4" hose and configurations with 25 coils, 20 coils and 15 coils were tested for the 1/2" hose.
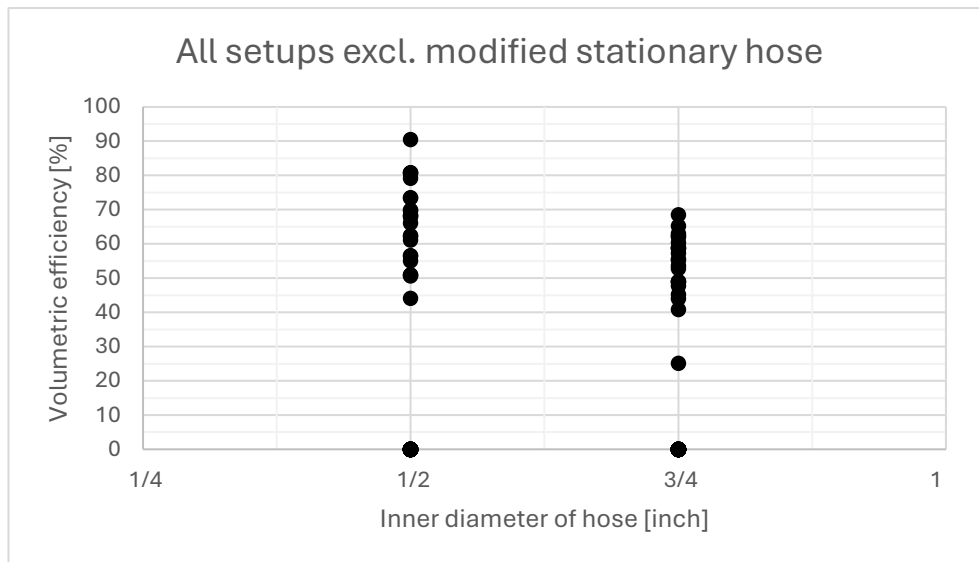
Figure 50: Calculated volumetric efficiencies for all setups excluding modified stationary hose (Own diagram)

3.2.3.5 Qualitative Observations

During the measurements of the flow rates, it was observed several times that the plugs of air and water behaved differently than expected. It was particularly noticeable in vertically aligned sections of the stationary hose that some air plugs moved upwards faster than their corresponding water plugs. This resulted in multiple individual air plugs merging to form one large plug, therefore creating a larger combined water plug. The larger plugs then moved at similar velocities. As a result, water and air were not emitted at short intervals as expected at the measuring head, but rather water was emitted continuously for longer periods with one or more longer pauses. Figure 51 illustrates the formation of those combined plugs. The described phenomenon occurred regardless of whether the stationary hose was positioned vertically upwards after touching the ground, strictly vertically or horizontally and then vertically. Only when the hose was routed horizontally and then diagonally upwards over the stairs, this behaviour was not observed. The inner diameter of the hoses employed also had no observable influence on the occurrence of this phenomenon. Yet, this observation contradicts the

Figure 51: Illustration of initial plugs (left) and of large, combined plugs (right) (Own illustration)

plug assumption, at least for stationary tubing, which is used in the literature as a basis for modelling Wirtz pumps (Deane and Bevan 2018).

An observation that was expected from theory and did occur frequently during the testing was the spilling failure described in chapter 2.2.1. This phenomenon occurred, primarily at low rotational speeds, initially as a slow leakage from the rotating hose without the columns in the stationary hose collapsing. The maximum pump height fluctuated by a few centimetres during those leakages. This was followed by the sudden collapse of the column in the stationary hose and water was ejected from the hose in a jet. At high rotational speeds, no slow leakage was observed but the water was ejected straight out as a jet. When pumping was continued without interruption after a spilling failure, it was observed qualitatively that the previous maximum pump head could not usually be reached before spilling occurred again. However, no exact measurements of the differences in head were taken. No difference in the occurrence of the phenomenon when using hoses of different diameters could be determined, apart from the absolute head at which spilling occurred.

Another, though not entirely surprising, observation relates to the behaviour of the water in the IBC container during the tests. While there was hardly any movement noticeable on the water surface during tests at 6 rpm and 12 rpm, it was significantly disturbed at 20 rpm. Clearly visible water movements were also observed during the measurements of the energy efficiency whenever higher rotational speeds occurred. It is not possible to assess exactly how these movements in the tank affected the measurements and therefore the results. This would require more transparent hoses and detailed slow-motion video recordings.

3.2.4 Analysis and Interpretation of the Test Results

This chapter focuses on the analysis of the measured results. This involves first making statements about possible sources of inaccuracy and then examining the results using statistical methods.

3.2.4.1 Possible Inaccuracies during the Measurements

Despite all efforts to standardise the tests as much as possible and to carry them out consistently, it was not possible to rule out all sources of potential inaccuracies in the results obtained. As described in the chapter 3.2.2, the rotational speed was regulated by manually turning the drive unit. This meant that it was not possible to guarantee a completely uniform rotational speed. Any effects of uneven operation of the device could have an impact on the flow rate and the maximum achievable pump head measurements.

In order to limit the time required for the flow rate tests, each test was measured for 1 min or until the 5 l measuring cup was almost full. The first potential problem concerns the measurement of time, which was stopped manually and may therefore contain slight irregularities. However, a more serious problem was that, as described, the columns of air and water in the stationary hose sometimes connected. This meant that during the measurements, water was either pumped continuously or not at all for long periods of up to 30 s. If the time limit was reached during such an irregularity, this might have had an influence on the amount of water pumped, which should actually have been lower or higher. Since it is not entirely clear whether this behaviour is a fundamental characteristic of coil pumps or whether it could be prevented by improved designs, this is a potential source of inaccuracies in the measurements.

During the measurement of the energy efficiencies, several possible inaccuracies were observed. The first one concerned the setup in general: To achieve any results at all, the water had to be pumped up the stationary hose manually until just below the tested pump head. Once this state was reached, the pump had to be held in this position until the rest of the setup was prepared. As described earlier, the plugs of water and air did not always behave as expected. In some cases, the water level dropped slightly during the waiting period as the air moved upwards through the stationary hose, possibly influencing the measured volume during the test. The second and likely more impactful problem was observed when the bucket was released for driving the pump. Moving downwards the

bucket accelerated from a very slow movement to rather high velocities at the point of impact. This resulted in an increasing rotational speed during the measurement. Especially for measurements with low numbers of coils and for the small drum diameter the coil rotated significantly faster than during the tests of the flow rates and maximum achievable pump heads. As a possible improvement, the measurements could be done with a different weight, that can be adapted to achieve more constant rotational speeds during the tests. Furthermore, the values for the height of the bucket above the ground as well as its impact velocity could not be measured with exact accuracy. For the buckets height above ground inaccuracies of about 10 cm are possible. The impact velocities were estimated from videos and rounded. Referring back to the calculations it can be assumed that inaccuracies in the height above the ground would affect the measurements more than those in the impact velocity.

Additionally, it should be noted that even without the modifications described in the previous chapter, the stationary hose did not always follow the same path. The part that laid on the ground next to the tank was rolled up in neat coils for some tests, but not for others. As a result, some of the coils did not lie flat on the ground but formed arcs in different directions. Since the results alone already show that the course with and without modifications had an influence on the maximum achievable pump heights, changes in the results due to the hose routing on the ground cannot be ruled out here either.

3.2.4.2 Methods for the Analysis of Flow Rates and Maximum Pump Heads

In the following sections, the measurement results for the flow rate and the maximum pump head are analysed using statistical methods to identify correlations. First, simple linear regressions are performed to investigate the dependence of the flow rate on the variables of the test setup. The results with modified setup of the stationary hose are not considered as these were not performed for all configurations. If they were included, this would likely distort the results of the regression. To test significance, the p-value is calculated based on the two-tailed t-distribution.

Microsoft Excel was used for all calculations. For the linear regression, diagrams were created that directly output the slope of the trend line, the so-called regression factor. The CORREL function was applied to calculate the correlation coefficients as the basis for the p-values. Next, the t-statistic was calculated as shown in Equation 11 (The Pennsylvania

State University 2024). To then obtain the corresponding p-value based on the two-tailed t-distribution, the T.DIST.2T function was used.

Equation 11: Calculation of the t-statistic (The Pennsylvania State University 2024)

$$t = \frac{|r| * \sqrt{df}}{\sqrt{1 - r^2}} = \frac{|r| * \sqrt{n - 2}}{\sqrt{1 - r^2}}$$

With:

t	*t-statistic*	$[-]$
r	*correlation coefficient*	$[-]$
df	*degrees of freedom*	$[-]$
n	*number of correlated value pairs*	$[-]$

It should be noted that the results of the statistical analyses are, of course, influenced by possible inaccuracies in the measurement results themselves. Furthermore, the accuracy of the linear regression is limited by the relatively small number of measurement results.

3.2.4.3 Statistical Analysis: Flow Rates

Since the evaluation should refer to a functioning configuration, all results with a flow rate of 0.0 l/min are excluded from the analysis. It should also be noted that the aim of the linear regression is not to prove a linear relationship. The aim of the analyses is merely to determine whether a relationship exists at all and whether it is statistically significant. To prove a linear correlation, more tests with higher resolution of the variables would be required. In principle, it can be assumed that for each configuration of three of the four variables drum diameter, number of coils, pump head, and rotational speed, there is a critical setting of the fourth variable at which the pump would no longer function.

For the flow rate versus the drum diameter, the linear regression yields a trend line with a correlation coefficient of 0.05997. The calculated p-value of 0.00783 indicates a correlation of high significance. The tests therefore demonstrated that higher flow rates can be achieved with larger drum diameters. The measurement results thus confirm the results of the experimental investigation presented in chapter 2.2.2.4 (Kassab et al. 2006). Figure 52 displays the diagram with the results for the flow rate as a function of the drum diameter including the automatically calculated trend line.
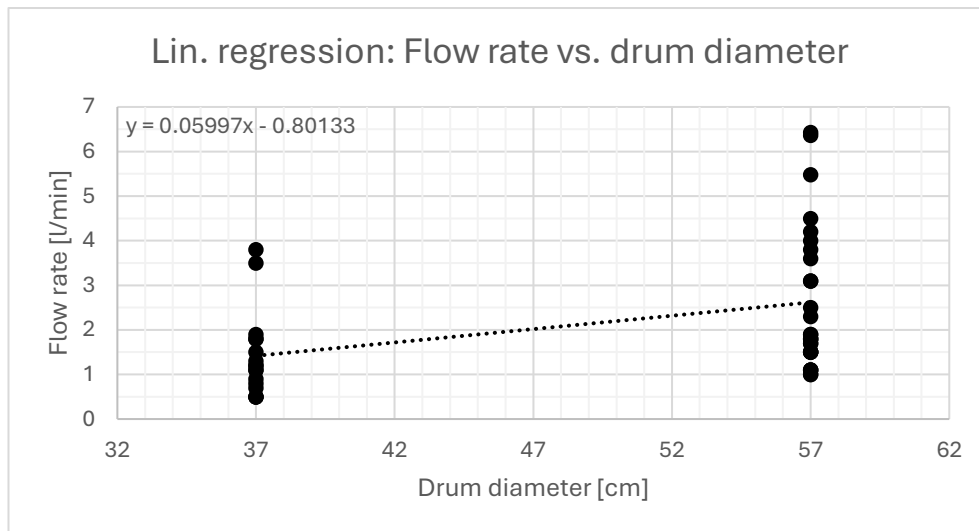
Figure 52: Trend line for the linear regression of flow rate versus drum diameter (Own diagram)

When examining the relationship between the number of coils and the flow rate, linear regression yields a trend line with a correlation coefficient of -0.02003. However, at 0.65675, the calculated p-value indicates no statistically significant correlation. Although the trend line points downwards as the number of turns increases, it cannot be concluded that more turns result in a lower flow rate. The authors of the previous experimental study come to a similar conclusion (Kassab et al. 2005). The results for the flow rate as a function of the number of coils are illustrated in Figure 53.
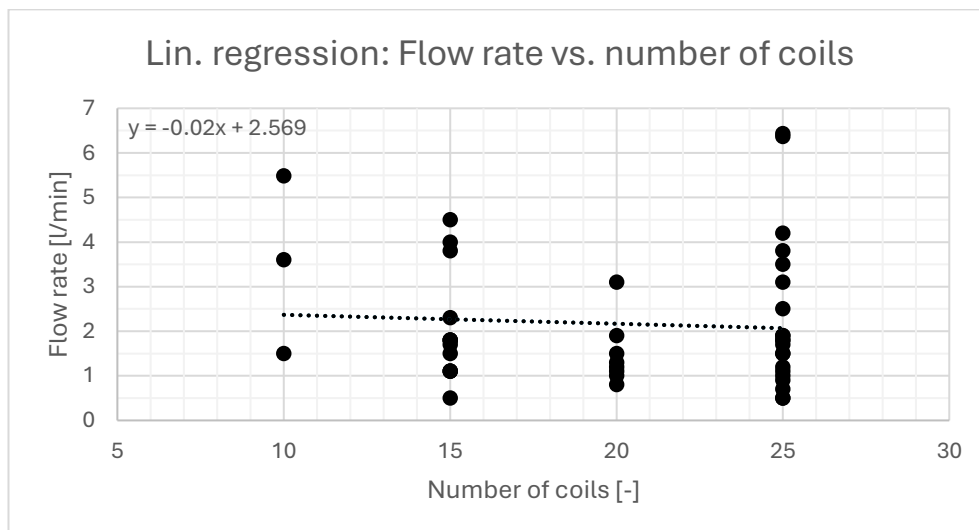
Figure 53: Trend line for the linear regression of flow rate versus number of coils (Own diagram)

For the linear regression of the flow rate versus the pump head, the correlation coefficient of the trend line comes out at -0.03631. While this could indicate a negative correlation between those two variables, the p-value of 0.95392 suggests differently. No statistically

significant correlation was found between the flow rate and the pump head, as long as the tests with a flow rate of 0.0 l/min are excluded from the analysis. The graph for the linear regression is displayed in Figure 54. No investigation of this correlation could be found in the literature, and it can therefore not be compared.
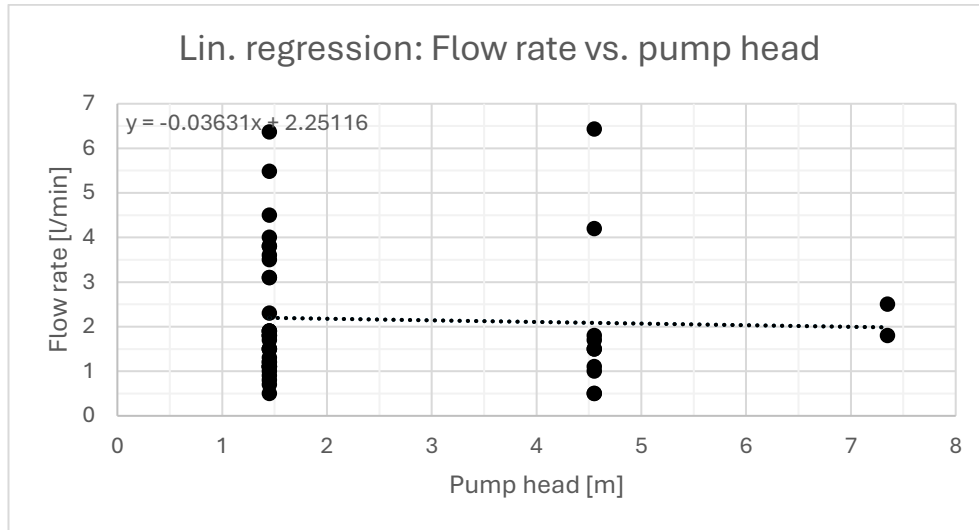
Figure 54: Trend line for the linear regression of flow rate versus pump head (Own diagram)

For the flow rate versus the rotational speed, the trend line yielded by the linear regression is characterized by a correlation coefficient of 0.17624. The calculated p-value of less than 0.000001 indicates a correlation of very high significance. The tests therefore demonstrated that higher flow rates can be achieved with higher rotational speeds, as long as the configuration is still operational. Figure 55 displays the diagram with the results for the flow rate as a function of the rotational speed including the trend line. Here too, the measurements taken and the analysis confirm the findings of the experimental study cited (Kassab et al. 2005).
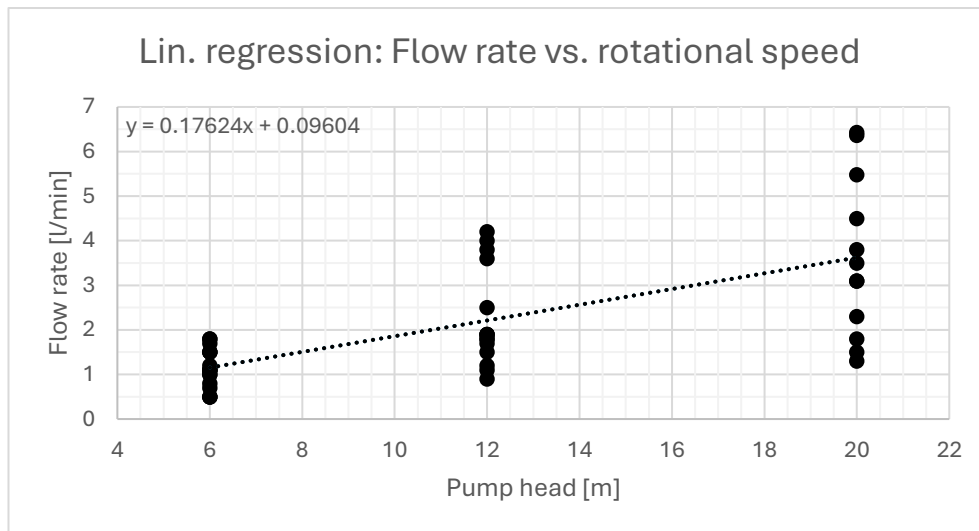
Figure 55: Trend line for the linear regression of flow rate versus rotational speed (Own diagram)

Finally, the influence of the hose diameter used on the flow rate is analysed. In order not to distort the results, only configurations that were carried out with both hose diameters are evaluated here. The results of the configurations with 10 coils for the 3/4" hose and those with 20 coils for the 1/2" hose are therefore not taken into account here. Figure 56 depicts the results for the flow rate as a function of the hose diameter. The correlation coefficient of the trend line comes out at 5.74651. Together with the p-value of 0.00504 this strongly indicates a positive statistical significance. It can be concluded that the utilization of a wider hose will lead to higher flow rates. The results are again consistent with the findings in Chapter 2.2.2.5 (Kassab et al. 2006). However, it is questionable up to what diameter this connection applies and whether the water and air plugs remain stable at significantly larger hose diameters. If this stability is lost, negative effects on the flow rate are to be expected at the very least. In extreme cases, the pump might lose its functionality completely.
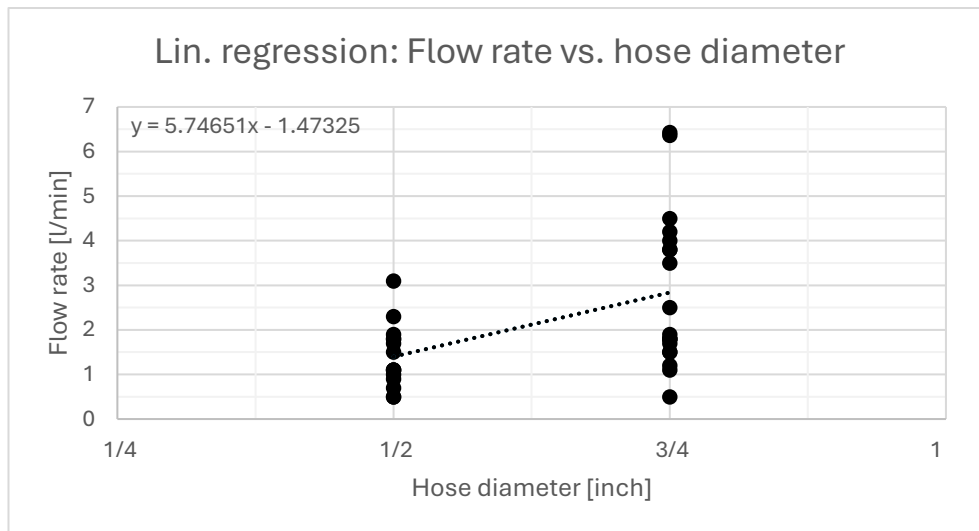
Figure 56: Trend line for the linear regression of flow rate versus hose diameter (Own diagram)

3.2.4.4 Statistical Analysis: Maximum Pump Heads

Here, too, the evaluation is not intended to identify linear relationships between the maximum achievable pump height and the variables. The data set generated by the tests is insufficient for this purpose. Rather, the aim is to show whether relationships exist at all and whether they are positive or negative.

The linear regression of the maximum achievable pump height versus the drum diameter shows a positive correlation coefficient of 0.08917 on the trend line. The p-value for the analysis is low at 0.00563, clearly indicating statistical significance. From these results, it can be concluded that an increase in drum diameter is accompanied by an increase in maximum achievable pump height. This finding confirms the results of previous experimental studies (Kassab et al. 2006). The corresponding diagram is presented in Figure 57.
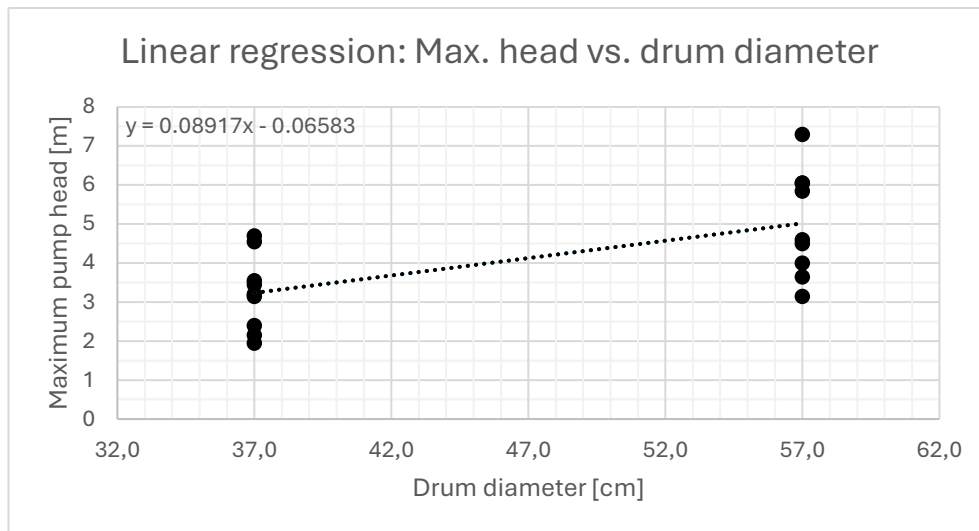
Figure 57: Trend line for the linear regression of maximum achievable pump head versus drum diameter (Own diagram)

When examining the relationship between the number of coils and the maximum achievable pump head, the correlation coefficient of the linear regression is given as 0.20417. The calculated p-value of 0.01103 suggests a statistical significance. It can therefore be deduced that a higher maximum achievable pump head can be expected with an increasing number of coils. The result of this analysis was to be expected, as both theory and previous experiments had come to the same conclusion (Deane and Bevan 2018; Kassab et al. 2005). The trend line of the related linear regression is depicted in Figure 58.
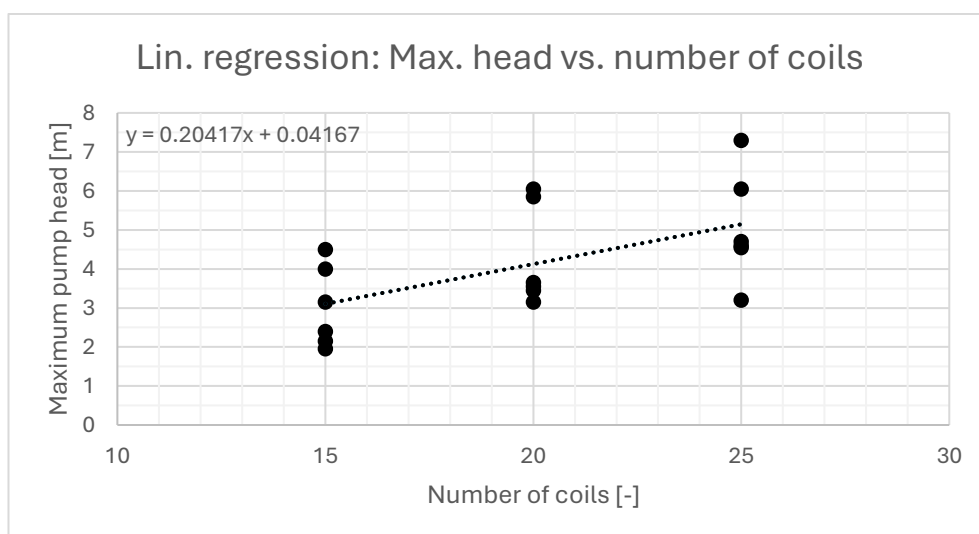
Figure 58: Trend line for the linear regression of maximum achievable pump head versus number of coils (Own diagram)

The final variable to be examined in relation to the maximum achievable pump height is the rotational speed. Linear regression yields a correlation coefficient of -0.10625, displayed in Figure 59. However, the p-value of 0.07754 is relatively high and does not indicate statistical significance. Even though it was suspected after the measurements and suggested in experimental studies, this analysis therefore does not confirm a clear correlation between the rotational speed and the maximum achievable pump height (Kassab et al. 2005).
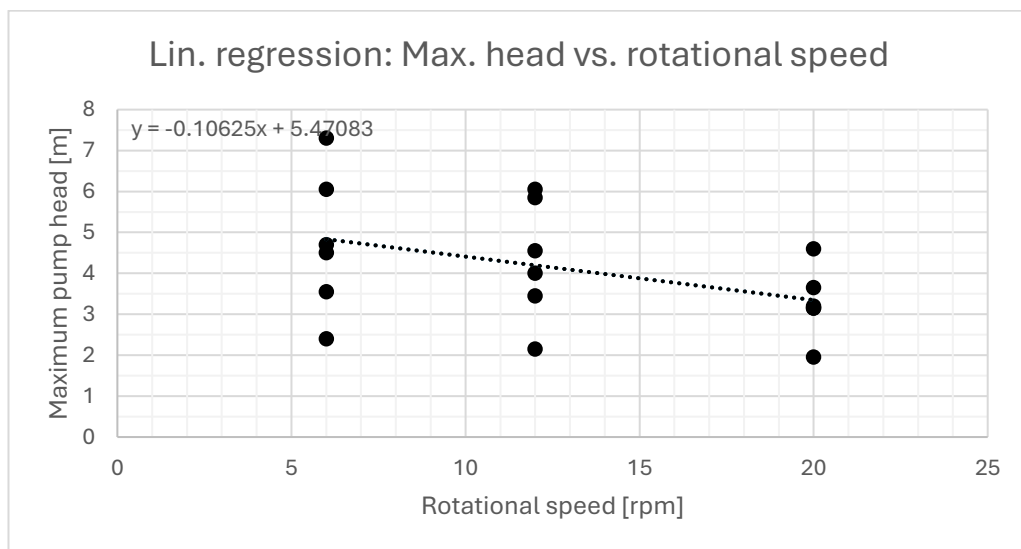
Figure 59: Trend line for the linear regression of maximum achievable pump head versus rotational speed (Own diagram)

3.2.4.5 Analysis: Energy Efficiencies

As described previously, the measurements for the tests on the energy efficiencies of the different configurations were exposed to several, partly severe, inaccuracies due to the limited time for the tests and the limitations of the testing apparatus. The results should therefore only be interpreted with the utmost caution. This can be seen when looking for instance at the result of the configuration 1/2" | ⌀ 37 cm | 25. The corresponding measurement in this configuration resulted in 0.0 l/min at a head of 4.55 m and the efficiency was therefore determined as 0.0 %, while the maximum achievable pump head for the same configuration was measured at 4.70 m. This discrepancy is most likely due to the irregular and excessive rotational speed. With a better adjustment of the total weight of the bucket, a slower and more consistent rotation of the pump could possibly have been achieved and thus water could have been pumped. In addition, this would significantly reduce the losses caused by the acceleration and therefore impact speed of

the bucket on the ground. Attempts were made to take the losses into account in the calculation. However, the losses are based on estimates from videos taken during the tests, which are highly susceptible to errors. An analysis using statistical methods comparable to the other tests does therefore not appear to be of use.

Nevertheless, the first results of the energy efficiency measurements in the configuration 3/4" | ⌀ 57 cm | 25, once again displayed in Figure 60, still offer informative insights. It can be concluded that, given the right circumstances, the testing apparatus performs surprisingly efficient at over 60 %. These circumstances were achieved during the measurement at a head of 7.35 m. What is also clear to see is that if these circumstances change, in this case only by reducing the pump head, the efficiency of the pump quickly drops. In this case, it halved to about 30 % at 4.55 m and is reduced to as low as 7.2 % at 1.45 m. It should be noted that given the results of other configurations this trend cannot be verified with other values and might therefore not be applicable in general. Yet, combining the observations during the testing and the test results, this seems to be a reasonable assumption.
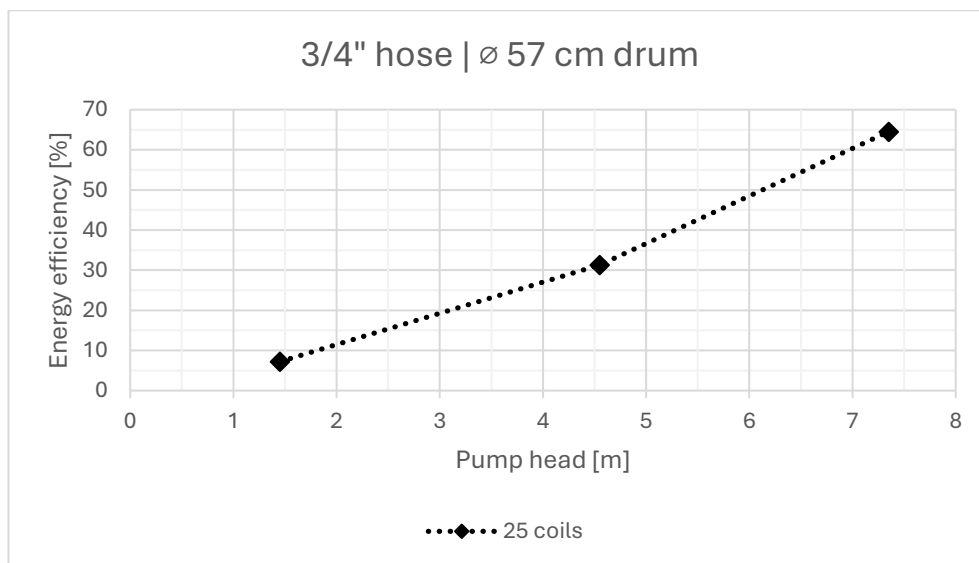
Figure 60: Energy efficiencies for the 3/4" hose with a ⌀57 cm drum and 25 coils (Own diagram)

3.2.4.6 Analysis: Volumetric Efficiencies

Since volumetric efficiency is only of secondary importance for real-world applications, no in-depth statistical analysis will be carried out here given the scope of this paper. Assuming that the pump behaves as theoretically expected, the results would have been expected to be in the range of roughly 50 % to 70 % based on the submerged ratio during

the tests, as long as water is being pumped at all. The average value for all tests of 60.1 % as well as both average values for the individual hose diameters of 66.1 % for the 1/2" hose and 53.8 % for the 3/4" hose all fall within this range.

Larger deviations can possibly be explained by the behaviour of the plugs in the stationary hose: Lower values may have been caused by a combined and therefore large air plug interrupting the water flow for a longer period after the start of the 1 min measurement. Upward deviations could be explained by larger air plugs working their way completely upwards through the water plugs before the start of the measurement period. This would have caused the respective measurement to start directly with a long, uninterrupted water flow, thereby influencing the measurement.

3.2.4.7 Analysis: Modified Stationary Hoses

The following briefly outlines how modifications to the stationary hose affected the measurement results. 'Standard' always refers to the setup in which the stationary hose laid on the ground next to the tank and was then pulled upwards. 'Vertical' describes the setup in which the stationary hose was pulled vertically upwards immediately after the outlet on the shaft. 'Horizontal variant 1' refers to the horizontal route after the tank and subsequent routing over the stairs, and 'horizontal variant 2' refers to the horizontal route after the tank and subsequent vertical routing upwards.

The impact of the modifications on flow rate was tested with the vertical setup at a pump head of 1.45 m in the two configurations 1/2" | ⌀ 37 cm | 20 and 1/2" | ⌀ 37 cm | 15. Regardless of the rotational speed, the results were almost identical in all measurements compared to the standard setup. The deviations of up to 0.1 l/min are more likely to be explained by general inaccuracies of the measurements than by an actual influence of the stationary hose routing on the flow rate.

The same configurations were used with the vertical setup to identify possible influences of the stationary hose routing onto the energy efficiency. Again, the pumped water volumes differed by a maximum of 0.1 l/min from the standard setup, resulting only in minor changes in the energy efficiencies. Therefore, based on the measurements, it cannot be assumed that the modified vertical routing of the stationary hose influenced the measurement results.

The influence of a modified stationary hose on the maximum achievable pump height was tested in a first step with a vertical setup in configurations 1/2" | ∅ 37 cm | 20 and 1/2" | ∅ 37 cm | 15. The values measured here differ so greatly from those of the standard setup that this change cannot be explained by measurement inaccuracies alone. The results for the configuration 1/2" | ∅ 37 cm | 15 with the setups horizontal 1 and horizontal 2 also show significant deviations from the standard setup for every measurement. The deviation in percent of the respective modification from the standard routing of the stationary hose is illustrated in Figure 61.
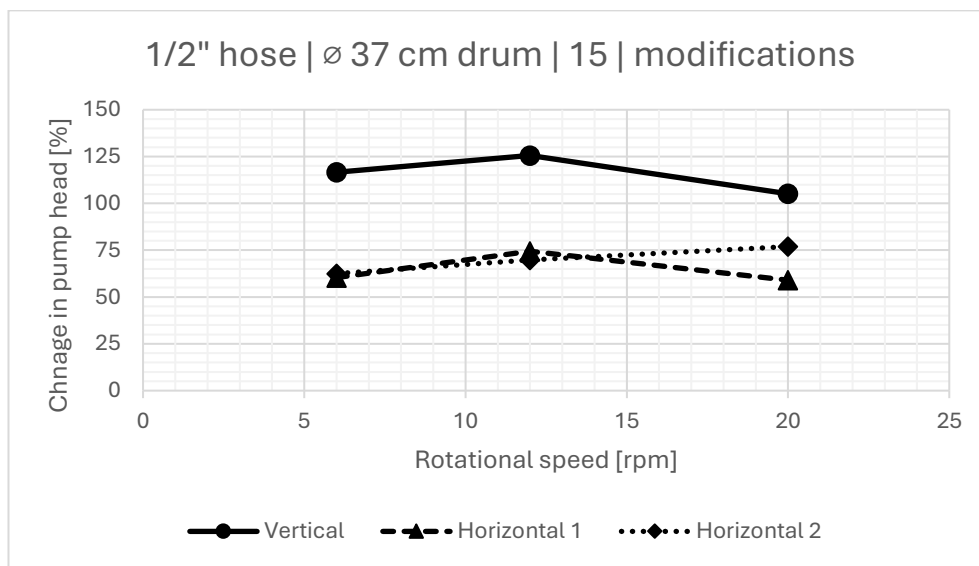
Figure 61: Change in the maximum achievable pump head with modified stationary hose setups for the 1/2" hose with a ∅ 37 cm drum and 15 coils (Own diagram)

4   Floating Turbine Coil Pump: Proof of Concept

The following sections describe the path to a practical floating turbine coil pump (FTCP) based on the tests described in the previous chapter. The chapter is divided into one subchapter concerning the construction and assembly of the FTCP and one illustrating the testing of the pump. The goal of the implementation is explicitly not to repeat the measurements in large numbers. It is merely to demonstrate that the FTCP concept is feasible in practice.

4.1   Assessment of Possible Test Sites

In order to be able to test the pump later, several test sites on the river Vils were examined. In consultation with the relevant authorities, due care was taken to pick locations that had already been artificially developed if feasible. This was to prevent damage to protected natural shore areas. Additionally, only locations that meet the following criteria were considered:

- Within Amberg's city limits
- Accessibility by car
- Easy water access

After inspecting the Vils, three locations were identified as possible options and examined in more detail: Eichenforstgäßchen, Schiffbrück-gasse and the pedestrian bridge underneath the street B85. The locations are shown in Figure 62 (Landesamt für Digitalisierung, Breitband und Vermessung 2025). All locations are situated south of the market square and north of the Kurfürstenbad.

Since the Vils is not a fast-flowing river, the flow velocities at these locations were investigated.
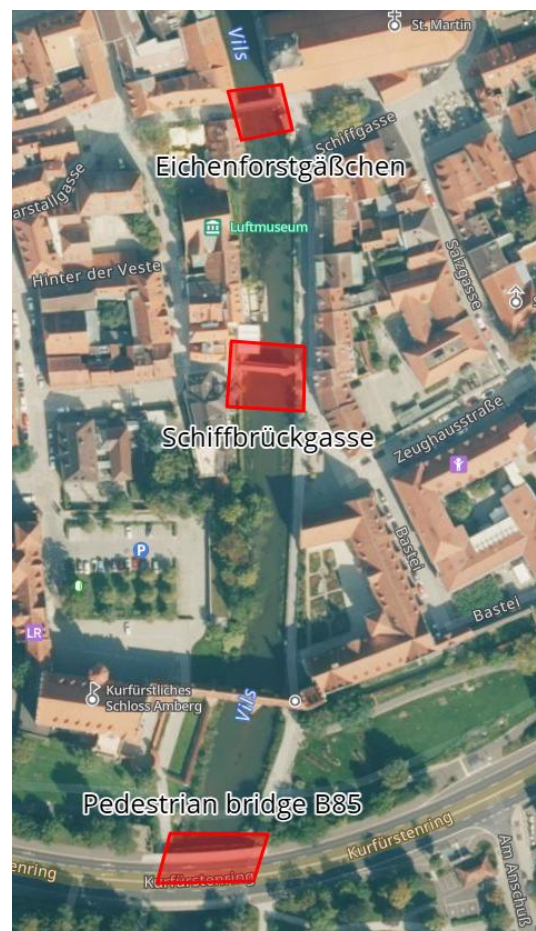
Figure 62: Possible test sites (Own screenshot from Landesamt für Digitalisierung, Breitband und Vermessung 2025)

The aim was to find the location with the highest flow velocity. To do this, the bucket used in the previous tests was attached to a rope and partially filled with water. The rope was then marked at two points: 5 m and 14 m away from the bucket. This resulted in a distance of 9 m between the marks. To take the measurements, the bucket was placed in the river and the time between the two marks was measured. Ten measurements were taken at each measuring point to calculate the average flow velocity. The measurements found average flow velocities of 0.3 m/s at the locations Eichenforstgäßchen and Schiffbrückgasse and 0.1 m/s at the location B85. The individual measurements can be found in the appendix. It should be noted that the measurements were taken on 03 June 2025, four weeks prior to the first test of the pump.

4.2   Construction of the Floating Turbine Coil Pump

The basic idea behind this project is to design an FTCP that is easy to replicate and as inexpensive as possible. An online video with a barrel as the basis for the pump served as inspiration (Tiller 2018).

Since metal bung barrels were already available at the OTH in Amberg, the first approach was to use one of these barrels. The 60-liter barrels have an inner diameter of just over 37 cm and a height of 57 cm. In addition to their availability at the university, another advantage was that these barrels were still new, which meant that contamination of water by oil residues, for example, could be ruled out. They are made of 0.6 mm sheet steel. However, the material thickness was not yet known at the time of selection.

Since there were two bungs on the lid of the selected barrel for filling, it was decided to remove the lid completely. Figure 63 depicts the processed barrel compared to an identical new one. This was done using an angle grinder. In the next step, four turbine blades were to be cut into the bottom of the barrel and then bent into shape. For this purpose, Prof. Dr.-Ing. Andreas P. Weiß created a wooden stencil that was used to outline the blades on the metal. Again, an angle grinder was used for this

Figure 63: Top view of metal barrels before processing (left) and after removing the lid (right) (Own photograph)

process. Due to the thinness of the sheet steel, the blades could be easily bent into shape by hand.

However, even slight pressure caused them to bend back out of shape. It was concluded that the stability of the turbine blades would not be sufficient for practical application. Various ideas for reinforcing the structures were rejected due to their complexity and the resulting difficulty in replicating them for users. Figure 64 compares the processed metal barrel from the bottom in comparison to an identical, unprocessed barrel. At the turbine blades, it is clearly visible how thin the material of the barrel is.

Figure 64: Bottom view of metal barrels before processing (left) and after manufacturing of the turbine blades (right) (Own photograph)

After a brief search, a plastic barrel was procured at short notice due to the problem with the metal barrel. This barrel has a capacity of around 200 litres, had only been used for collecting rainwater to date, and, with an inner diameter of around 57 cm, also fits the measurements carried out on the test apparatus. With a height of 93 cm, compared to the steel barrel, the barrel also offers more space for hose coils as a base for the pump. Furthermore, the material thickness of 5 mm indicated significantly improved stability for the turbine blades.

Similar to the steel barrel, the lid was removed as its bungs made it unsuitable for the manufacturing of turbine blades. However, a jigsaw was used for this purpose as an angle grinder would have led to the plastic melting in the process. Due to the changed dimensions of the barrel, the stencil for the turbine blades also had to be adjusted. For this purpose, the original stencil was transferred to CAD by hand and scaled up. Care was taken to ensure that sufficient material remained at the edge of the barrel bottom in order not
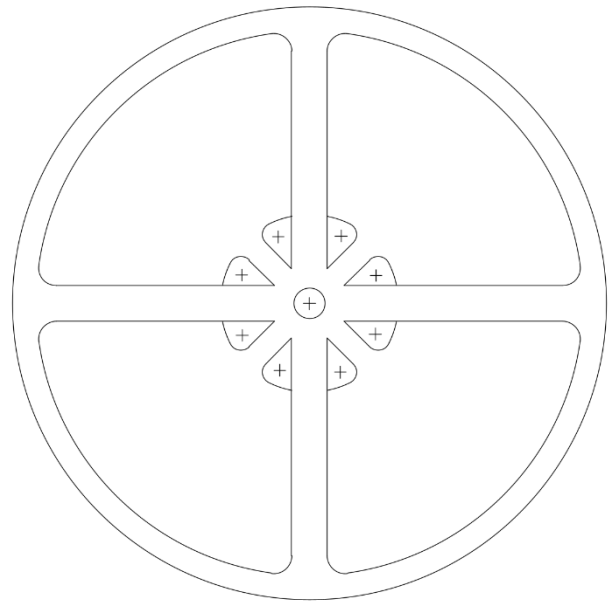
Figure 65: CAD model of the stencil for the turbine blades (Own CAD model)

to compromise the stability of the barrel as a whole. The CAD model of the stencil, displayed in Figure 65 in reduced size, was then printed out on DIN A1 paper. The lines represent the cut edges, and the areas marked with '+' are to be completely removed. After the turbine blades had been cut out, they had to be shaped. To achieve this, the blades were heated with a hot air gun until the material became pliable. Compared to the rest of the barrel bottom, the blades were first twisted by 45° and then the river facing side was bent further by about 20°. Due to the shape of the barrel bottom and the simple processing, it proved impossible to achieve exactly the same bend for all blades. The hole resulting from the circle in the centre of the stencil will later be used to feed the hose through and was created using a peel drill. For additional stability, the turbine blades were connected to the barrel at the outer edge using small metal plates.

In theory, it would have been possible to calculate the exact shape of the turbine blades based on the turbine radius and flow velocity. However, in real-world applications, varying flow velocities depending on location, season and weather conditions must be assumed. Furthermore, it cannot be assumed that this geometry could be replicated by non-experts due to the difficulty in processing. A less-than-optimal turbine design should therefore not be considered a disadvantage for the proof of concept.

The results of the tests conducted were considered when selecting the hose. These tests showed that higher flow rates could rather be achieved with the 3/4" hose than with the 1/2" hose. In addition, the pump performed more frequently in comparable configurations with the 3/4" hose than with the 1/2" hose. Therefore, the 3/4" hose was selected for implementation in this project. To minimise costs and to avoid additional plastic waste, no new hose was procured. Instead, three pieces of hose left over from testing, with a total length of just over 45 m, were connected using hose connectors. The hose was then arranged in the barrel in a total of 25 coils and secured with cable ties. To achieve this, small holes were drilled into the barrel on opposite sides using a shell drill and three coils each were bundled together with the cable ties.

On the turbine side, at the barrel bottom, the hose was then fed through the hole in the centre of the barrel. Therefore, it was first attached to a 90° pipe elbow using Geka couplings. The elbow was then fed through the hole in the centre of the template shown in Figure 65. On the other side, the ABA Beul coupling, which had already been used on the test apparatus, was screwed onto the elbow. A rotatable hose nozzle was inserted into the coupling, to which the stationary hose will later be connected. Care had to be taken to ensure that the hose did not open the Geka couplings again by itself due to torsion. Additionally, in retrospect of the tests, sealing tape was applied to the screw thread of the Geka coupling before screwing. Unlike the ABA Beul coupling, no rubber seal is provided
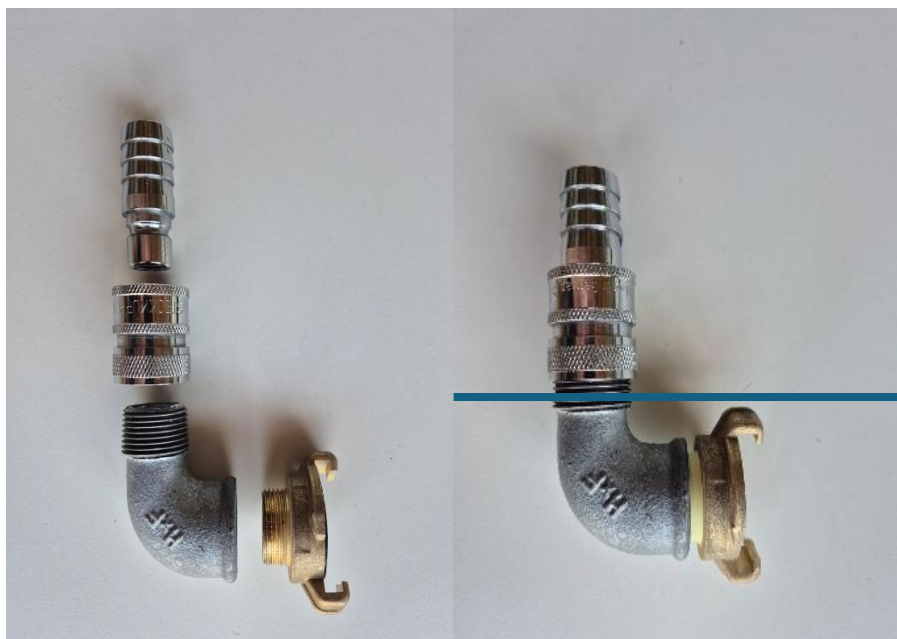
Figure 66: Exploded (left) and assembled (right) view of the transition from rotating to stationary hose (Own photographs)

on this screw connection. Using the tape is intended to prevent any leaks before they even occur. Figure 66 shows the used components individually and in their assembled state. The barrel bottom is symbolised in the assembled view by the blue line. The section above the line is located outside the barrel, the section below it is located inside.

Since the barrel could no longer float on the surface of the water in this form, bicycle inner tubes were used to provide buoyancy. In total, eight 24" tubes were required to ensure that the barrel remained stable in the water. Due to the barrels' weight distribution, four tubes were placed at the front of the pump near the turbine, three at the rear and one in the middle. To prevent the tubes from moving along the barrel, a hole was drilled in the barrel casing for each but the middle tube, and the valves were inserted through these holes. The middle tube was not fixated in this way. The ability to move it along and around the barrel was intended to ensure that

Figure 67: Uneven shape of an inflated bicycle tube (Own photograph)

any imbalance during testing could be compensated for. Still, two problems arose: Firstly, the tubes could not be inflated completely because, without an outer tire encasing the tubes, their internal diameter increased with increasing pressure, meaning that they would no longer fit tightly against the barrel. However, reduced pressure per tube and therefore reduced volume resulted in less buoyancy. This explains why so many tubes were necessary. The second problem was likely caused by differences in the material thickness of the bicycle inner tubes. As a result, some of the tubes did not develop a uniform torus shape when inflated but instead had irregular bulges with different diameters. Figure 67 displays a tube where this was particularly evident. The uneven shape of the bicycle inner tubes caused the barrel to float unevenly. This meant that it remained stable in the water but did not rotate as planned. In order to move it out of its stable position, a considerable amount of force had to be applied during buoyancy tests in the IBC container, which was still present from the tests. As soon as the barrel was no

longer rotated manually, it rolled back into its starting position on its own, sometimes even against the previous direction of rotation.

As a short-term solution to the irregular buoyancy, connectors made for foam pool noodles were purchased. These are shown in Figure 68 in their original form and cut up for use on the barrel. Four cut pieces were attached with screws, washers and nuts through holes drilled in the barrel so that the buoyancy was more evenly distributed. However, this did not completely compensate for the irregularities.
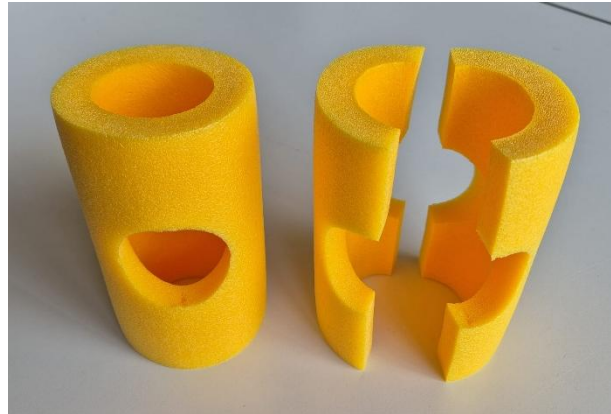
Figure 68: Foam connectors for pool noodles (Own photograph)

No further technical modifications were made to the pump before the first test. However, as with the test setup, a red mark was added again. This was intended to measure the rotational speed while testing. In addition, the university logo was printed on a foil sticker and glued to the barrel. Figure 69 depicts the pump at this point in time from the front and Figure 70 from the side. Neither image shows the stationary hose that was later attached to the coupling in the centre of the turbine.

Figure 69: First version of the pump prepared for testing (front view) (Own photograph)

Figure 70: First version of the pump prepared for testing (side view) (Own photograph)

4.3   First Test in the Vils

The first practical test in the Vils took place on 1 July 2025 close to the location Schiffbrückgasse. This day was preceded by several weeks of very little rainfall, and the Vils therefore carried significantly less water than normal, just from a visual perspective. The flow velocity also appeared to be lower than at the time of the earlier measurements. A quick test with a PET bottle yielded a velocity of about 0.25 m/s, confirming the impression.

The stationary hose was attached to the pump on site. In addition, a rope was attached to the stationary hose to hold the pump in position. The stationary hose could thus be guided to the shore independently of the retaining rope. A measuring cup and stopwatch were prepared there to measure the flow rate of the pump. However, after the pump was lowered into the water, it quickly became clear that the experiment would fail. The pump did not start to rotate as planned. An attempt to rotate the pump manually was successful. However, the pump stopped rotating almost immediately after the support was withdrawn.

Figure 71: First test of the pump in the Vils (Photograph: Prof. Dr.-Ing. A. P. Weiß)

After inspecting the pump, a material defect could be ruled out. The low flow velocity of the Vils river on that day is a much more likely cause of the test failure. As such, the turbine

blades of the pump were probably unable to generate enough torque to start the pump or keep it rotating. It is also possible that the uneven lift of the pump contributed to its failure. As there was no prospect of success on site that day, the first test of the pump was therefore discontinued at this point.

Nevertheless, it was positive that no air bubbles were visible at the transition from the rotating hose to the stationary hose as long as it was under water. This indicates that the selected coupling and its connections are suitable for the pump. The control of the pump's buoyancy position via the middle, non-fixed bicycle tube also worked as expected.

4.4   Optimisation of the Pump

Since modifications to the pump were anyway necessary in order to successfully prove the concept, the opportunity was taken to optimise the floats as well. The new approach was to use inner tubes for motorcycle tyres. In discussions with experts at a local bike shop, attention was drawn to the thicker material, which would inflate more evenly than bicycle inner tubes even without a casing. In addition, a single motorcycle inner tube holds significantly more air than a bicycle inner tube and can therefore provide more buoyancy. This would mean that fewer inner tubes would be needed.

After the bicycle inner tubes greatly increased their internal diameter under higher pressure and similar behaviour was expected from the motorcycle inner tubes, two inner tubes with an internal diameter of 19" were procured. These were then inflated to just under 1 bar of overpressure and attached to the existing holes in the barrel with their valves. The bicycle inner tubes as well as the pool noodle connectors were removed beforehand. Figure 72 shows the pump from behind with the motorcycle inner tubes attached to it. The pump's internal hose coils as well as their fixation with cable ties are also visible from this angle.

Figure 72: Pump with the motorcycle inner tubes attached from behind (Own photograph)

However, this did not solve the fundamental problem of insufficient torque due to the slow flow velocity of the Vils. Since the turbine cut out of the barrel bottom could not be improved significantly, another solution had to be found. This consisted of attaching additional turbine blades to the barrel bottom around the existing turbine. These were, on the one hand, intended to contribute to higher torque due to their additional surface area. On the other hand, they were also to be mounted so that they acted at a greater distance from the centre of the barrel. A larger lever arm allows a higher torque to be generated with the same surface area (Kuypers 2012).

Since it was primarily the torque that needed to be increased, rather than the rotational speed of the pump, it was decided to manufacture eight turbine blades instead of four, as a higher number of turbine blades results in higher torque. However, such turbines tend to spin more slowly, as more drag is generated at the same time (Hau 1996). Here, too, the geometry was to be as simple as possible to enable reproduction. For the production, a design was first created in AutoCAD and the shape was then transferred to cardboard.

This design is shown in reduced size in Figure 73. The blades with a surface area of almost 300 cm^2 each were cut from 3 mm aluminium sheet. They were then bent into shape by hand and holes were drilled for attaching them to the pump. Markings for the additional blades were etched on the edge of the existing turbine at an offset of 45° and holes were drilled into the barrel. The blades were then each attached with two screws, along with washers and nuts.
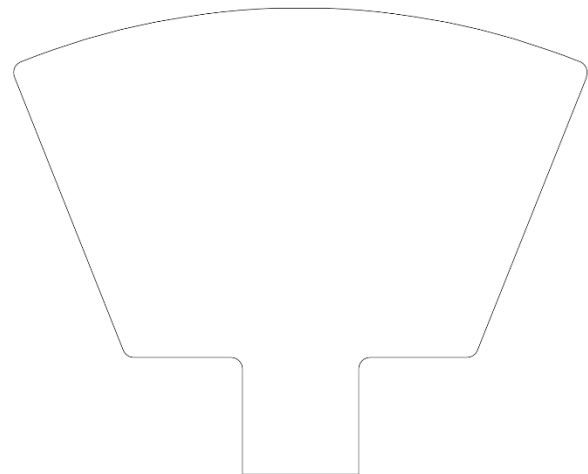
Figure 73: CAD model of the stencil for the additional turbine blades (Own CAD model)

With the additional turbine blades, the optimisation for the next pump test was complete. Figure 74 depicts the optimised pump from different angles, again without the stationary hose.

Figure 74: Optimised version of the pump prepared for testing from different angles (Own photographs)

4.5 Second Test in the Vils

The second test, now with the optimised pump, took place on 10 July 2025 at the same location near Schiffbrückgasse. As there had been several instances of precipitation in Amberg and the surrounding area in the meantime, the Vils carried more water than during the first test. The flow velocity was also significantly higher at 0.5 m/s, which greatly improved the test conditions.

After the stationary hose with the rope attached to it was secured to the pump, the pump was lowered into the water and held in position by hand using the rope. Due to the increased buoyancy of the motorcycle tubes, only a small part of the pump was under water at this point. Nevertheless, the pump began to rotate almost immediately. The rotation slowly filled the hose coils inside the pump, which in turn increased its weight. This caused the pump to sink slowly further into the water.

Due to the fact that the hose coils in the pump begin directly at the turbine but do not extend to the end of the barrel, and the additional turbine blades shifted the pump's centre of gravity even further towards the turbine, the pump sank lower at the front than at the rear. This behaviour can be seen in the angled shot in Figure 75. Comparing the water edge on the barrel with the black cable ties clearly indicates the pumps inclined position.
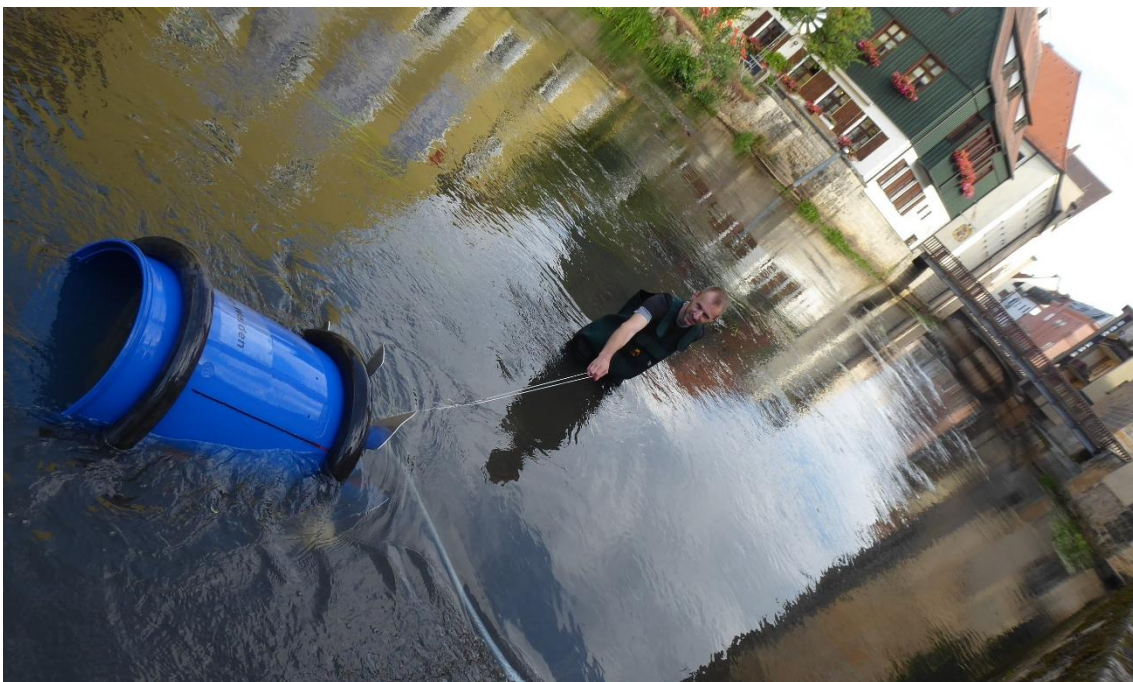
Figure 75: Inclination of the pump in the water during the measurement (Photograph: Prof. Dr.-Ing. A. P. Weiß)

However, this behaviour is desirable, as this position allows a larger part of the turbine to be surrounded by water, while the pump at the water inlet is still only submerged by 50 %. This means that a higher share of the turbine surface can be used for propulsion, which can be particularly important at low flow rates. During the test, the position of the pump was adjusted by releasing air from the motorcycle hoses until the tilt shown in Figure 75 was reached.

It was observed that, despite the optimisations, the rotation was still not constant. During each rotation, the barrel encountered a rotational resistance peak, causing a brief deceleration before regaining its angular momentum. This behaviour is likely caused by the floats utilized. The motorcycle tubes also showed slight differences in thickness when inflated and may therefore have led to uneven buoyancy. It was also noted that the entire pump oscillated slightly from left to right during operation, relative to the direction of flow of the Vils. Since the test took place near the shore, it seems likely that this behaviour was exacerbated by the turbulences occurring there. Other possible reasons include the geometry of the FTCP, which is not exactly symmetrical, mainly due to the hand-made turbine, and the fact that it was held in position by hand. It is possible that small movements while holding the pump by the rope were transferred to the pump.

During operation, the pump reached a rotational speed of approximately 8 rpm. In doing so, 5 l of water were pumped to a head of 1.7 m in 253 s. This results in a flow rate of 1.2 l/min or 71.1 l/h or 1.7 m^3/d. Comparing this value with the tests carried out at the university, the appropriate configuration must first be identified. The structure of the FTCP corresponds almost exactly to the configuration 3/4" | ⌀ 57 cm | 25. A flow rate of 1.5 l/min was measured at a rotational speed of 6 rpm in this configuration. It would have been expected that the flow rate in the practical test would be slightly higher because of the higher rotational speed. Why this expectation was not met cannot be conclusively determined at this point. The most likely explanation however is the stationary hose, which was laid out differently during the test at the university compared to the test in the Vils. Nevertheless, both values are within the same magnitude.

Shortly after the end of the measurement, another problem with the design of the FTCP became apparent. The movements of the pump in the water had caused the rotary coupling to slowly unscrew from the rotating hose. Since the pump was only connected

to the rope at the stationary hose, the pump briefly drifted downstream with the current. In the practical application of the FTCP this would result in the total loss of the pump, as it is unlikely that the pump can continuously be monitored and therefore recovered in time. An obvious solution to this problem would be to permanently connect the ABA Beul coupling to the rotating hose. To do this, it could be welded to the pipe bend used. However, this would require extreme caution, as the entire pump relies on the coupling remaining tight during operation. The high temperatures during welding might cause the entire component to deform slightly and thus leak. The probably better option would be to change the sense of rotation of the pump by changing the orientation of the turbine blades. In addition, the rotating hose would have to be wound in the opposite direction. This would prevent the coupling from unscrewing and would instead screw itself tight due to the rotation. However, due to the time constraints of this thesis, neither of these solutions could be implemented and tested in practice.

4.6 Evaluation of the Tested Pump's Efficiency

The results of the measurement and the theoretical considerations can be used to calculate the energy efficiency as well as the volumetric efficiency of the tested pump. The following paragraphs display the respective necessary calculations.

4.6.1 Energy Efficiency of the Tested Floating Turbine Coil Pump

The energy efficiency of the FTCP is based on the pumped water volume and the kinetic energy of the river Vils at the time of the testing. It describes, which proportion of the power available in the Vils that the pump was actually able to utilise. Various assumptions are made for this purpose:

1. The inner turbine blades did not contribute significantly to driving the pump.
2. Based on the image and video documentation, the submerged ratio is 75 %.
3. The flow velocity of the Vils was 0.5 m/s and was exactly perpendicular to the turbine. Turbulence is not a factor.
4. The density of the water was 1,000 kg/m³ at the time of the testing.

The first step is to calculate the flow contained in the Vils that is theoretically available to drive the pump. For this purpose, the power coefficient according to Betz is considered. The calculation is shown in Equation 12 and is derived from Equation 4.

Equation 12: Available power input for the tested floating turbine coil pump (Own calculation)

$$P_{input} = \frac{1}{2} * r_{tur}^2 * \pi * \rho_{H_2O} * v_{H_2O}^3 * c_{p,Betz} * SR_{tur} =$$

$$= \frac{1}{2} * ((0.45\ m)^2 - (0.30\ m)^2) * \pi * 1{,}000\ \frac{kg}{m^3} * \left(0.5\ \frac{m}{s}\right)^3 * \frac{16}{27} * 0.75 = 9.82\ W$$

The output power can be calculated based on the potential energy of the pumped water. Equation 6 can be used for this and adjusted as shown in Equation 13.

$$P_{output} = \frac{E_{H_2O}}{\Delta t} = \dot{V}_{H_2O} * \rho_{H_2O} * g * H_{H_2O} =$$

$$= 1.2 \ \frac{l}{min} * \frac{1 \ m^3}{1,000 \ l} * \frac{1 \ min}{60 \ s} * 1,000 \ \frac{kg}{m^3} * 9.81 \ \frac{m}{s^2} * 1.7 \ m = 0.33 \ W$$

Similar to Equation 8, the energy efficiency of the pump can now be calculated using the ratio of these two values. To obtain a value in percent, the result of the ratio in Equation 14 is multiplied by 100 %.

$$\eta_{energy,FTCP} = \frac{P_{output}}{P_{input}} * 100 \ \% = \frac{0.33 \ W}{9.82 \ W} * 100 \ \% = 3.36 \ \%$$

A review of the calculations shows that the density of the water has no influence on the calculated efficiency in this procedure.

It should be noted that the result of the calculation indicates the efficiency of the entire FTCP and not that of the turbine. All other losses, such as friction, that occur in the system are also included. It should also be considered that the efficiency also depends significantly on the pump head. As shown in chapter 3.2.4.3, however, the flow rate does not necessarily depend on the pump head. It would therefore be possible for the FTCP to generate a similarly high flow rate at a higher pump head, which in turn would result in higher power output and thus in increased energy efficiency.

4.6.2 Volumetric Efficiency of the Tested Floating Turbine Coil Pump

Volumetric efficiency also considers the amount of water pumped as output. However, only the volume flow rate of the pumped water is taken into account here, not the potential energy. In this case, the output volume flow rate amounts to 1.19 l/min as calculated in Equation 15.

Equation 15: Volume flow rate of water at the output (Own calculation)

$$\dot{V}_{H_2O,outlet} = \frac{V_{H_2O,outlet}}{t} = \frac{5.0\ l}{253\ s * \dfrac{1\ min}{60\ s}} = 1.19\ \frac{l}{min}$$

As shown in Equation 16, the maximum volume that the FTCP could have absorbed at the inlet is considered as a possible input. This value is based on the configuration, specifically on the hose diameter and drum diameter, and the rotational speed of the FTCP during operation.

Equation 16: Total volume flow rate at the input (Own calculation)

$$\dot{V}_{inlet} = \left(\left(\frac{D_{hose}}{2}\right)^2 * \pi\right) * [(D_{drum} * \pi) * \omega] * 1000\ \frac{l}{m^3} =$$

$$= \left(\left(\frac{0.75\ inch * 0.0254\ \dfrac{m}{inch}}{2}\right)^2 * \pi\right) * [(0.57\ m * \pi) * 8\ rpm] * 1000\ \frac{l}{m^3} = 4.08\ \frac{l}{min}$$

The volumetric efficiency of the pump can now be calculated using the ratio of these two values. To obtain a value in percent, the result is again multiplied with 100 %. The calculation is displayed in Equation 17.

Equation 17: Volumetric efficiency of the tested floating turbine coil pump (Own calculation)

$$\eta_{volumetic,FTCP} = \frac{\dot{V}_{H_2O,outlet}}{\dot{V}_{inlet}} * 100\ \% = \frac{1.19\ \dfrac{l}{min}}{4.08\ \dfrac{l}{min}} * 100\ \% = 29.17\ \%$$

Reviewing the footage from the tests, the FTCPs submerged ratio at the inlet was about 50 %. Consequently, a volumetric efficiency of 50 % would have been expected. A major water leak in the system as an explanation can be ruled out, as otherwise air would have escaped as well and the pump would not have been able to function. The observation of the combining air plugs from the experiments on the test apparatus, however, could be a

possible explanation. If the plug assumption (Deane and Bevan 2018) does not necessary apply, this could lead to air plugs surpassing parts of water plugs, thus reducing the share of water delivered at the output.

However, this would mean that the proportion of water in the system would increase. If the proportion of water increased in the stationary hose, sooner or later this increased proportion would also reach the outlet in the form of longer water plugs, thereby increasing the flow rate and thus also the volumetric efficiency again. This theory could be validated or rejected by conducting a longer test with a specific focus on this behaviour. Based on observations made on the test equipment, an increase in the water proportion in the rotating hose appears unlikely.

5 Economic Analysis of Floating Turbine Coil Pumps

Since this work has demonstrated that it is possible to build a functioning FTCP using simple means, the next step is to conduct an economic analysis including alternative pumping options. As the proof of concept was only of limited duration and no studies on the long-term use of FTCPs are available, the costs for maintaining FTCPs are not taken into account. For the sake of comparability, this also applies to the alternatives presented. Fuel costs are considered for alternatives where applicable. No fuel costs are incurred for the FTCP due to its turbine drive.

To provide price transparency for the estimation of investment costs in Germany, only offers available online are used and delivery costs are included in the calculations. Where possible, stainless-steel parts have been chosen both to prevent rust and to enable welded connections. If several items were available at low cost from the same supplier, the delivery costs were only added to the first item listed, provided that this was compatible with the delivery terms. The price quoted always refers to the total number of products required, including shipping costs. Care is taken to select functional and inexpensive items. The online search for offers was carried out using the Google search engine, as well as on Amazon, eBay and Idealo, using the respective specifications. There is no guarantee that the cheapest available offer has been found and listed. The costs for small parts such as screws, nuts and washers are estimated.

As available online date on prices in Mozambique is found to be insufficient, the investment costs for Mozambique are based on information provided by local staff of the INKOTA-netzwerk e.V. organization.

5.1 Costs of the Constructed Pump in Germany

The first consideration relates to the new price of all items used to construct the FTCP as described in the previous chapter. For a better overview of the items required, these are listed in Table 2. Please note that these are not necessarily the exact same items that were used for the FTCP tested in Vils, as long as they offer the same functionality.

Usage	Product (supplier)	Price [EUR]
Drum	220 l plastic bung barrel (Amazon.de 2025j)	62.90
Rotating hose	50 m garden hose with textile fabric 3/4" (Hans Kraeft GmbH & Co.KG 2025c)	52.35
Stationary hose	25 m garden hose with textile fabric 3/4" (Hans Kraeft GmbH & Co.KG 2025a)	23.70
Coupling rotating hose	Geka coupling brass 3/4" hose fitting (GWT Technik Versand 2023c)	7.47
Coupling rotating hose	Geka coupling brass 3/4" external thread (GWT Technik Versand 2023b)	2.40
Sealing tape	12 m sealing tape (GWT Technik Versand 2023d)	0.97
Connecting piece	Pipe elbow 90° stainless steel 3/4" internal/ external thread (GWT Technik Versand 2023a)	2.67
Rotary coupling	ABA Beul coupling 65004.006 stainless steel (Amazon.de 2025e)	22.52
Rotary coupling	Aba Beul plug stainless steel 12022.106 (Amazon.de 2025d)	11.14
Fixation of hoses on fittings	4 × hose clamp ⌀ 16-27 mm (GWT Technik Versand 2023e)	1.92
Fixation of hoses on drum	Cable ties in different lengths (Amazon.de 2025i)	3.99
Fixation of inner turbine blades	4 × Connecting plate 50 mm × 15 mm × 2 mm (Amazon.de 2025c)	4.95
Floats	2 × Motorcycle tyre 19" (Amazon.de 2025b)	17.99
Outer turbine blades	Aluminium sheet 1000 mm × 400 mm × 3 mm (K&D Handel 2025)	54.83
Handling rope	Polypropylene rope ⌀ 2,5 mm × 100 m (Amazon.de 2025g)	8.67
Small parts	Screws, nuts, washers	15.00
	TOTAL	**293.56**

Table 2: Investment costs for the parts of a new FTCP in Germany (Own table)

Based on the prices listed in Table 2 the total costs for the parts of a new FTCP with the same specifications as in the test amount to about 290 EUR. In accepting these costs, it is assumed that all tools required for manufacture are already available. It is also assumed that suitable structures for securing the pump, such as bridges or trees, are located in the vicinity of the river where the pump can be secured for operation. For unattended long-term operation, it would also be necessary to check how the pump can be secured so that the fastening cannot break, and the pump operates safely. This may result in additional costs.

5.2   Costs for Alternative Pumping Options in Germany

For pumping small quantities of river water, it would be conceivable to use small electric submersible pumps (FengQui Pumps n.d.). To keep negative environmental impacts to a minimum, the following sections take a closer look at the two options of grid-connected and solar-powered systems. Pumps powered by fossil fuels such as diesel are not examined. To ensure low-maintenance operation, only dirty water pumps are considered.

5.2.1   Grid-connected Submersible Pump

The following Table 3 illustrates the approximate investment costs required to set up a water supply system based on a grid-connected submersible pump comparable to that of the FTCP. It is assumed that an additional power cable will be required outdoors for connection to the power grid. All other requirements for installation are considered to be met.

Usage	Product (supplier)	Price [EUR]
Pump	Dirty water submersible pump (Amazon.de 2025h)	26.79
Delivery hose	25 m garden hose with textile fabric 1" (Hans Kraeft GmbH & Co.KG 2025b)	44.65
Fixation of delivery hose on pump	2 × hose clamp ⌀ 20 - 32 mm (GWT Technik Versand 2023f)	5.88
Power cable	25 m outdoor-rated power cable (Amazon.de 2025k)	35.41
	TOTAL	**112.73**

Table 3: Investment costs for a new grid connected submersible pump in Germany (Own table)

In addition to the investment costs of approximately 110 EUR, fuel costs, in this case electricity costs, must be taken into account here. In order to estimate these costs, the efficiency of the pump shall be estimated based on the data provided in the data sheet (Güde GmbH & Co. KG 2025). The calculation is shown in Equation 18. It should be noted that, due to the limited data available, this is only a very rough estimate of the pump's efficiency.

$$\eta_{pump} = \frac{P_{hydraulic}}{P_{electric}} * 100\ \% = \frac{\rho_{H_2O} * g * \dot{V}_{pump} * H_{H_2O}}{P_{electric}} * 100\ \% =$$

$$= \frac{1{,}000\ \frac{kg}{m^3} * 9.81\ \frac{m}{s^2} * 7{,}500\ \frac{l}{h} * \frac{1}{1000}\ \frac{m^3}{l} * \frac{1}{3600}\ \frac{h}{s} * 5\ m}{400\ W} = 25.55\ \%$$

To ensure comparability, the submersible pump should not run continuously at full load in this analysis, as it would otherwise pump a significantly larger volume of water than the FTCP tested. Therefore, the following analysis of annual power consumption is based on a flow rate of 1.7 m^3 per day. The annual amount of energy required is calculated as shown in Equation 19.

Equation 19: Annual required electric energy for the submersible pump (Own calculation)

$$E_{electrical} = \frac{E_{hydraulic}}{\eta_{pump}} = \frac{\rho_{H_2O} * g * V_{H_2O} * H}{\eta_{pump}} =$$

$$= \frac{1{,}000\ \frac{kg}{m^3} * 9.81\ \frac{m}{s^2} * 1.7\ \frac{m^3}{d} * 365.25\ \frac{d}{a} * 1.7\ m}{25.55\ \%} = 40.53\ \frac{MJ}{a} = 11.26\ \frac{kWh}{a}$$

The average electricity price for German households in 2024 is used to calculate the annual electricity costs and therefore the operational expenditures (OPEX) in Equation 20 (Bocksch 2025).

Equation 20: Annual operational costs for the submersible pump (Own calculation)

$$c = OPEX = E_{electrical} * p = 11.26\ \frac{kWh}{a} * 40.22\ \frac{ct}{kWh} = 4.53\ \frac{EUR}{a}$$

With:

c	*operational expenditures*	$\left[\frac{EUR}{a}\right]$
p	*price*	$\left[\frac{ct}{kWh}\right]$

Even in this very rough calculation of annual operating costs, it is evident that these are negligible as long as electricity is available. A more detailed analysis with reduced operating costs, for example through dynamic electricity tariffs, is therefore not necessary.

5.2.2 Solar-powered Submersible Pump

In early summer and summer in Germany the total precipitation in absolute numbers decreases and more often appears as heavy rainfall events (Umweltbundesamt 2023). Therefore, solar-powered submersible pumps appear to be a sensible option for additional irrigation as an adaptation to climate change.

The following Table 4 shows the investment costs for the components of a solar-based pump system that can be used without an additional energy source and is therefore location-independent.

Usage	Product (supplier)	Price [EUR]
Pump	DC 12 V dirty water submersible pump (Amazon.de 2025f)	69.99
Power supply	100 W 12 V Solar panel with controller (Amazon.de 2025a)	67.98
Delivery hose	25 m garden hose with textile fabric 1" (Hans Kraeft GmbH & Co.KG 2025b)	44.65
Fixation of delivery hose on pump	2 × hose clamp ⌀ 20 - 32 mm (GWT Technik Versand 2023f)	5.88
	TOTAL	**188.50**

Table 4: Investment costs for a new solar-powered submersible pump in Germany (Own table)

Assuming a comparable pump efficiency to that calculated in the previous chapter and a required water quantity of 1.7 m³ per day, the energy consumption per day can be calculated as shown in Equation 21.

Equation 21: Daily electricity requirement of the submersible pump (Own calculation)

$$E_{electrical} = \frac{E_{hydraulic}}{\eta_{pump}} = \frac{\rho_{H_2O} * g * V_{H_2O} * H}{\eta_{pump}} =$$

$$= \frac{1{,}000 \ \frac{kg}{m^3} * 9.81 \ \frac{m}{s^2} * 1.7 \ \frac{m^3}{d} * 1.7 \ m}{25.55 \ \%} = 110.96 \ \frac{kJ}{d} = 30.82 \ \frac{Wh}{d}$$

The calculation shows that the 100 W solar panel should generally be able to cover the daily water requirements. An additional battery is therefore optional. Operating with solar energy and without a connection to the power grid, no fuel costs are incurred here.

5.3   Costs of the Constructed Pump in Mozambique

Since even an intensive online search failed to yield any reliable prices for the required materials, various organisations working in Mozambique were contacted. The support provided by INKOTA-netzwerk e.V., which is active in various projects including irrigation in the country, was very helpful (INKOTA-netzwerk e.V. 2025).

A request was made with a list of materials, which was forwarded to local staff in Mozambique. The list was translated into Portuguese by a member of staff. The prices shown in Table 5 are based on information provided by local staff and have been converted using an exchange rate of 1 EUR = 75 MZN MT.

Usage	Product (supplier)	Price [EUR]
Drum	220 l plastic bung barrel	45.33
Rotating hose	50 m garden hose with textile fabric 3/4"	24.67
Stationary hose	25 m garden hose with textile fabric 3/4"	14.00
Coupling rotating hose	Geka coupling brass 3/4" hose fitting + Geka coupling brass 3/4" external thread	13.00
Sealing tape	12 m sealing tape	0.67
Connecting piece	Pipe elbow 90° stainless steel 3/4" internal/ external thread	3.07
Rotary coupling	ABA Beul coupling + plug stainless steel	4.67
Fixation of hoses on fittings	4 × hose clamp ⌀ 16 - 27 mm	No information
Fixation of hoses on drum	Cable ties in different lengths	2.00
Fixation of inner turbine blades	4 × connecting plate 50 mm × 15 mm × 2 mm	20.00
Floats	2 × motorcycle tyre 19"	16.67
Outer turbine blades	Metal sheet 1000 mm × 400 mm × 3 mm	69.53
Handling rope	Polypropylene rope ⌀ 2,5 mm × 10 m	26.67
Small parts	Screws, nuts, washers	0.33
	TOTAL	**242.53**

Table 5: Investment costs for the parts of a FTCP in Mozambique (Own table based on information provided by INKOTA-netzwerk e.V.)

5.4   Economic Comparison and Evaluation

This section examines the economic performance of the pump variants presented. To this end, the economically relevant aspects capital expenditures (CAPEX), operational expenditures as well as data on the flow rate of each pumping system are considered. The FR is economically relevant, as a higher value allows irrigation of a larger area. This increases the economic benefit per system. For ease of reference, this key data is presented in Table 6.

The information in the tables shown was used to calculate the CAPEX values. Due to a lack of information, the German price was used for the hose clamps in Mozambique. As already described, only fuel costs are included in the OPEX values. These only occur to the grid-connected submersible pump. For all other systems, 0.00 EUR/a is assumed.

Flow rate value for the FTCP in Germany were taken from the described measurements at the river Vils. It should be noted that the value is not a maximum value as it depends on the local conditions and the setup. The values for the submersible pumps were taken from the respective data sheets, with the value for solar-powered pumps adjusted to a reduced power input of 100 W instead of 120 W (Güde GmbH & Co. KG 2025; Amazon.de 2025f). No flow rate value was assumed for FTCP in Mozambique, as it can vary greatly depending on the location.

Pumping System	CAPEX [EUR]	OPEX [EUR/a]	Potential flow rate [l/min]
FTCP Germany at the Vils	293.56	0.00	Measured: 1.2
Submersible pump (grid) Germany	112.73	4.53	125.0
Submersible pump (solar) Germany	188.50	0.00	66.7
FTCP Mozambique	242.53	0.00	unknown

Table 6: Economic comparison of the presented pumping systems (Own table)

It can be seen that, in absolute terms, the FTCP in Mozambique is around 17 % cheaper than in Germany. However, the available per capita income should normally also be taken into account in this context. Given the projections for 2025 in Mozambique at around 450 EUR/a, this is significantly lower than in Germany, where it is projected to stand at

93

33,120 EUR/a in 2025 (Statista GmbH 2025a, 2025b). This would mean that, in relation to available income, the pump is considerably more expensive in Mozambique than in Germany. In the case of Mozambique, however, it is questionable whether these projections are comparable. The proportion of people who are mainly self-sufficient through agriculture is very high (Deutsche Gesellschaft für Internationale Zusammenarbeit (GIZ) GmbH 2024). It can be assumed that this and other factors significantly distort the available per capita income. A final assessment of whether an average household in Mozambique could afford to invest in an FTCP can therefore not be given here. More detailed information about the financial possibilities of local farmers would be required to evaluate the financial burden associated with the investment FTCP. An assessment of available rivers and their flow velocities as well as of the water requirement for agriculture would be required to quantify the benefits of an FTCP. However, this data was not collected due to the scope of this work.

For the comparison in Germany, it can be stated that the submersible pumps presented are significantly superior to the developed FTCP in terms of CAPEX. The low OPEX of the grid-connected submersible pump is negligible. If the possibilities of increased flow rates are also taken into account, it becomes clear that the FTCP cannot prevail in applications where submersible pumps are also possible. While the flow rate of the grid-connected pump is only limited by its power, the flow rate of the solar-powered pump depends on the power generated by the solar panel and thus on the amount of sunlight. The flow rate of the FTCP, on the other hand, is directly dependent on the flow velocity of a flowing body of water and cannot be adjusted manually.

It should be noted, however, that even in Germany there are locations where connection to the power grid is either impossible or only possible at great expense due to long distances. Given the cost of cables listed above, the CAPEX advantage would be wiped out by material costs alone for distances exceeding approximately 100 m. Additional costs for installing the cables have not yet been factored in.

Factors not considered so far for both countries relate to local value creation and the manageability of the systems. While submersible pumps have to be purchased and possibly imported as finished systems, FTCPs can be manufactured locally from individual components. Local producers could create jobs on a small scale by

manufacturing FTCPs. In terms of system manageability, FTCPs also outperform submersible pumps: The repair of complex electric pumps requires a high level of expertise and, in some cases, special tools. Neither of these can necessarily be expected to be available to the local population, either in Germany or in Mozambique. A failure of individual components could therefore mean that the pumps have to be replaced. Thanks to its simple mechanical design, it is expected that individual components of the FTCP can be repaired without external assistance, allowing both faster and more cost-effective maintenance.

Depending on the application, both submersible pumps and FTCPs have their own economic advantages and disadvantages. In Germany, due to the existing infrastructure and fast delivery times, it can be assumed that FTCPs will not be able to compete with electrically powered pumps. Local production of FTCPs would also be impractical due to high costs, particularly for labour. As mentioned above, it is not possible to conclusively assess whether investing in FTCPs is economically viable for Mozambique. Data on the costs of electrical submersible pumps were not collected in this study. However, if irrigation is essential, FTCPs outperform electric pumps due to their simplicity and the fact that the system is easy to understand, allowing users to intervene independently and therefore cost-effectively in the event of potential issues.

6   Conclusion and Outlook

This thesis investigated technical and economic aspects of floating turbine coil pumps (FTCPs). To this end, theoretical and experimental preliminary work was carried out to analyse how they work. The pump is based on the Wirtz pump principle and generates pressure by alternately absorbing air and water while rotating continuously. This allows water to be pumped through a delivery pipe to an output point located higher than the pump itself. If the system pressure becomes too high, water is suddenly forced back towards the inlet through a process known as spilling, and the plugs of water and air in the delivery pipe fall accordingly. This limits the performance of the FTCP.

The studies cited identified the submerged ratio, the number of coils, the rotational speed, the drum diameter, and the pipe or hose diameter as decisive parameters in operating conditions. The correlations are not generally applicable to borderline cases, as the pump may lose its functionality in such cases. The submerged ratio has little effect on the maximum pump head. The flow rate, on the other hand, increases with an increasing submerged ratio. Increasing the number of coils increases the maximum pump head, while there is hardly any noticeable effect on the flow rate. As the rotational speed increases, the maximum pump head decreases while the flow rate increases. Increasing the drum diameter increases both the maximum pump head and the flow rate. The effect of the hose diameter on the maximum pump head has not been discussed in the literature. However, it has been shown that larger flow rates can be achieved with larger hoses.

Since the FTCP is to be powered exclusively by an existing flowing watercourse in its later implementation, the power available to it depending on the conditions was examined. The most important parameter here is the flow velocity, which influences the power to the third potency. Next, the possible power is dependent on the radius of the turbine squared and therefore its area. Other influencing factors are primarily the submerged ratio and the efficiency of the turbine.

In order to validate the theoretical findings, a test apparatus was constructed on which various parameters of the pump could be tested depending on configuration and operation. The tests were carried out on the university premises in Amberg, and 186

measurements were recorded. Despite some possible sources of error and inaccuracies in the measurements, most of the findings examined were confirmed by theory. Additionally, it was found that the routing of the stationary delivery pipe can have a major influence on the maximum pump head. Furthermore, it was observed that the air and water plugs do not always behave as stably as assumed in theory. Due to their design, the results of the energy efficiency tests are only reliable to a limited extent, but they do indicate that the pump can operate both very efficiently and very inefficiently, depending on the configuration and pump head. As expected, the results for volumetric efficiency were based on the submerged ratio.

The FTCP concept was then put into practice and tested. The tests were carried out in the river Vils in Amberg, which is characterised by low flow velocities of significantly less than 1 m/s. After the first test failed due to the pump not rotating, additional turbine blades were installed, along with other modifications. With this adjustment and an increased flow velocity on the day of the test, the pump was able to successfully deliver 1.2 l/min to a head of 1.7 m. The energy efficiency of the pump, based on the available power of the flow, is relatively low at less than 5 %. At less than 30 %, the volumetric efficiency is below the expected value.

The economic analysis yielded investment costs of just under EUR 300 in Germany and, in Mozambique, a potential country for FTCP deployment due to its development and the local impacts of climate change, investment costs equivalent to around EUR 250. The alternatives presented, submersible pumps, perform better in Germany in economic terms in terms of both investment costs and benefits due to more flexible and potentially higher flow rates. Even though the investment costs in developing countries such as Mozambique have not been recorded, the FTCP offers advantages over electric submersible pumps due to its simplicity and manageability. Still, a final economic assessment of the use of FTCPs in developing countries could not be completed due to a lack of data.

In summary, the research questions can be answered as follows: It is possible to produce a functioning FTCP. However, in addition to the technical implementation, success also depends to a large extent on the flowing water body in which the system is to be used. Economically, despite its relatively low price, the FTCP cannot compete with submersible

pumps in Germany, provided that these are suitable for use. No final assessment could be made for use in developing countries such as Mozambique.

Due to the scope of this work, not all questions could be conclusively clarified and designs optimised. For future investigations, it could therefore be interesting to test the test apparatus more extensively. A different and more precise method of measuring the energy efficiency, for example using a controllable electric motor, would be one approach here. Furthermore, the developed FTCP could be tested further under different conditions, such as flow velocity and pump head, at different times and in different locations. For instance, the inner blades could be removed to determine whether they still make a significant contribution to the drive with the additional outer turbine blades. Improvements could also be made to the floats and the pump attachment, which does not provide sufficient security in its current state and must be held in place by hand if there is no suitable vegetation or structure available.

Publication Bibliography

General Literature

Baruah, Pranab; Coleman, Brendan (2019): Country Brief: Mozambique. Off-grid solar power in Mozambique: opportunities for universal energy access and barriers to private sector participation. The Global Green Growth Institute.

Betz, Albert (1926): Wind-Energie und Ihre Nutzung durch Windmühlen. Göttingen: Vandenhoeck & Ruprecht. Available online at https://openelec.moodle-nds.de/pluginfile.php/4004/mod_resource/content/2/Windenergie%20und%20ihre%20Ausnutzung%20durch%20Windm%C3%BChlen.pdf.

Bocksch, René (2025): Strompreise 2025 auf dem Niveau des Vorjahres. Statista GmbH. Available online at https://de.statista.com/infografik/33667/strompreise-fuer-haushalte-und-industrie-in-deutschland/, checked on 7/20/2025.

Bundesverband WindEnergie e.V. (2022): Betz und Leistungsentnahme. Theorie nach Betz – maximal entnehmbare Windleistung. Available online at https://www.wind-energie.de/themen/anlagentechnik/funktionsweise/betz-und-leistungsentnahme/, checked on 10/9/2024.

Deane, Jonathan H. B.; Bevan, Jonathan J. (2018): A hydrostatic model of the Wirtz pump. In *Proc. R. Soc. A*. 474 (2211), p. 20170533. DOI: 10.1098/rspa.2017.0533.

Deutsche Gesellschaft für Internationale Zusammenarbeit (GIZ) GmbH (2024): Mosambik. Available online at https://www.giz.de/de/weltweit/320.html, checked on 7/28/2025.

FengQui Pumps (n.d.): 7 Key Benefits of Submersible Pumps in Water Management. Available online at https://fengqiupumps.com/blog/7-key-benefits-of-submersible-pumps-in-water-management.html#Agricultural_Benefits, checked on 7/19/2025.

Hau, Erich (1996): Windkraftanlagen. Grundlagen, Technik, Einsatz, Wirtschaftlichkeit. Zweite, überarbeitete und aktualisierte Auflage. Berlin, Heidelberg, s.l.: Springer Berlin Heidelberg (Springer eBook Collection Computer Science and Engineering).

INKOTA-netzwerk e.V. (2025): Wasser für die Felder. Land als Lebensgrundlage erhalten. Available online at https://www.inkota.de/projekte/mosambik/land-fuer-ein-gutes-leben, checked on 7/25/2025.

Kassab, Sadek Z.; Naby, Ahmed A. Abdel; Basier, El Sayed I. Abdel (Eds.) (2005): COIL PUMP PERFORMANCE UNDER VARIABLE OPERATING CONDITIONS. Ninth International Water Technology Conference. Egypt. Available online at https://www.researchgate.net/publication/228421671_Coil_Pump_Performance_under_variable_Operating_Conditions, checked on 7/15/2025.

Kassab, Sadek Z.; Naby, Ahmed A. Abdel; Basier, El Sayed I. Abdel (Eds.) (2006): PERFORMANCE OF MULTI-LAYERS COIL PUMP. Tenth International Water Technology Conference. Egypt. Available online at https://www.researchgate.net/publication/228458768_PERFORMANCE_OF_MULTI-LAYERS_COIL_PUMP, checked on 7/16/2025.

Kuypers, Friedhelm (2012): Physik für Ingenieure und Naturwissenschaftler. Band 1. 3., überarbeitete und erw. Aufl (Online-Ausg.). Weinheim, Germany: Wiley-VCH Verlag GmbH & Co. KGaA. Available online at http://site.ebrary.com/lib/alltitles/Doc?id=10612547.

Landesamt für Digitalisierung, Breitband und Vermessung (2025): BayernAtlas. Available online at https://atlas.bayern.de/?c=707065,5480684&z=18&r=0&l=luftbild_labels&mid=1, checked on 7/23/2025.

Makar, Randa S.; Shahin, Sahar A.; El-Nazer, Mostafa; Wheida, Ali; Abd El-Hady, Mohamed (2022): Evaluating the Impacts of Climate Change on Irrigation Water Requirements. In *Sustainability* 14 (22), p. 14833. DOI: 10.3390/su142214833.

Meneses, Ariel (2015): waterdragon river pump. Available online at https://www.youtube.com/watch?v=5TO6PY6ohA8, checked on 7/3/2025.

Meseret, Million; Wami, Dawit; Nallamothu, Ramesh Babu (2024): Experimental study on the parameters affecting the performance of spiral tube pump. In *Scientific reports* 14 (1), p. 22425. DOI: 10.1038/s41598-024-73234-w.

Mindú, Arsénio José; Capece, Jó António; Araújo, Rui Esteves; Oliveira, Armando C. (2021): Feasibility of Utilizing Photovoltaics for Irrigation Purposes in Moamba, Mozambique. In *Sustainability* 13 (19), p. 10998. DOI: 10.3390/su131910998.

Mortimer, Geoffrey H. (1988): The coil pumps. Doctoral Thesis. Loughborough University of Technology. Available online at https://repository.lboro.ac.uk/articles/thesis/The_coil_pumps/9454172?file=17076791, checked on 7/15/2025.

Ruff, Robin (2022): Entwicklung eines mobilen, hydrokinetischen Kleinstenergiewandlers für den Einsatz in Schwellen- und Entwicklungsländern. Dissertation. Technische Universität Darmstadt, Darmstadt. Bau- und Umweltingenieurwissenschaften. Available online at https://tuprints.ulb.tu-darmstadt.de/21603/3/Dissertation_Robin_Ruff.pdf.

SKF GmbH (2025): UCP 205. Available online at https://www.skf.com/de/products/mounted-bearings/ball-bearing-units/pillow-block-ball-bearing-units/productid-UCP%20205, checked on 6/28/2025.

Statista GmbH (2025a): Konsumindikatoren - Deutschland. Available online at https://de.statista.com/outlook/co/konsumindikatoren/deutschland, checked on 7/28/2025.

Statista GmbH (2025b): Konsumindikatoren - Mosambik. Available online at https://de.statista.com/outlook/co/konsumindikatoren/mosambik, checked on 7/28/2025.

The Pennsylvania State University (2024): 1.9 - Hypothesis Test for the Population Correlation Coefficient. Available online at https://online.stat.psu.edu/stat501/lesson/1/1.9, checked on 7/5/2025.

Thornton, P. K.; Loboguerrero, A. M.; Campbell, B. M.; Kavikumar, K. S.; Mercado, L.; Shackleton, S. (2019): Rural livelihoods, food security and rural transformation under climate change. Global Commission on Adaptation. Available online at https://gca.org/wp-content/uploads/2020/12/RuralLivelihoodsFoodSecurityRuralTransformation_V2.pdf, checked on 7/19/2025.

Tiller, Matthew (2018): River Powered Coil Pump. Available online at https://www.youtube.com/watch?v=9K1zLVABB0U, checked on 7/3/2025.

Umweltbundesamt (2023): Monitoringbericht 2023 zur Deutschen Anpassungsstrategie an den Klimawandel. LW-R-6: Landwirtschaftliche Bewässerung. Bundesministerium für Umwelt, Klimaschutz, Naturschutz und nukleare Sicherheit (BMUKN). Available online at https://www.umweltbundesamt.de/monitoring-zur-das/handlungsfelder/landwirtschaft/lw-r-6/indikator, checked on 7/20/2025.

Suppliers Pumping Parts

Amazon.de (2025a): 100W Solarpanel 12V Monokristallines Solarpanel-Kit 100 Watt Solarmodul mit 20 A Laderegler für netzunabhängige 12 Volt Energieladung für Wohnmobil, Boot, Wohnwagen, Haushalt. Available online at https://www.amazon.de/100W-Monokristallines-Solarpanel-Kit-netzunabh%C3%A4ngige-Energieladung/dp/B0CL34XYF7/ref=sr_1_5?__mk_de_DE=%C3%85M%C3%85%C5%BD%C3%95%C3%91&crid=395410EUZCJFY&dib=eyJ2IjoiMSJ9.B1ak39wxt5CrVynkN5yBnONZzJAWfgvauEVyB3yLP-jeC04COC6oecGV_WQuK9Y-TQk5co12PVWglOLydcCwXh4Hov2H9fUHmewpkE8x8p6SXJ9J_gfnqWBL7UC6pTkbvTGInHag9K71pc9b2bNE194N94V1wbZuyl1pN1BeQ2AUVkl0KCRBuZzF3-5T_LARdn2JZLu-7XcmCioOXFKhVwuQ895pZd-Yk29FXGEloMi_rTH0y697GKOuNMWo7WE4L2dzvhDXWaMgNdZlN8gzYanGHlBI30krXiOTfgkRlf4.io3agHOw-me4tfdl5ytLHdkqA89TCbkjGxO3vaq1cl0&dib_tag=se&keywords=solarpanel%2B12%2Bv%2B100%2Bw&qid=1753862956&sprefix=solarpanel%2B12%2Bv%2B100%2Bw%2Caps%2C89&sr=8-5&th=1, checked on 7/20/2025.

Amazon.de (2025b): 2.75/3.00-19 Innenschlauch, Heavy Duty Dirt Bike Schlauch für Honda CRF 100F 125FB 150F 450R KX Surron Light Bee X UltraBee Talaria Offroad Motocross Motorrad mit TR4-Ventil 2 Stück. Available online at https://www.amazon.de/Innenschlauch-Schlauch-UltraBee-Motocross-TR4-Ventil/dp/B0D5QRHZTS/ref=sr_1_7?dib=eyJ2IjoiMSJ9.zU7vs_a37mkTPR5FdujgD5Jvax6iHKDLNCZ8NE5SpigFx8D7_AL7Pg7BIUjQ2d72IH-PTsfnFlgnLwSdxNUiczyhDY0YQu1r30eWKLOwMJ_JRjt_AN-kGSEij6qcg-KuYSg50tUyVhC3czS1sbTKpwVUPkk4Uk3Fbr3ZewOaVJsu_ETKeG-PP6jPZn0LiNiw7A1TPza92LOVoCsx2lDsuthHpsfL0z_S_8TlI9ltEynYrti6gRx5DFcUUNi6ZUAaLfTb0MYtM8q1XiX35hVZx-asc0vgYxQWYFsM1Zc7jFo.mwqYuSDrCt2ecdzhlt0aRVKz9s7CRq9Jal_iSkNasbE&dib_tag=se&keywords=schlauch%2Bmotorrad%2B19&qid=1752960906&sr=8-7&th=1, checked on 7/17/2025.

Amazon.de (2025c): 5 Stück Verbindungsblech 50 x 15 mm verzinkt - Flachverbinder Holzverbinder Lochplatte Lochblech Blauverzinkt I DIOS24®. Available online at https://www.amazon.de/St%C3%BCck-Verbindungsblech-verzinkt-Flachverbinder-Holzverbinder/dp/B0B869J9WZ/ref=sr_1_6?__mk_de_DE=%C3%85M%C3%85%C5%BD%C3%95%C3%91&crid=3M51B12F7XZMO&dib=eyJ2IjoiMSJ9.5vSZJd7qJaaHBSab5P7sTB18LM-lgJLNsNJWj6Sv3HlXW2yn_PtdHcpKoK-vBMckDzW9Lmqw2ZhMCcXgzpYqEnGsDgNyHZU80dfe8de5Dd5NMrVKGcDzwJM7PnhvsbfV2ccUjO5s6Lw4FJGfSPcYGanEZRXncS6IX6R5pVDotbRhVrbndlbXDObQZBp0079PhCtXuUrgSX66riFWDcUWEyW15DI5QatRoYZG_AKDWZt4ONGAFDMEHx-8HVrOLfhVcelKM9b0N9KKf1yhI_ZXCUbjSbwmbbbDwecSfZpkpmTw.so2fhQNnqGFhiZ0r9

dc_zSJQr84AAzbCxxFjhwucGcw&dib_tag=se&keywords=verbindungsblech%2B15%2B5 0%2Bmm&qid=1753271891&sprefix=verbindungsblech%2B15%2B50%2Bmm%2Caps %2C88&sr=8-6&th=1, checked on 7/17/2025.

Amazon.de (2025d): ABA Beul 12022.106.11 Schlauchstecker für Schlauch 3/4 (19 mm) zur Wassersteckkupplung System 3/4, Edelstahl. Available online at https://www.amazon.de/ABA-Beul-12022-106-11-Schlauchstecker-Wassersteckkupplung/dp/B07XYM4PNW?pd_rd_w=y2ITK&content-id=amzn1.sym.835616c4-491b-47d1-828e-9b3e74551c5d&pf_rd_p=835616c4-491b-47d1-828e-9b3e74551c5d&pf_rd_r=5M9AJDWWK5ZVAFY4CXSZ&pd_rd_wg=5myp3&pd_rd_r=a217 c882-1d58-40e7-93ad-91a9e4128b61&ref_=sspa_dk_detail_sbb_img_2&sp_csd=d2lkZ2V0TmFtZT1zcF9kZXRh aWxfdGhlbWF0aWM&th=1, checked on 7/17/2025.

Amazon.de (2025e): ABA Beul 65004.006.11 Wasser-Steckkupplung System 3/4, Edelstahl. Available online at https://www.amazon.de/ABA-Beul-65004-006-11-Wasser-Steckkupplung-Edelstahl/dp/B07XYLRB38/ref=sr_1_2_sspa?crid=34X68W5PEFIMH&dib=eyJ2IjoiMSJ9.4 cr3MAZa264kXjdfy5peMjinEZWALSRi74D-OZe9UN0u_5KthEvhRyAxdP05suTLOAGo4S-7eCTtbjiCJoBAvFKHvw2OZklzUKu1Y0NOttKQXwpHZekesxJcHDAVFGhdnOvaBTrmk4pN brd-yid2NY1qzbVRnTlqy-GQw44a2LkJOdxv7xxjBWhkBwYX_K3FK0ln_F8iBnOMPMQufKaVB0V0VI6sVe8ArDVRlbS BAxo0mlXUg-R-CbR8nclivxSxVlk77IqhKHTx3Fc-kT5K0-O0XQpwtpGcohsddlu-_PE.2cQ9w_JMhHUj2VTCPfSAlpMGsotaecMoS7gxYqMF0wE&dib_tag=se&keywords=ab a%2Bbeul%2Bwasser-steckkupplung%2Bsystem%2B1%2F2&qid=1752953078&sprefix=aba%2Bbeul%2B1%2 F2%2Bsteckkupplung%2Caps%2C430&sr=8-2-spons&ufe=app_do%3Aamzn1.fos.00b1ec55-3783-4b8e-9430-16820cd5ad16&sp_csd=d2lkZ2V0TmFtZT1zcF9hdGY&th=1, checked on 7/17/2025.

Amazon.de (2025f): BACOENG DC 12V Tauchpumpe Solar Wasserpumpe, Geeignet zum Pumpen von Sauberem/Schmutzwasser. Available online at https://www.amazon.de/dp/B017E7UBN2/ref=sspa_dk_detail_right_aax_0?sp_csd=d2lk Z2V0TmFtZT1zcF9kZXRhaWxfcmlnaHRfc2hhcmVk&th=1, checked on 7/20/2025.

Amazon.de (2025g): Flandria Geflochtenes Seil Polypropylen PP weiß Ø 2,5 mm L 100 m G425. Available online at https://www.amazon.de/geflochten-Polypropylen-Durchmesser-L%C3%A4nge-G425/dp/B09NYJ14RZ/ref=sr_1_4?__mk_de_DE=%C3%85M%C3%85%C5%BD%C3%95 %C3%91&crid=1ZTX0N1FM92YS&dib=eyJ2IjoiMSJ9.iD78dmgHip5qEiNUAqRs7NzDmcz d7uzpCaviUNIyGMfrTaBbzPUhWIKos58HNqVxlZCOsaKpbC14iknfgbAIwY9-ljl3SfhyIHdq6CMkUj4wcX4d4rH8ij9PlMkUBf0RclqX32WOBr06ePUpR9hfNslrr_Q4TIePU VnOYTBslCVwmJT6hx-FhDjO_SQHtyeLdiZ_UJddWRW6HO-

9vXK0FF5gywxPN8GF7FzeuCspLmasbKrOhCSKCuYVkjXuWlkFBcZuxmJlDknr_C05rOU
wsiPdyDPISryHJmPr57E_7Ds.Cnc9flFgUmN0y6625aQeznenVEavxc9PZ9t5nOsMKxY&di
b_tag=se&keywords=polypropylenseil+2%2C5&qid=1753270856&rdc=1&s=industrial&s
prefix=polypropylen+seil+2+5%2Cindustrial%2C85&sr=1-4, checked on 7/17/2025.

Amazon.de (2025h): Güde Schmutzwassertauchpumpe GS 4002 P (400 W, 7500 l/h,
Förderhöhe max 5 m, Eintauchtiefe max 4 m, Noryllaufrad, 10 m Anschlusskabel,
variabel einstellbarer Schwimmerschalter, Thermoschutz). Available online at
https://www.amazon.de/G%C3%BCde-Schmutzwassertauchpumpe-GS4002P-var-
Schwimmerschalter-
94630/dp/B00FAMEG4E/ref=sr_1_4?__mk_de_DE=%C3%85M%C3%85%C5%BD%C3%
95%C3%91&crid=3O6GWL8LTH37A&dib=eyJ2IjoiMSJ9.5-
uCZnaSFkodeufwZ50jEJZogr1YMU4eZziDaqJ6vwcessdkt6Jjcr8PbyHaYskz0UQhNK2iTQa
E8gjf4ahhL-18hsWLjQMk9zhL1V-9Uhp1OHotE1mZs2_dZekP0TPlfNBHJXnpg_Y-
1vJq8dg9CesMi3xCrR-
ojtMNqNuxhOL4gnDq30RhbeqVdwqWkYZ1TvtCGUlqnEsuMW2nWm6zjU1E7uGIKTyTGV
4BEipylKs.le4UyZ_hS63Rm8jlriuqqZdzP0L857YQ8fx0juSWWfU&dib_tag=se&keywords=t
auchpumpe&qid=1753345391&s=diy&sprefix=tauchpumpe%2Cdiy%2C122&sr=1-
4&th=1, checked on 7/22/2025.

Amazon.de (2025i): Kabelbinder schwarz set 100/150/200/300mm, 200 Stück,
Kabelbinder UV-beständige für Innen- und Außenbereich, TASKTACKER. Available online
at https://www.amazon.de/Kabelbinder-schwarz-UV-best%C3%A4ndige-
Au%C3%9Fenbereich-
TASKTACKER/dp/B0CT5Q8TWM/ref=sr_1_5?__mk_de_DE=%C3%85M%C3%85%C5%BD
%C3%95%C3%91&crid=7O8KC3BW0E18&dib=eyJ2IjoiMSJ9.l-
ZplB6P3k7hyPStfJ7lU7iOCBpjz8uJ99XaN_-B1d-
jLB8c9d9bWeTp7cczp3hprfdb5MxZWtoZEytbdGDsOqWFwFgf4PM7p-9IFQ-
whAb5izeFOWR3brdKMxjO3MsAPKXw8gJNjm5mokMIlVuxtOr3cVlUv58z2RPIuO_WDtxR
N3N359HE7_uIGtbJtiLRD07YnyUO1ezftXSOOkYG4PUjsneQKOVMYnR_oJpKO_c.t9lGiv5
kFeQbymB3Qbej3QM9vhr0ayf4XZEeEFJCVRA&dib_tag=se&keywords=Kabelbinder&qid
=1752960231&s=diy&sprefix=kabelbinder%2Cdiy%2C130&sr=1-5, checked on
7/17/2025.

Amazon.de (2025j): kanister-vertrieb® 220 Liter Spundfass, Wasserfass, Fass HDPE
Kunststoff, Farbe blau (220 Fass blau neu) + Etikett. Available online at
https://www.amazon.de/dp/B0CN9N91YF/?smid=A3O7I2LQQHDA7V&tag=idealode-
ysm1-
21&linkCode=asn&creative=6742&camp=1638&creativeASIN=B0CN9N91YF&ascsubta
g=2025-07-
19_d5033f595852850aaecd0280a912c5f3d4f391980fb41c1387402834ede7998e&th=1
&psc=1, checked on 7/19/2025.

Amazon.de (2025k): REV Verlängerung, Verlängerungskabel mit Winkelstecker 25m, 3680W, orange. Available online at https://www.amazon.de/REV-Verl%C3%A4ngerungskabel-Verl%C3%A4ngerung-Winkelstecker-orange/dp/B004UFT1K6/ref=sxin_14_pa_sp_search_thematic_sspa?content-id=amzn1.sym.a242ad73-69d0-4a8d-978f-6d53f9236b99%3Aamzn1.sym.a242ad73-69d0-4a8d-978f-6d53f9236b99&crid=3MB6MSJ7EF4NL&cv_ct_cx=verl%C3%A4ngerungskabel%2Bau%C3%9Fen%2B25m&keywords=verl%C3%A4ngerungskabel%2Bau%C3%9Fen%2B25m&pd_rd_i=B004UFT1K6&pd_rd_r=3642ca35-c8b7-40fc-8129-d4f4ef3fd438&pd_rd_w=ubaxr&pd_rd_wg=nfERE&pf_rd_p=a242ad73-69d0-4a8d-978f-6d53f9236b99&pf_rd_r=V1KT7GBH51D9G66D0VKH&qid=1753789407&sbo=RZvfv%2F%2FHxDF%2BO5021pAnSA%3D%3D&sprefix=verl%C3%A4ngerungskabel%2Bau%C3%9Fen%2B25%2Caps%2C104&sr=1-1-6e6ea531-5af4-4866-af75-1ef299d1c279-spons&ufe=app_do%3Aamzn1.fos.00b1ec55-3783-4b8e-9430-16820cd5ad16&sp_csd=d2lkZ2V0TmFtZT1zcF9zZWFyY2hfdGhlbWF0aWM&th=1, checked on 7/20/2025.

Güde GmbH & Co. KG (2025): Schmutzwassertauchpumpe GS 4002 P. Available online at https://www.guede.com/temp/1753798594/p94630_de.pdf, checked on 7/20/2025.

GWT Technik Versand (2023a): Edelstahl Winkel 90 Grad - 3/4 Zoll / Innengewinde x Aussengewinde. Available online at https://www.gwt-versandhandel.de/de/Edelstahl-Winkel-90-Grad-IG-x-AG-3-4-Zoll.html, checked on 7/19/2025.

GWT Technik Versand (2023b): Messing Schnellkupplung | 3/4 Zoll | AG. Available online at https://www.gwt-versandhandel.de/de/messing-schnellkupplung-mit-aussengewinde-3-4-zoll-ag.html, checked on 7/20/2025.

GWT Technik Versand (2023c): Messing Schnellkupplung Schlauchtülle | 3/4 Zoll (Ø19mm). Available online at https://www.gwt-versandhandel.de/de/product_info.php?info=p7897_messing-schnellkupplung-schlauchtuelle---3-4-zoll----19mm-.html&no_boost=1, checked on 7/17/2025.

GWT Technik Versand (2023d): PTFE Teflonband 12 Meter - Gewindedichtband DVGW Geprüft. Available online at https://www.gwt-versandhandel.de/de/Teflonband-Gewindedichtband-DVGW.html, checked on 7/17/2025.

GWT Technik Versand (2023e): Schlauchschelle | Ø16-27mm. Available online at https://www.gwt-versandhandel.de/de/product_info.php?info=p9040_schlauchschelle-----16-27mm.html&no_boost=1, checked on 7/17/2025.

GWT Technik Versand (2023f): Schlauchschelle | Ø20-32mm. Available online at https://www.gwt-versandhandel.de/de/Schlauchschelle-20-32mm.html, checked on 7/20/2025.

Hans Kraeft GmbH & Co.KG (2025a): IDRO YELLOW Standard Gartenschlauch mit Textilgewebe, gelb. Available online at https://www.schlauch-profi.de/IDRO-YELLOW-Standard-Gartenschlauch-mit-Textilgewebe-gelb/10111419-25, checked on 7/19/2025.

Hans Kraeft GmbH & Co.KG (2025b): IDRO YELLOW Standard Gartenschlauch mit Textilgewebe, gelb. Available online at https://www.schlauch-profi.de/IDRO-YELLOW-Standard-Gartenschlauch-mit-Textilgewebe-gelb/10111425-25, checked on 7/20/2025.

Hans Kraeft GmbH & Co.KG (2025c): IDRO YELLOW Standard Gartenschlauch mit Textilgewebe, gelb. Available online at https://www.schlauch-profi.de/IDRO-YELLOW-Standard-Gartenschlauch-mit-Textilgewebe-gelb/10111419-50, checked on 7/19/2025.

K&D Handel (2025): Alublech 3mm. Available online at https://www.metallparadies.de/alublech-3mm.html, checked on 7/17/2025.

Appendix

Vils: Flow Velocity Measurements

Measured distance: 9 m

	Time at Bridge Eichenforstgäßchen [s]	Time at Bridge Schiffbrückgasse [s]	Time at Bridge B85 [s]
Value 1	25.4	27.0	55.9
Value 2	28.0	27.4	64.7
Value 3	27.5	24.1	56.2
Value 4	31.5	29.9	51.4
Value 5	31.6	34.9	52.7
Value 6	27.5	28.1	70.7
Value 7	27.8	27.7	59.6
Value 8	28.6	27.1	80.6
Value 9	29.7	23.5	72.4
Value 10	29.7	28.4	69.2
Mean value	**28.7**	**27.8**	**63.3**

	Velocity at Bridge Eichenforstgäßchen [m/s]	Velocity at Bridge Schiffbrückgasse [m/s]	Velocity at Bridge B85 [m/s]
Mean value	**0.31**	**0.32**	**0.14**

Test Apparatus: Flow Rate and Volumetric Efficiency Results for the 3/4" Hose

Test-No.	Variables				Results	
	Drum diameter [cm]	No. of coils [-]	Pump head [m]	Rotational speed [rpm]	Flow rate [l/min]	Volumetric efficiency [%]
F1	57.0	25	7.35	20	0.0	0.0
F2	57.0	25	7.35	12	2.5	40.8
F3	57.0	25	7.35	6	1.8	58.8
F4	57.0	25	4.55	20	6.4	63.0
F5	57.0	25	4.55	12	4.2	68.6
F6	57.0	25	4.55	6	1.8	58.8
F7	57.0	25	1.45	20	6.4	62.4
F8	57.0	25	1.45	12	3.8	62.0
F9	57.0	25	1.45	6	1.5	49.0
F10	37.0	25	7.35	20	0.0	0.0
F11	37.0	25	7.35	12	0.0	0.0
F12	37.0	25	7.35	6	0.0	0.0
F13	37.0	25	4.55	20	0.0	0.0
F14	37.0	25	4.55	12	0.0	0.0
F15	37.0	25	4.55	6	0.5	25.2
F16	37.0	25	1.45	20	3.5	52.8
F17	37.0	25	1.45	12	1.9	47.8
F18	37.0	25	1.45	6	1.2	60.4
F19	57.0	15	7.35	20	0.0	0.0
F20	57.0	15	7.35	12	0.0	0.0
F21	57.0	15	7.35	6	0.0	0.0
F22	57.0	15	4.55	20	0.0	0.0
F23	57.0	15	4.55	12	0.0	0.0
F24	57.0	15	4.55	6	1.5	49.0
F25	57.0	15	1.45	20	4.5	44.1
F26	57.0	15	1.45	12	4.0	65.3
F27	57.0	15	1.45	6	1.7	55.5

Test-No.	Variables				Results	
	Drum diameter [cm]	No. of coils [-]	Pump head [m]	Rotational speed [rpm]	Flow rate [l/min]	Volumetric efficiency [%]
F28	37.0	15	7.35	20	0.0	0.0
F29	37.0	15	7.35	12	0.0	0.0
F30	37.0	15	7.35	6	0.0	0.0
F31	37.0	15	4.55	20	0.0	0.0
F32	37.0	15	4.55	12	0.0	0.0
F33	37.0	15	4.55	6	0.0	0.0
F34	37.0	15	1.45	20	3.8	57.3
F35	37.0	15	1.45	12	1.8	45.3
F36	37.0	15	1.45	6	1.1	55.3
F37	57.0	10	7.35	20	0.0	0.0
F38	57.0	10	7.35	12	0.0	0.0
F39	57.0	10	7.35	6	0.0	0.0
F40	57.0	10	4.55	20	0.0	0.0
F41	57.0	10	4.55	12	0.0	0.0
F42	57.0	10	4.55	6	0.0	0.0
F43	57.0	10	1.45	20	5.5	53.7
F44	57.0	10	1.45	12	3.6	58.8
F45	57.0	10	1.45	6	1.5	49.0
F46	37.0	10	7.35	20	0.0	0.0
F47	37.0	10	7.35	12	0.0	0.0
F48	37.0	10	7.35	6	0.0	0.0
F49	37.0	10	4.55	20	0.0	0.0
F50	37.0	10	4.55	12	0.0	0.0
F51	37.0	10	4.55	6	0.0	0.0
F52	37.0	10	1.45	20	0.0	0.0
F53	37.0	10	1.45	12	0.0	0.0
F54	37.0	10	1.45	6	0.0	0.0

Test Apparatus: Flow Rate and Volumetric Efficiency Results for the 1/2" Hose

Test-No.	Variables				Results	
	Drum diameter [cm]	No. of coils [-]	Pump head [m]	Rotational speed [rpm]	Flow rate [l/min]	Volumetric efficiency [%]
F55	57.0	25	7.35	20	0.0	0.0
F56	57.0	25	7.35	12	0.0	0.0
F57	57.0	25	7.35	6	0.0	0.0
F58	57.0	25	4.55	20	0.0	0.0
F59	57.0	25	4.55	12	1.7	62.5
F60	57.0	25	4.55	6	1.1	80.8
F61	57.0	25	1.45	20	3.1	68.3
F62	57.0	25	1.45	12	1.9	69.8
F63	57.0	25	1.45	6	1.0	73.5
F64	57.0	20	7.35	20	0.0	0.0
F65	57.0	20	7.35	12	0.0	0.0
F66	57.0	20	7.35	6	0.0	0.0
F67	57.0	20	4.55	20	0.0	0.0
F68	57.0	20	4.55	12	1.5	55.1
F69	57.0	20	4.55	6	1.0	73.5
F70	57.0	20	1.45	20	3.1	68.3
F71	57.0	20	1.45	12	1.9	69.8
F72	57.0	20	1.45	6	1.1	80.8
F73	37.0	25	7.35	20	0.0	0.0
F74	37.0	25	7.35	12	0.0	0.0
F75	37.0	25	7.35	6	0.0	0.0
F76	37.0	25	4.55	20	0.0	0.0
F77	37.0	25	4.55	12	0.0	0.0
F78	37.0	25	4.55	6	0.5	56.6
F79	37.0	25	1.45	20	1.5	50.9
F80	37.0	25	1.45	12	0.9	50.9
F81	37.0	25	1.45	6	0.7	79.2

Test-No.	Variables				Results	
	Drum diameter [cm]	No. of coils [-]	Pump head [m]	Rotational speed [rpm]	Flow rate [l/min]	Volumetric efficiency [%]
F82	57.0	15	7.35	20	0.0	0.0
F83	57.0	15	7.35	12	0.0	0.0
F84	57.0	15	7.35	6	0.0	0.0
F85	57.0	15	4.55	20	0.0	0.0
F86	57.0	15	4.55	12	0.0	0.0
F87	57.0	15	4.55	6	0.0	0.0
F88	57.0	15	1.45	20	2.3	50.7
F89	57.0	15	1.45	12	1.8	66.1
F90	57.0	15	1.45	6	1.1	80.8
F91	37.0	20	7.35	20	0.0	0.0
F92	37.0	20	7.35	12	0.0	0.0
F93	37.0	20	7.35	6	0.0	0.0
F94	37.0	20	4.55	20	0.0	0.0
F95	37.0	20	4.55	12	0.0	0.0
F96	37.0	20	4.55	6	0.0	0.0
F97	37.0	20	1.45	20	1.3	44.1
F98	37.0	20	1.45	12	1.2	67.9
F99	37.0	20	1.45	6	0.8	90.6
F100	37.0	15	7.35	20	0.0	0.0
F101	37.0	15	7.35	12	0.0	0.0
F102	37.0	15	7.35	6	0.0	0.0
F103	37.0	15	4.55	20	0.0	0.0
F104	37.0	15	4.55	12	0.0	0.0
F105	37.0	15	4.55	6	0.0	0.0
F106	37.0	15	1.45	20	1.8	61.1
F107	37.0	15	1.45	12	1.1	62.3
F108	37.0	15	1.45	6	0.5	56.6

Test-No.	Variables				Results	
	Drum diameter [cm]	No. of coils [-]	Pump head [m]	Rotational speed [rpm]	Flow rate [l/min]	Volumetric efficiency [%]
F97*	37.0	20	1.45	20	1.4	47.5
F98*	37.0	20	1.45	12	1.1	62.3
F99*	37.0	20	1.45	6	0.8	90.6
F106*	37.0	15	1.45	20	1.7	57.7
F107*	37.0	15	1.45	12	1.0	56.6
F108*	37.0	15	1.45	6	0.6	67.9

*   Vertical stationary hose

Test Apparatus: Maximum Pump Head Results for the 1/2" Hose

Test-No.	Variables			Results
	Drum diameter [cm]	No. of coils [-]	Rotational speed [rpm]	Max. pump head [m]
H1	57.0	25	20	4.60
H2	57.0	25	12	6.05
H3	57.0	25	6	7.30
H4	57.0	20	20	3.65
H5	57.0	20	12	5.85
H6	57.0	20	6	6.05
H7	37.0	25	20	3.20
H8	37.0	25	12	4.55
H9	37.0	25	6	4.70
H10	57.0	15	20	3.15
H11	57.0	15	12	4.00
H12	57.0	15	6	4.50
H13	37.0	20	20	3.15
H14	37.0	20	12	3.45
H15	37.0	20	6	3.55
H16	37.0	15	20	1.95
H17	37.0	15	12	2.15
H18	37.0	15	6	2.40
H13*	37.0	20	20	3.95
H14*	37.0	20	12	5.15
H15*	37.0	20	6	6.60
H16*	37.0	15	20	4.00
H17*	37.0	15	12	4.85
H18*	37.0	15	6	5.20

Test-	Variables			Results
No.	Drum diameter [cm]	No. of coils [-]	Rotational speed [rpm]	Max. pump head [m]
H16**	37.0	15	20	3.10
H17**	37.0	15	12	3.75
H18**	37.0	15	6	3.85
H16***	37.0	15	20	3.45
H17***	37.0	15	12	3.65
H18***	37.0	15	6	3.90

*   Vertical stationary hose

**   Horizontal stationary hose, then pulled up via the stairs

***   Horizontal stationary hose, then pulled up vertically

Test Apparatus: Energy Efficiency Results for the 3/4" Hose

B. bucket

Test-No.	Variables					Measurements		Results			
	Drum diameter [cm]	No. of coils [-]	Pump head [m]	Height B. [m]	Weight B. [kg]	Impact speed B. [m/s]	Pumped volume [l]	Energy input B. [J]	Energy output water [J]	Kin. Energy B. [J]	Energy Efficiency [%]
E1	57.0	25	7.35	7.5	3.5	0.50	2.3	257.5	165.8	0.4	64.5
E2	57.0	25	4.55	7.5	3.5	0.50	1.8	257.5	80.3	0.4	31.3
E3	57.0	25	1.45	7.5	3.5	0.75	1.3	257.5	18.5	1.0	7.2
E4	37.0	25	7.35	7.5	3.5	0.75	0.0	257.5	0.0	1.0	0.0
E5	37.0	25	4.55	7.5	3.5	0.75	0.0	257.5	0.0	1.0	0.0
E6	37.0	25	1.45	7.5	3.5	1.00	1.5	257.5	21.3	1.8	8.3
E7	57.0	15	7.35	7.5	3.5	0.75	0.0	257.5	0.0	1.0	0.0
E8	57.0	15	4.55	7.5	3.5	0.75	0.0	257.5	0.0	1.0	0.0
E9	57.0	15	1.45	7.5	3.5	1.00	1.5	257.5	21.3	1.8	8.3
E10	37.0	15	7.35	7.5	2.5	0.75	0.0	183.9	0.0	0.7	0.0
E11	37.0	15	4.55	7.5	2.5	0.75	0.0	183.9	0.0	0.7	0.0
E12	37.0	15	1.45	7.5	2.5	1.00	0.5	183.9	7.1	1.3	3.9

Test-No.	Variables					Measurements		Results			
	Drum diameter [cm]	No. of coils [-]	Pump head [m]	Height B. [m]	Weight B. [kg]	Impact speed B. [m/s]	Pumped volume [l]	Energy input B. [J]	Energy output water [J]	Kin. Energy B. [J]	Energy Efficiency [%]
E13	57.0	10	7.35	7.5	2.5	1.00	0.0	183.9	0.0	1.3	0.0
E14	57.0	10	4.55	7.5	2.5	1.00	0.0	183.9	0.0	1.3	0.0
E15	57.0	10	1.45	7.5	2.5	1.00	1.4	183.9	19.9	1.3	10.9
E16	37.0	10	7.35	7.5	2.5	1.00	0.0	183.9	0.0	1.3	0.0
E17	37.0	10	4.55	7.5	2.5	1.00	0.0	183.9	0.0	1.3	0.0
E18	37.0	10	1.45	7.5	2.5	1.00	0.0	183.9	0.0	1.3	0.0

Test Apparatus: Energy Efficiency Results for the 1/2" Hose

B. bucket

Test-No.	Variables					Measurements		Results			
	Drum diameter [cm]	No. of coils [-]	Pump head [m]	Height B. [m]	Weight B. [kg]	Impact speed B. [m/s]	Pumped volume [l]	Energy input B. [J]	Energy output water [J]	Kin. Energy B. [J]	Energy Efficiency [%]
E19	57.0	25	7.35	7.5	2.5	0.50	0.0	183.9	0.0	0.3	0.0
E20	57.0	25	4.55	7.5	2.5	0.50	1.0	183.9	44.6	0.3	24.3
E21	57.0	25	1.45	7.5	2.5	0.75	0.8	183.9	11.4	0.7	6.2
E22	57.0	20	7.35	7.5	2.5	0.75	0.0	183.9	0.0	0.7	0.0
E23	57.0	20	4.55	7.5	2.5	0.75	1.0	183.9	44.6	0.7	24.4
E24	57.0	20	1.45	7.5	2.5	1.00	0.8	183.9	11.4	1.3	6.2
E25	37.0	25	7.35	7.5	2.5	0.75	0.0	183.9	0.0	0.7	0.0
E26	37.0	25	4.55	7.5	2.5	0.75	0.0	183.9	0.0	0.7	0.0
E27	37.0	25	1.45	7.5	2.5	1.00	0.8	183.9	11.4	1.3	6.2
E28	57.0	15	7.35	7.5	2.5	0.75	0.0	183.9	0.0	0.7	0.0
E29	57.0	15	4.55	7.5	2.5	0.75	0.0	183.9	0.0	0.7	0.0
E30	57.0	15	1.45	7.5	2.5	1.00	0.7	183.9	10.0	1.3	5.5

Test- No.	Variables					Measurements		Results			
	Drum diameter [cm]	No. of coils [-]	Pump head [m]	Height B. [m]	Weight B. [kg]	Impact speed B. [m/s]	Pumped volume [l]	Energy input B. [J]	Energy output water [J]	Kin. Energy B. [J]	Energy Efficiency [%]
E31	37.0	20	7.35	7.5	2.5	1.00	0.0	183.9	0.0	1.3	0.0
E32	37.0	20	4.55	7.5	2.5	1.00	0.0	183.9	0.0	1.3	0.0
E33	37.0	20	1.45	7.5	2.5	1.00	0.6	183.9	8.5	1.3	4.7
E34	37.0	15	7.35	7.5	2.5	1.00	0.0	183.9	0.0	1.3	0.0
E35	37.0	15	4.55	7.5	2.5	1.00	0.0	183.9	0.0	1.3	0.0
E36	37.0	15	1.45	7.5	2.5	1.00	0.1	183.9	1.4	1.3	0.8
E31*	37.0	20	7.35	7.5	2.5	1.00	0.0	183.9	0.0	1.3	0.0
E32*	37.0	20	4.55	7.5	2.5	1.00	0.0	183.9	0.0	1.3	0.0
E33*	37.0	20	1.45	7.5	2.5	1.00	0.7	183.9	10.0	1.3	5.5
E34*	37.0	15	7.35	7.5	2.5	1.00	0.0	183.9	0.0	1.3	0.0
E35*	37.0	15	4.55	7.5	2.5	1.00	0.0	183.9	0.0	1.3	0.0
E36*	37.0	15	1.45	7.5	2.5	1.00	0.1	183.9	1.4	1.3	0.8

* Vertical stationary hose